INFORMATION TO USERS

This manuscript has been reproduced from the microfilm master. UMI films the text directly from the original or copy submitted. Thus, some thesis and dissertation copies are in typewriter face, while others may be from any type of computer printer.

The quality of this reproduction is dependent upon the quality of the copy submitted. Broken or indistinct print, colored or poor quality illustrations and photographs, print bleedthrough, substandard margins, and improper alignment can adversely affect reproduction.

In the unlikely event that the author did not send UMI a complete manuscript and there are missing pages, these will be noted. Also, if unauthorized copyright material had to be removed, a note will indicate the deletion.

Oversize materials (e.g., maps, drawings, charts) are reproduced by sectioning the original, beginning at the upper left-hand corner and continuing from left to right in equal sections with small overlaps.

Photographs included in the original manuscript have been reproduced xerographically in this copy. Higher quality 6" x 9" black and white photographic prints are available for any photographs or illustrations appearing in this copy for an additional charge. Contact UMI directly to order.

ProQuest Information and Learning
300 North Zeeb Road, Ann Arbor, MI 48106-1346 USA
800-521-0600

Robustness analysis for power systems based on the structured singular value tools and the ν gap metric

by

Chuanjiang Zhu

A dissertation submitted to the graduate faculty
in partial fulfillment of the requirements for the degree of
DOCTOR OF PHILOSOPHY

Major: Electrical Engineering (Electric Power)
Major Professors: Vijay Vittal and Mustafa Khammash

Iowa State University
Ames, Iowa
2001

Graduate College
Iowa State University

This is to certify that the Doctoral dissertation of

Chuanjiang Zhu

has met the dissertation requirements of Iowa State University

Signature was redacted for privacy.

Co-major Professor

Signature was redacted for privacy.

Co-major Professor

Signature was redacted for privacy.

For the Major Program

Signature was redacted for privacy.

For the Graduate College

TABLE OF CONTENTS

LIST OF TABLES

LIST OF FIGURES

ACKNOWLEDGMENTS

The experience at Iowa State University has been both productive and enjoyable for me. I had the chance to meet a number of talented and warm-hearted people. First, I would like to thank my co-major advisors, Dr. Vijay Vittal and Dr. Mustafa Khammash for their invaluable guidance and continual support throughout this research project.

I would also like to express my gratitude to graduate committee members, Drs. V. Ajjarapu, Wolfgang Kliemann, Gerry Sheblé and James McCalley for their generous contributions of time and effort in the process of this research project.

Various colleagues have influenced my work and helped during the course of the research. I appreciate Dr. Miodrag Djukanovic's kind and prompt help in providing me with valuable suggestions. Although I never had the chance to work with him, I am impressed with his smart, knowledgeable, hard-working and thorough research notes, papers and codes he gave us. I would like to thank Dr. Nicola Elia for helping me understand new concepts in robust control area. I am very grateful to Zhe Lin, Xin Qi, Rajeev Rajaram, Songzhe Zhu, Nagaraj Balijepalli, Dede O. Subakti, and Jiang Huang for numerous helpful discussions. In addition, I am grateful to all the professors and graduate students in the electric power program at Iowa State University. They have shared their views and friendship with me.

Finally I would like to offer my sincerely appreciation to my parents and my in-laws. They overcame great difficulties and have been continuously giving me strong support. And my thanks also go to my husband, Jianwei, for his encouragement and support. All my thanks, and all my love, to my son Dylan.

Robustness analysis for power systems based on the structured singular value tools and the ν gap metric

Chuanjiang Zhu

Major Professors: Vijay Vittal and Mustafa Khammash
Iowa State University

Modern power systems are operated more stressed than ever because of the advent of deregulation and competition. One of the important issues in the design of controllers for a stressed system is to evaluate the stability of the controlled system over a range of operating conditions.

The conventional controllers are designed to make the system stable under certain conditions of operation. The time consuming time domain simulation is then used to evaluate the controllers for a few selected operating conditions around which the controllers are designed. Such a design and evaluation procedure cannot guarantee robustness of the controller over the whole range of operating conditions.

In this dissertation, practical algorithms to perform robustness analysis based on two tools, structured singular value and the ν gap metric, are investigated. The power system stabilizer is used as the controller and small signal stability is of interest.

The robustness problem in the SSV framework is set up for the multimachine power system. In this formulation, an improved uncertainty characterization has been used to capture the effect of parameter variations in terms of the varying elements of the linearized system matries, which are derived from the component differantial equations and the network algebraic equations separately. SVD decomposition is used to reduce the size of the problem. Based on the resulting framework, a branch and bound scheme is proposed to intelligently select frequency intervals on which the frequency sweep test can be performed further to find the peak of μ. Instead of blindly choosing frequency intervals to sweep, which could ignore important frequency points on the μ plots, this scheme

provides searching under guidance. The analysis procedure accurately predicts the range of stable operating conditions which are verified by repeated eigenvalue analysis.

For the robustness in terms of ν gap metric, we set up the feedback configuration for multimachine power system. The frequency response of the ν gap metric is plotted and its relationship with that of the stability margin is used to determine the stability of the perturbed systems. A weighted ν gap metric is defined and its frequency domain interpretation is explored to further reduce the conservatism of the results.

Finally, a feedback configuration is carefully developed to carry out the McFarlane and Glover H_∞ loop shaping design procedure. The effect of the damping controller on improving system dynamic performance is also examined.

Comparisons are made between the two major analysis tools via the results on the same test systems with the same scenarios.

1 INTRODUCTION

1.1 Damping the Low Frequency Oscillation

Oscillations were observed in power systems when synchronous generators were interconnected to provide more power capacity and more reliability. Several instances of low frequency oscillations, which associated with machines in one part of the system swinging against machines in another part of the system, have been found in the North American interconnection in the past decade [44]. These phenomena are referred to as inter-area oscillations and have frequencies typically in the range of 0.1HZ to 0.7HZ. From an operating point of view, oscillations are acceptable as long as they decay. However, oscillations are a characteristic of the system; if sufficient damping is not provided, growing oscillations can even result in system collapse.

These oscillations are related to the small signal stability of a power system. Small signal stability is the ability of the power system to maintain synchronism under small disturbances. The more stressed the operating condition of the power system is, the more likely it is to lose small signal stability under a small variation in loads or generation. The disturbances are considered sufficiently small so that linearization of system equations is allowed for the purpose of analysis. Instability that may result can be of two forms: steady increase in rotor angle due to lack of sufficient synchronizing torque, or rotor oscillations of increasing amplitude due to lack of sufficient damping torque [10].

PSS are often used to provide positive damping. PSS are mostly single-loop local controllers, which use speed or power input signal and synthesize a control signal based

on appropriate phase-lead compensations to add to the reference voltage signal of the voltage regulate. The conventional power system stabilizer design involves time consuming tuning, and its design methodology results in its non-optimal damping in the entire operating range since they are usually designed for a particular operating points. In this research, the robustness of conventionally designed power system stabilizers were tested using the proposed algorithms. The results were verified by conventional eigenvalue test.

While the inter-area oscillation may be destabilized by a PSS tuned according to the conventional design way, it is desirable to design robust PSS so that when the operating conditions change within a wide range, the system can still maintain stability. In power system, the change of operating conditions involves a lot of uncertainty. To effectively handle the uncertaities is one of the main objectives of this research.

1.2 Handling Uncertainties in Power Systems

This research is concerned with the problem of small signal stability of power systems under uncertainties. There are various types of uncertainties in power systems, the most common of which is parametric uncertainty. The parameters of the power system models can never be known exactly. One reason is because of the accuracy of the measurements. There is no way to get the exact value of every parameter due to the errors in the measurements. Besides, the parameters in the linear model may vary due to nonlinearities or changes in the operating conditions. Furthermore, in most cases the uncertainties are even unpredictable. Power systems must typically perform over a wide range of operating conditions. For instance, the load demands at a certain bus can vary gradually or even sharply every hour throughout a given day; disturbances of differing extent of severity could happen during the normal operation, etc. Besides, uncertainties arise when we represent the real system by models that are linear, time-invariant and finite dimensional. Thus, it is usually possible to implement only approximate modeling.

All the above problems emphasize the necessity of including uncertainty in the model so that uncertainties can be handled when we do the stability analysis, the dynamic security assessment, and the controller design based on these models.

The existence of uncertainties requires good robustness of the control systems. A control system is robust if it is insensitive to differences between the actual system and the model of the system which was used to design the controller. These differences are referred to as model/plant mismatch or simply model uncertainty. As for power systems, the control system will have to regulate the system under a diversity of operating conditions; it must have the ability to tolerate model uncertainties, suppress potential instability and damp the system oscillations that might threaten the system stability as the system is operating under more stressed conditions.

One of the major tasks in the design of control systems in a power system is to evaluate the stability robustness. The conventional controllers are designed to make the system stable under certain conditions of operation. Because the time domain simulation used to evaluate the controller is time consuming, evaluation of the controller is then performed only for a few selected operating conditions around which the controllers are designed. The simulation obviously cannot cover the whole operating range; thus, the resulting evaluation procedure cannot guarantee robustness of the controller over the whole range. Another disadvantage is that such evaluation does not provide any indicator of the stability margin. As for the controller design, we require the controller to achieve robust performance, that is, the performance requirements to be satisfied for all possible plants, including the worst-case uncertainty. This requirement cannot be satisfied using the conventional design methodology.

In order to take into account these problems in the evaluation, it is necessary to use a technique that could capture the uncertainties precisely and include them into the model. It should also indicate the distance to instability. This technique should be analytical in contrast to the simulation method.

Modern robust control theories have been developed significantly in the past two decades. The key idea in a robust control paradigm is to check whether the design specifications are satisfied even for the "worst-case" uncertainty. Many efforts have been taken to investigate the application of robust control techniques to power systems. such as Kharitonov's theorem [24], H_∞ [8. 9. 6. 25. 1], L_1 [23. 45], and Structured Singular Value (SSV or μ) [32. 33. 34] techniques.

Among them, H_∞ optimization techniques are the most popular ones that have been applied to robust design problem and have many applications in power systems. But it is restricted to the additive and/or multiplicative uncertainty representation which overbounds the parametric uncertainty. and tends to give conservative results. Actually all of the above mentioned techniques suffered from the conservatism problem due to overbounding of the uncertainty set.

By taking advantage of the fact that in many problems uncertainty can be represented in a structured form. e.g.. a block-diagonal form. the Structured Singular Value (or μ) based tools have been proven to be promising. Algorithms were developed to compute upper and lower bounds for μ. and the computed bounds were usually tight enough for practical applications (see [17. 39]). This lead to a significant reduction in conservatism over methods which simply lump all uncertainty into a single norm-bounded block. This has been demonstrated in previous research [32. 33. 34]. But the μ approach involves complex computation. It encounters difficulty in application to large scale systems due to the heavy computational burden. It has been shown that the mixed μ problem is NP hard [53]. which means that no algorithm can evaluate μ in polynomial time. This property of the problem suggests that instead of trying to evaluate the exact μ. a more practical approach would be to evaluate good bounds. In fact. even bounds calculation takes considerable time. Thus it is desirable to propose feasible algorithms to perform the bounds calculation. This research extends existing methods to more practical algorithms for achieving the μ bounds to deal with the robustness analysis

problem in power systems. This sheds light on the application of SSV based robustness analysis on large-scale systems.

The efficiency of using feedback systems to control dynamical systems promotes the study of the notion of uncertainty appropriate to the plant. We will introduce a new notion of uncertainty, namely the ν gap metric, and its application in analysis problems. This metric is of interest since we are interested in comparing the closed loop behavior of different plants connected to the same feedback compensator instead of just the open loop behavior as what the norm metric captured. This metric introduces the graph topology. The graph topology has been used to quantitatively measure the distance of two plants. In this topology, two plants are deemed "close" if any reasonable compensator for the first gives similar closed loop behavior with the second of the plants in the standard feedback configuration of Figure 1.1.

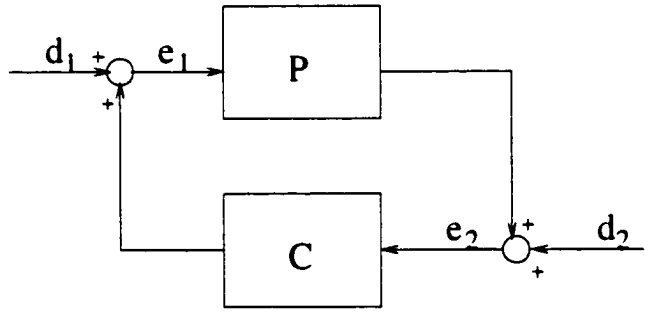

Figure 1.1 Standard feedback configuration.

The ν gap metric provides a sufficient condition for the stability of a perturbed plant/compensator pair, in terms of the gain of the transfer functions from the input and output of the plant to the input output of the controller. But to date, no effort has been made to study the power system behavior in terms of the ν gap metric. Research has been conducted here to develop the frequency response interpretation of the ν gap

metric in power systems. And its application in power system robust analysis has been studied in depth.

1.3 Robust PSS Design

Although the μ approach is successful in tackling analysis problem, it is too complicated to be used in controller synthesis. To conduct the μ synthesis problem, one need to first set up the framework which involves extracting uncertainties, choosing the weighting functions. Then the DK-iteration needs to be carried on. The iteration is not guaranteed to be convergent and sometimes it is slow to converge due to bad fitting of the scaling factors. Furthermore, the resulting controller is of very high order. This brings difficult for controller model reduction.

It has been shown that the problem of robustness optimization in the gap metric is equivalent to robustness optimization for normalized coprime factor perturbations [20]. That is, a ball of uncertainty in the gap metric of a given radius is equal to a ball of uncertainty in the same radius defined by perturbations of a normalized right coprime fraction. For the stabilization of the coprime factor type uncertainties, McFarlane and Glover have developed a nice method, namely H_∞ loop shaping design procedure [35]. This design procedure combines the loop shaping and H_∞ synthesis together. It allows one to shape the nominal plant singular value without considering the phase information, with the guaranteed stability properties of H_∞ design methods. In this research, the power system stabilizer (PSS) has been designed using an H_∞ loop shaping design procedure.

1.4 Objectives and Scope of Research Work

The objective of this research is to answer the following problem: given a controller, subject to parametric uncertainties within a certain range, will the system be stable?

At the same time, this study should provide a number indicating how large the worst case uncertainty can be before the system loses stability. Two major concepts in robust control area are explored thoroughly to apply to power system: the structured singular value and the ν gap metric.

The scope of this research work includes the following:

1. In the structured singular value section,

   (a) Formulate a general framework for the inclusion of the PSS model in order to apply the μ-based robustness approach. This involves writing a parameter-dependent system as a linear fractional transformation involving a fixed LTI plant with a structured perturbation operator. The parameter dependence in the system gives rise to a repeated real perturbation block. A novel way to characterize uncertainties incorporates the variations of parameters into both the differential and algebraic equations, further minimizing conservatism. The varying parameters include changes in generation setting and interface power flows.

   (b) To eliminate the frequency search for robustness tests, the frequency is extracted and treated as an additional uncertainty. Namely, a bounded frequency test is performed for evaluating μ at a certain frequency range. This effectively reduces the original frequency sweep test which is time-consuming and tends to miss important frequency points to a single μ test.

   (c) In order to analyze the worst case perturbation, the bounded frequency test is further developed to achieve a branch and bound scheme. By branching on the frequency intervals, this scheme provides a systematic way to narrow the frequency range upon which a frequency sweep test could be performed. Instead of blindly selecting frequency ranges to perform frequency sweep tests, this scheme could intelligently select narrow enough intervals to do the test.

thus avoiding the possibility of ignoring important frequency points when there are sharp spikes or discontinuities at the μ plots.

2. In the ν gap metric section.

   (a) A plant set at various operating points due to the existence of the uncertainty is formulated. The distance between each plant in this set is calculated in terms of the ν gap metric.

   (b) The robustness of the interconnected system is investigated making use of the robustness properties for the ν gap metric.

   (c) The frequency response interpretation of the stability in the ν gap metric is explored. A weighted gap metric test with its frequency response is shown to be particularly sharp in robustness analysis.

   (d) PSS is designed using the H_∞ loop shaping design procedure. The resulting PSS has been tested to perform well in the whole operating range. It achieves robust stability as well as good performance in the design parameter range. The results are verified by performing nonlinear simulation. The robustness of the designed controller is validated by the structured singular value based analysis tools.

3. Comparisons are made between the structure singular value approach and the gap metric approach both in terms of robust analysis and synthesis.

During the course of this research, an artificial two-area four-machine system was used to study the control of power system oscillations. Its model was created for a research report commisioned from Ontario Hydro by the Canadian Electrical Association [27, 28] to exhibit the different types of oscillations that occur in both large and small interconnected power systems. The results were also tested on an IEEE 50-machine generator system [50]. In this system, six generators are represented in the detailed model

and the remaining generators are represented in the classical model. This system exhibits complex behavior and is often used to analyze the efficacy of the controls in damping inter-area oscillations.

1.5 Summary of the Contents

This thesis consists of four chapters. Chapter 1 proposes the problem and introduces the objective and scope of this research work.

Chapter 2 focuses on the structured singular value based robustness analysis, and is organized as follows:

- **Section 2.1** is a brief literature review on structured singular value based concepts and bounds calculation. The two subsections introduce recent studies on the uncertainty characterization in robustness assessment and the μ bounds calculation algorithms respectively.

- **Section 2.2** consists of introductory materials on the existing robust methodology. After explaining these methods in detail, it is easy to recognize the need for improvement.

- **Section 2.3** gives a detailed description of the mathematical models of the power system components and the overall system dynamic equations.

- **Section 2.4** presents a systematic way to characterize the parametric uncertainty and constructs the robustness analysis framework. The uncertainties in the power system models are characterized in the algebraic and differential equations separately. Singular Value Decomposition is used to reduce the order of the system.

- **Section 2.5** describes in detail several practical algorithms to perform the robustness analysis. It is based on the canonical $M - \Delta$ framework formed in Chapter

4. The real spectral radius calculation is for one uncertainty case. For the general case, in order to eliminate the frequency search from robustness tests, we transform a classical frequency dependent μ analysis problem into a bounded frequency test problem, in which the frequency is introduced as an additional uncertainty, i.e. by viewing frequency as a real scalar parameter. This gives a one-shot μ test instead of the time-consuming frequency sweep. In order to determine how large the perturbation besides the frequency uncertainty could be, the skewed-μ [42] is calculated. Finally the branch and bound test is used to assess the robustness by screening the frequency intervals. Numerical results for each method are presented.

Chapter 3 consists of four sections.

- **Section 3.1** gives a brief description of μ synthesis and summarizes its disadvantages, which promotes us to study the new topic in robust control area, the gap metric and the ν gap metric.

- **Section 3.2** provides the mathematical concepts related to the gap and the ν gap metric. We need a substantial amount of mathematical machinery for this topic. Despite the level of mathematical abstraction, it is important to bear in mind that, this theoretical research has a solid engineering motivation.

- **Section 3.3** gives a brief literature review on the application of gap metric in power systems.

- **Section 3.4** establishes detailed steps to perform robustness analysis in terms of the ν gap metric and presents simulation results on the test systems. The frequency domain explanation of the ν gap is investigated thoroughly. A weighted ν gap metric is defined and used in the robustness assessment.

- **Section 3.5** describes the design of an H_∞ loop shaping controller to damp power system low frequency oscillation. The design procedure for power system stabi-

lizer is shown in detail and simulation results on the comparison of the controller performance with the conventional PSS and μ controller are given.

Chapter 4 includes the conclusions and also provides some suggestions for future research.

2 STRUCTURED SINGULAR VALUE BASED ROBUSTNESS ANALYSIS

2.1 Review of Relevant Literature

2.1.1 Uncertainty characterization

Over the years, precise and fixed linear control schemes have been used extensively in many engineering applications. These kinds of designs do not take into account the uncertainties that could be encountered in both the plant and controller model. The uncertainty may have several origins:

1. There are many parameters in the linear model which are only known approximately or are simply in error;
2. The parameters in the linear model may vary due to changes in the operating conditions;
3. Measurement devices cause error;
4. There are neglected dynamics when simplifying the system model;
5. Uncertainties can be caused by the controller model reduction or implementation inaccuracies.

The first step of the robust control methodology is to model and bound the above uncertainties in an appropriate way. The next step is to try to design a controller that

is insensitive to the difference between the actual system and the model of the system, i.e. a controller that can handle the worst case perturbations.

In current literature, modeling of uncertainty is considered from two viewpoints.

- In the frequency domain, the perturbation is considered to be a transfer function, separate from the system model [12]. This kind of uncertainty could be multiplicative or additive. For example, the normalized coprime factor uncertainty in [35] is a kind of additive uncertainty.

- In the state-space representation, the uncertainties in the matrices can be captured. This is usually used to deal with the parametric uncertainty.

If the uncertainty description represents one or several sources combined together to form a single lumped perturbation of a chosen structure, such uncertainty is called *unstructured uncertainty*. Parametric uncertainty is usually modeled in a structured way. However, sometimes there can be several levels of structure. For example, when the uncertainties include both parametric uncertainties and unmodeled dynamics the whole uncertainty block could be a structured one and arranged in a diagonal form, while in particular, each block for the unmodeled dynamics could be a lumped unstructured block. In this research, we focus on the parametric uncertainties characterized in a structured way, and the uncertainties are captured in a state-space representation context.

In [32], a framework for robust stability assessment of controls in multimachine power systems was used. Starting from the algebraic and differential equations, all the algebraic variables in the component differential equations were eliminated according to the relationship derived from the network algebraic equations. The resulting differential equations were linearized at the nominal operating point to create a simplified linear system. The parametric uncertainties on the elements of the coefficient matrix of the system equations were then characterized by polynomial approximation. The disad-

vantage of this approach is that the uncertainties in the algebraic equations and the differential equations cannot be characterized separately so as to exploit the specific nature of power system dynamics. This results in a more natural way to characterize uncertainties and has been investigated in this research.

2.1.2 Computation of the μ bounds

When the uncertainty is characterized in a structured manner, more information about the uncertainty is captured since the unstructured uncertainty is assumed to be bounded but otherwise unknown. In practical problems, it is generally the case that the uncertainty consists of multiple norm bounded perturbations. Consequently, using only a single norm-bounded perturbation for analysis is rarely adequate.

The structured singular value is defined based on the structured uncertainty representation. It is a function which provides a generalization of the singular value (for a single full complex block) and the spectral radius (for a single repeated complex scalar block) and gives the smallest size of the uncertainty (measured by the maximum singular value of the uncertainty block) which makes the system lose stability. Since it is based on an uncertainty characterization which makes use of much more information than most other robust approaches, it gives much less conservative results.

In practice, the major difficulty in the application of the μ approach lies in the computational burden, especially when the system dimension and the number of uncertain parameters are large.

The major issues in computing μ, or its equivalent are generality of the problem description, the exactness of analysis, and the ease of computation. Many works in literature deal with the computation of μ bounds. They may be divided into two categories: one includes those methods that emphasize refining the bounds by reducing gaps between the upper and lower bounds as much as possible to achieve high accuracy; the other kind of method aims at reducing the computational complexity, which tends

to obtain μ quickly at the expense of getting relatively cruder results. To explore the algorithms obtaining μ, we need to make proper trade-offs between the accuracy and the computation time.

The upper and lower bounds are derived as two optimization problems. The lower bound of μ is derived as a real eigenvalue maximization problem, and an improved power iteration has been developed for the generalized mixed μ case. Although it can be proved that μ is exactly equal to the maximal of this optimization problem, this problem is not convex; in general only local maxima can be achieved instead of global maxima. Thus usually we can find only the lower bound. The commercial MATLAB Toolbox "μ analysis and synthesis" [7] uses the power algorithm to compute the lower bound. An upper bound was presented by Fan et. al [18] which involves minimizing the eigenvalues of a Hermitian matrix. We will use these bounds in our calculation.

The general μ analysis procedure is to compute the bounds of $\mu(\omega)$ as a function of frequency ω. In practice, this function is usually computed at each point of a frequency grid. This frequency sweep technique may, however, be unreliable in the case when narrow and high peaks exist on the μ plot, since critical frequencies can be missed.

Doyle in [11] gave a state space test for the fast calculation of μ. This test first performs a bilinear transformation where the frequency variable is treated as another Δ block to give a larger problem which converts the continuous-time μ problem to a discrete time μ problem. Since the bilinear transformation is a one to one mapping between the frequency axis and the unit circle, no frequency will be missed. Moreover, this transforms the frequency domain calculation to a single constant μ calculation involving larger M and Δ matrices. This gives a one-shot state-space μ test. But this kind of test does not have the flexibility to evaluate μ over a specified frequency interval. And to get the worst case parameter, it needs an α searching procedure which is time consuming and usually relies heavily on the tightness of the bounds to give information on the value of α.

Based on the development of μ related theory, this research will explore more practical algorithms to perform the μ analysis.

2.2 Robustness Methodology

2.2.1 Definition of μ

Suppose we have a complex matrix $M \in C^{n\times n}$ and three non-negative integers m_r, m_c, and m_C (with $m = m_r + m_c + m_C \leq n$), which specify the number of uncertainty blocks of repeated real scalars, repeated complex scalars, and full complex blocks, respectively. Then the block structure $\mathcal{K}(m_r, m_c, m_C)$ is an m-tuple of positive integers:

$$\mathcal{K} = (k_1, \ldots, k_{m_r}, k_{m_r+1}, \ldots, k_{m_r+m_c}, k_{m_r+m_c+1}, \ldots, k_m). \tag{2.1}$$

This m-tuple specifies the dimensions of the perturbation blocks and determines the set of allowable perturbations:

$$X_{\mathcal{K}} = \{\Delta | \Delta = \text{block diag}(\delta_1^r I_{k_1}, \ldots, \delta_{m_r}^r I_{k_{m_r}}, \delta_1^c I_{k_{m_r+1}}, \ldots, \delta_{m_c}^c I_{k_{m_r+m_c}}, \Delta_1^c, \ldots, \Delta_{m_C}^c) : \\ \delta_i^r \in R, \delta_i^c \in R, \Delta_i^c \in C^{k_{m_r+m_c+i}\times k_{m_r+m_c+i}}\}. \tag{2.2}$$

This block structure is a general form for any combination of repeated real scalars, repeated complex scalars, and full complex blocks. The purely complex case corresponds to $m_r = 0$, and the purely real case to $m_c = m_C = 0$.

The SSV, $\mu_{\mathcal{K}}(M)$ of a matrix $M \in C^{n\times n}$ with respect to a block structure $\mathcal{K}(m_r, m_c, m_C)$, is defined as follows:

$$\mu_{\mathcal{K}}(M) = [\min_{\Delta\in X_{\mathcal{K}}} \bar{\sigma}(\Delta) : \det(I - M\Delta) = 0]^{-1}. \tag{2.3}$$

with $\mu_{\mathcal{K}}(M) = 0$ if $\det(I - M\Delta) \neq 0$ for all $\Delta \in X_{\mathcal{K}}$.

There are two special cases in which the definition of μ can be simplified:

1. Δ is a repeated real scalar block, i.e., $m_r = 1$ and $m_c = m_C = 0$, we have

$$\mu_{\mathcal{K}}(M) = \rho_R(M).$$

where $\rho_R(M) := max\{|\lambda| : \lambda \text{ is a real eigenvalue of } M\}$, with $\rho_R(M) = 0$ if M has no real eigenvalues. Thus μ is the real spectral radius of M.

2. Δ is a full complex block (unstructured uncertainty), i.e., $m_r = m_c = 0$ and $m_C = 1$, we have

$$\mu_{\mathcal{K}}(M) = \overline{\sigma}(M).$$

For a general type of uncertainty $\Delta \in \mathcal{X}_{\mathcal{K}}$, the following holds:

$$\rho_R(M) \leq \mu_{\mathcal{K}}(M) \leq \overline{\sigma}(M). \tag{2.4}$$

So μ can be viewed as a generalization of both the real spectral radius and the maximal singular value.

From the definition of μ in (2.3), it is not obvious how the value of μ may be computed. In fact, the exact calculation of μ is generally very difficult [53]. Equation (2.4) provides lower and upper bounds for μ, however, both bounds are too crude since the gap between them can be arbitrarily large in some cases. In order to reduce the gap, we define the following sets of scaling matrices $Q_{\mathcal{K}}$ and $D_{\mathcal{K}}$:

$$Q_{\mathcal{K}} := \{\Delta \in \mathcal{X}_{\mathcal{K}} : \delta_i^r \in [-1, 1], \delta_i^{c*}\delta_i^c = 1, \Delta_i^{C*}\Delta_i^C = I_{k_{m_r+m_c+i}}\} \tag{2.5}$$

$$D_{\mathcal{K}} := \{\text{block diag}(D_1, \ldots, D_{m_r+m_c}, d_1 I_{k_{m_r+m_c+1}}, \ldots, d_{m_C} I_{k_m}) :$$
$$0 < D_i = D_i^* \in \mathbf{C}^{k_i \times k_i}, 0 < d_i \in \mathbf{R}\} \tag{2.6}$$

then the lower bound and upper bound can be refined as

$$\max_{Q \in Q_{\mathcal{K}}} \rho_R(QM) \leq \mu_{\mathcal{K}}(M) \leq \inf_{D \in D_{\mathcal{K}}} \overline{\sigma}(DMD^{-1}) \tag{2.7}$$

It has been proven in [13] that the first inequality in (2.7) is actually an equality. However, the function $\rho(QM)$ is not convex in $Q \in Q_{\mathcal{K}}$ and therefore it is not guaranteed

that a global maximum can be found. The practical computation uses a power iteration algorithm to find a local maximum and thus obtains a lower bound for μ. On the other hand, the calculation of an upper bound from (2.7) is a convex minimization problem for the maximal singular value, so all local minima are global. Hence, this bound is computationally attractive. In this research, we will use the commercially available MATLAB μ-toolbox to compute μ upper and lower bounds [7].

2.2.2 Linear fractional transformation

Linear fractional transformation (LFT) is an important concept when forming the standard μ analysis framework. It is defined as follows.

Consider a matrix $M \in \mathbf{C}^{n\times n}$ partitioned as

$$M = \begin{bmatrix} M_{11} & M_{12} \\ M_{21} & M_{22} \end{bmatrix} \tag{2.8}$$

with $M_{11} \in \mathbf{C}^{n_1\times n_1}$, $M_{22} \in \mathbf{C}^{n_2\times n_2}$ and $n_1 + n_2 = n$. Suppose we have block structures $\mathcal{X}_{\mathcal{K}_1}$ and $\mathcal{X}_{\mathcal{K}_2}$ defined as follows:

$$\begin{aligned} \mathcal{X}_{\mathcal{K}_1} &= \{\Delta : \Delta \in \mathbf{C}^{n_1\times n_1}\} \\ \mathcal{X}_{\mathcal{K}_2} &= \{\Delta : \Delta \in \mathbf{C}^{n_2\times n_2}\} \end{aligned}$$

then the block structure of $\mathcal{X}_{\mathcal{K}}$ defined as

$$\mathcal{X}_{\mathcal{K}} := \{\Delta = \text{block diag}(\Delta_1, \Delta_2) : \Delta_1 \in \mathcal{X}_{\mathcal{K}_1}, \Delta_2 \in \mathcal{X}_{\mathcal{K}_2}\} \tag{2.9}$$

is compatible with M. Now given any $\Delta_1 \in \mathcal{X}_{\mathcal{K}_1}$, the LFT $F_u(M, \Delta_1)$ is said to be well-posed if and only if there exists a unique solution to the loop equations shown in Figure 2.1, namely

$$\begin{aligned} w &= M_{11}z + M_{12}d \\ e &= M_{21}z + M_{22}d \end{aligned}$$

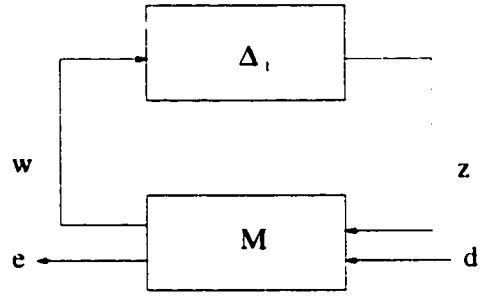

Figure 2.1 Upper LFT

$$z = \Delta_1 w$$

It is easy to see that $F_u(M, \Delta_1)$ is well posed if and only if $(I_{n_1} - M_{11}\Delta_1)$ is invertible. When the LFT is well-posed, it is defined to be an unique mapping from d to ϵ, i.e., the vectors e and d satisfy $\epsilon = F_u(M, \Delta_1)d$ where

$$F_u(M, \Delta_1) := M_{22} + M_{21}\Delta_1(I_{n_1} - M_{11}\Delta_1)^{-1}M_{12} \tag{2.10}$$

Note that in the above derivation we always assume that the feedback is closed around the top inputs and outputs, and hence we obtain an upper LFT (denoted by F_u). We can analogously define lower LFT (denoted by F_l) as

$$F_l(M, \Delta_2) := M_{11} + M_{12}\Delta_2(I_{n_2} - M_{22}\Delta_2)^{-1}M_{21} \tag{2.11}$$

A fundamental property of the LFT is that the interconnections of LFTs are again LFTs. Therefore, the LFT is very flexible in representing both parametric uncertainty and unmodeled dynamics.

2.2.3 Robust stability and the frequency sweep method

The general definition of μ is now extended to the linear system case. Instead of being a constant complex matrix, M is now a transfer function matrix.

The following theorem addresses the robust stability of linear systems and gives rise to the most common usage of μ as a frequency domain robustness test.

Let $\mathcal{M}(X_{\mathcal{K}})$ denote the set of all block diagonal and stable rational transfer functions that have block structures such as $X_{\mathcal{K}}$. And for $\Delta \in \mathcal{M}(X_{\mathcal{K}})$, define $\|\Delta\|_\infty := \sup_\omega \bar{\sigma}\{\Delta(j\omega)\}$.

Theorem(Robust Stability [53]) Suppose $M(s)$ is a nominal stable system(otherwise the problem is trivial), then for all $\Delta \in \mathcal{M}(X_{\mathcal{K}})$ with $\|\Delta\|_\infty < \frac{1}{\beta}$, the perturbed closed-loop system is well posed and internally stable if and only if

$$\sup_{\omega \in R} \mu_{\mathcal{K}}(M(j\omega)) < \beta. \tag{2.12}$$

This theorem means that we can evaluate the robustness properties of a closed-loop system by using a frequency evaluation of μ. For any given frequency point we have a constant matrix μ problem, and the peak value of the frequency μ-plot determines the maximal size of the uncertainty for which the close-loop system can maintain stability.

As mentioned above, the μ-toolbox software does not compute μ exactly, but bounds it from above and below by several optimization steps. Hence, the conclusion can be restated in terms of upper and lower bounds. If we let β_u and β_l be upper and lower bounds of μ respectively, then we can expect the following rules:

- For all uncertainty matrices Δ in $\mathcal{M}(X_{\mathcal{K}})$ satisfying $\|\Delta\|_\infty < \frac{1}{\beta_u}$, the closed-loop system is stable;
- There is a particular uncertainty matrix Δ in $\mathcal{M}(X_{\mathcal{K}})$ satisfying $\|\Delta\|_\infty = \frac{1}{\beta_l}$ that causes instability.

The restatement of the theorem suggests the need to search for $\max_{i=1,\cdots,n} \bar{\mu}_{\mathcal{K}}(M(j\omega_i))$ and $\max_{i=1,\cdots,n} \underline{\mu}_{\mathcal{K}}(M(j\omega_i))$ instead of $\sup_{\omega \in R} \mu_{\mathcal{K}}(M(j\omega))$. This search involves a fairly large amount of computation. In practice one has to decide on the appropriate frequency range and the fineness of the grid. Thus there is possibility of missing important points.

Moreover, in general, μ may be discontinuous so that the use of frequency sweeps may be misleading.

2.2.4 The state space test

The state space test method [11] for the analysis of robust stability can avoid the frequency sweep. The main idea is that a transfer function can be expressed as a linear fractional transformation (LFT) of a constant matrix with respect to the frequency variable, and the frequency variable can then be treated as an uncertainty so that the SSV technique can be applied directly.

Given a transfer function $M(s)$ in the $M-\Delta$ framework, we write it as an upper LFT:

$$M(s) = C(sI_p - A)^{-1}B + D = F_u\left(\begin{bmatrix} A & B \\ C & D \end{bmatrix}, \frac{1}{s}I_p\right) \tag{2.13}$$

where p is the dimension of the state space and (A, B, C, D) is a state space realization of $M(s)$.

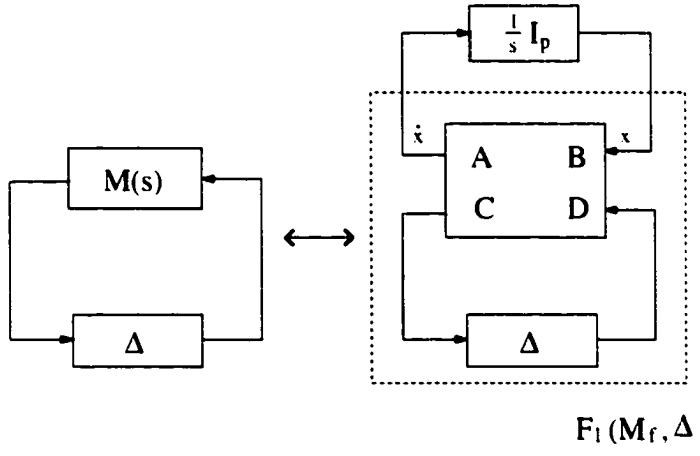

Figure 2.2 Transfer function in state space equation form with LFT.

We denote

$$M_f := \begin{bmatrix} A & B \\ C & D \end{bmatrix}$$

then the state equation for the robust stability problem of $M - \Delta$ can be written as

$$\dot{x} = F_l(M_f, \Delta)x \tag{2.14}$$

where $F_l(M_f, \Delta) = A + B\Delta(I - D\Delta)^{-1}C$. This is illustrated in Figure 2.2.

Next we want to remove the frequency search and include $\frac{1}{s}I_p$ as one of the uncertainties. Since μ usually considers uncertainty inside the unit disk, while $\frac{1}{s}I_p$ covers the right half of the s-plane, we may apply a bilinear transformation to map the right half of the s-plane into the unit disk on the complex plane (see Figure 2.3).

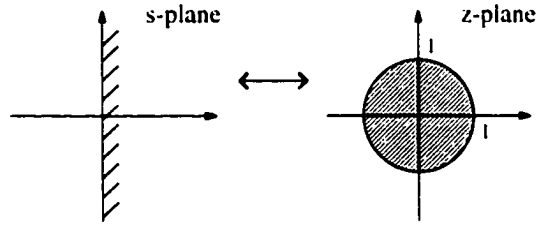

Figure 2.3 Bilinear transformation: the right half of the s-plane to the unit disk in z-plane.

i.e.,

$$s = \frac{1 - z}{1 + z}, z \in \mathbf{C}, |z| \leq 1$$

therefore,

$$\frac{1}{s}I_p = \frac{1 + z}{1 - z}I_p$$

This can be written in an LFT form again

$$\frac{1}{s}I_p = F_u(Q, zI_p) \text{ where } Q := \begin{bmatrix} I_p & 2I_p \\ I_p & I_p \end{bmatrix}$$

Now we can replace $\frac{1}{s}I_p$ with the LFT of this constant matrix Q with respect to the new frequency variable z, as shown in Figure 2.4. The interconnection of Q and M_f in lower and upper LFT can be simplified using Redhaffer's star product [42]. This results in a new connection shown in Figure 2.4.c with matrix T in the following form

$$T = \begin{bmatrix} I_p + 2A(I_p - A)^{-1} & 2(I_p - A)^{-1}B \\ C(I_p - A)^{-1} & D + C(I_p - A)^{-1}B \end{bmatrix}$$

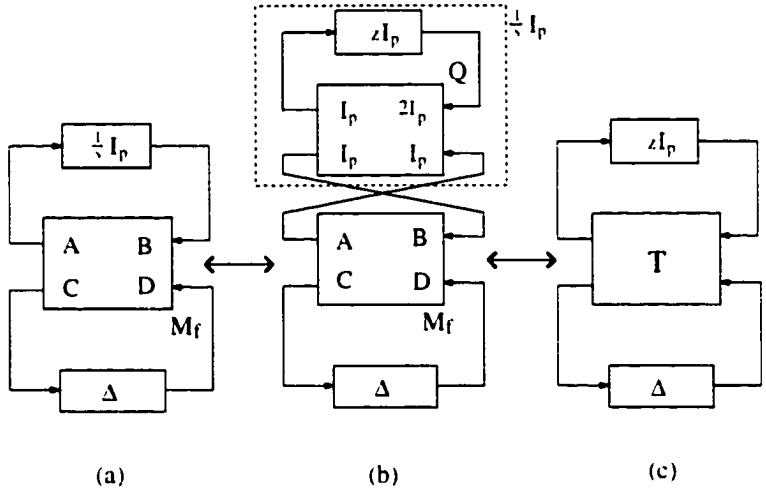

Figure 2.4 Frequency sweep transformed to state space test: A constant μ problem.

From Figure 2.4, we eliminate the frequency sweep by including the frequency variable as one of the uncertainty parameters (a repeated complex scalar block). In this way, we obtain a one-shot μ test involving a constant matrix μ problem. This is formally stated in the following theorem:

Theorem(Robust stability with state space test) [11]

$$\sup_{\omega \in \mathbf{R}} \mu_{\Delta}(M(j\omega)) \leq 1 \quad \textit{if and only if} \quad \mu_{\tilde{\Delta}}(T) \leq 1$$

where $\tilde{\Delta} = \{diag(zI_p, \Delta), z \in \mathbf{C}, |z| \leq 1\}$.

Note that this theorem only tells us whether $\sup_{\omega} \mu_{\Delta}(M(j\omega))$ is less than or equal to 1, which is a direct test for robust stability/instability. In order to compute the value of $\sup_{\omega} \mu_{\Delta}(M(j\omega))$, we need to define:

$$T_{\alpha} = \begin{bmatrix} T_{11} & \frac{1}{\alpha} T_{12} \\ T_{21} & \frac{1}{\alpha} T_{22} \end{bmatrix} \tag{2.15}$$

$$\tilde{\mu}(T) = \inf_{\alpha} \left\{ \alpha \geq 0 : \mu_{\tilde{\Delta}}(T_{\alpha}) \leq 1 \right\} \tag{2.16}$$

Then Theorem 2.2.4 can be restated as:

$$\sup_{\omega \in \mathbf{R}} \mu_{\Delta}(M(j\omega)) = \tilde{\mu}(T) \tag{2.17}$$

Note that the right hand side of (2.16) involves a search over α: thus, we haven't totally eliminated the need to search. Since $\mu_{\tilde{\Delta}}(T_{\alpha})$ is monotonically decreasing as α increases, the binary search can be used for (2.16) which involves only several constant μ calculations.

As mentioned before, the μ-toolbox software computes the lower and upper bounds instead of the exact value of μ. Therefore, we also obtain lower and upper bounds for $\tilde{\mu}(T)$. Since the upper and lower bounds of $\mu_{\tilde{\Delta}}(T_{\alpha})$ may not be always monotonic, a linear search over α is still needed.

2.3 Power System Modeling

In order to perform the robust analysis on the power system, we need to set up the required framework. First, the nominal system model must be obtained. The power system models are described in detail in the following sections. The synchronous generators are represented by a classical model(see chapter 2 of [3]) or two-axis model(see chapter 4 of [3]), with an excitation system represented by ETMSP Type-30 model [26] and power system stabilizer in ETMSP Type-1 model [26]. The network is represented

by steady-state network parameters with a constant impedance load model. By assuming the generator internal reactance to be constant, the network representation can be reduced to generator internal buses. The equations representing the various power system components can be coupled with the reduced network equations through a reference frame transformation. As a result, we obtained a set of coupled differential algebraic equations in the following form:

$$\begin{aligned} \dot{X} &= f(X, Z, u) \\ 0 &= g(X, Z) \end{aligned} \tag{2.18}$$

where X is the vector of state variables governed by the differential equations, and Z is the vector of network variables.

The procedure for obtaining a linearized model of the system given in (2.18) is summarized as follows. A power flow solution is obtained for a given operating condition, specified in terms of real and reactive power load, real power generation schedules at generator buses, and voltage magnitudes at certain buses. This solution provides the voltage magnitudes and angles at all the buses. With the voltage solution and the power injection at each generator bus, initial conditions for the state variables are calculated. The state equations and the network equations are then linearized, and a set of state-space equations representing the power system are obtained in the following form:

$$\begin{aligned} \dot{X}_\Delta &= AX_\Delta + FZ_\Delta \\ GZ_\Delta &= HX_\Delta \end{aligned} \tag{2.19}$$

Where X_Δ is the vector of incremental state variables, Z_Δ is the vector of incremental network variables, and A, F, G, H are coefficient matrices with proper dimensions. Chapter 3 in [51] schematically describes the structure of the coupled equations.

2.3.1 Generator model

In this dissertation, we use two kinds of generator models: the two-axis model and the classical model [3]. We assume that in a power system with n generators, the first m generators are represented by the two-axis model and equipped with exciters and the remaining $n - m$ generators are represented by the classical model.

2.3.1.1 Classical model

The classical model is the simplest model to represent generators without excitation control in a multi-machine system (see Chapter 2 of [3]). It is based on the following assumptions:

1. Mechanical power input is constant.
2. Damping or asynchronous power is negligible.
3. Constant-voltage-behind-transient-reactance model for the synchronous machines is valid.
4. The mechanical rotor angle of a machine coincides with the angle of the voltage behind the transient reactance.

With the loads represented by constant impedance, the load nodes and the terminal voltage nodes of the generators are eliminated. The resulting network contains only the internal generator nodes (numbered from 1 to n). The generator reactance and the constant impedance loads are included in the bus admittance matrix Y_{bus} of the reduced network.

The dynamic equations for the classical model are given by

$$M_i\dot{\omega}_i = P_i - P_{ei} \tag{2.20}$$

$$\dot{\delta}_i = \omega_i - \omega_S \qquad i = m+1, m+2, \ldots, n \tag{2.21}$$

where,

$$P_i = P_{mi} - E_i^2 G_{ii}$$
$$P_{ei} = \sum_{j=1, j\neq i}^{n} [E_i E_j B_{ij} \sin(\delta_i - \delta_j) + E_i E_j G_{ij} \cos(\delta_i - \delta_j)]$$

and

E_i: internal bus voltage of generator i

M_i: inertia constant of generator i

P_{mi}: mechanical power input of generator i

G_{ii}: driving point conductance of node i

$G_{ij} + jB_{ij}$: the transfer admittance between node i and node j in the reduced network

ω_i: rotor speed of generator i(with respect to the synchronous frame)

ω_S: synchronous speed

δ_i: rotor angle of generator i

2.3.1.2 Two-axis model

Generators with excitation control are described by the two-axis model (see chapter 4 of [3]) in this work. The two-axis model accounts for the transient effects and requires the following assumptions.

1. In the stator voltage equations, the variation of flux linkages of d-q axes are negligible compared to the speed voltage terms.

2. $\omega \cong \omega_S = 1$ p.u.

The resultant dynamic equations are given by

$$\tau'_{d0i} \dot{E}'_{qi} = E_{FDi} - E'_{qi} + (x_{di} - x'_{di}) I_{di} \quad (2.22)$$
$$\tau'_{q0i} \dot{E}'_{di} = -E'_{di} - (x_{qi} - x'_{qi}) I_{qi} \quad (2.23)$$
$$M_i \dot{\omega}_i = P_{mi} - (I_{di} E'_{di} + I_{qi} E'_{qi}) + (x'_{qi} - x'_{di}) I_{qi} I_{di} - \frac{D_i}{\omega_S}(\omega_i - \omega_S) \quad (2.24)$$

$$\dot{\delta}_i = \omega_i - \omega_S \qquad i = 1, 2, ..., m \tag{2.25}$$

where,

E'_d, E'_q: direct and quadrature axes stator EMFs corresponding to rotor transient flux components, respectively

I_d, I_q: the d and q axes stator currents

τ'_{d0}, τ'_{q0}: open-circuit direct and quadrature axes transient time constants

x_d, x'_d: direct axis synchronous and transient reactances

x_q, x'_q: quadrature axis synchronous and transient reactances

E_{FD}: stator EMF corresponding to the field voltage

D_i: damping coefficient of generator i.

2.3.1.3 Angle reference

In (2.21) and (2.25), we used the absolute rotor angles (δ_i, $i = 1, 2, ..., n$) as state variables. Since these n state variables are not independent, we can introduce the relative rotor angles as new state variables which are independent. Without loss of generality, δ_1 is chosen as a reference; then, the relative rotor angles are defined as:

$$\delta_{i1} = \delta_i - \delta_1, \qquad i = 2, 3, ..., n$$

The dynamic equations (2.20) — (2.25) remain unchanged with each δ_i replaced by δ_{i1} and ω_S replaced by ω_1. Therefore (2.21) and (2.25) becomes

$$\dot{\delta}_{i1} = \omega_i - \omega_1 \qquad i = 2, 3, ..., n \tag{2.26}$$

2.3.2 Excitation system model

The type of excitation system used is ETMSP Type-30 [26] (same as IEEE AC-4, see [16]), as shown in Figure 2.5.

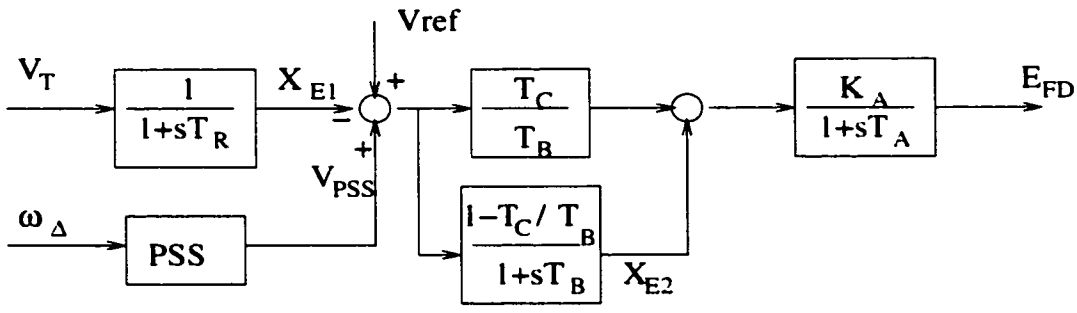

Figure 2.5 Excitation system model: ETMSP Type-30.

The state variables are E_{FD}, X_{E1}, and X_{E2}, and the dynamic equations are given by

$$\dot{E}_{FDi} = \frac{K_{Ai}}{T_{Ai}} X_{E2i} - \frac{1}{T_{Ai}} E_{FDi} + \frac{aK_{Ai}}{T_{Ai}} (V_{REFi} + V_{PSSi} - X_{E1i}) \tag{2.27}$$

$$\dot{X}_{E1i} = -\frac{1}{T_{Ri}} X_{E1i} + \frac{1}{T_{Ri}} V_{Ti} \tag{2.28}$$

$$\dot{X}_{E2i} = -\frac{1}{T_{Bi}} X_{E2i} + \frac{1-a}{T_{Bi}} (V_{REFi} + V_{PSSi} - X_{E1i}) \tag{2.29}$$

$$\begin{aligned} V_T &= V_{Tq} + jV_{Td} \\ &= (E'_q + x'_d I_d) + j(E'_d - x'_q I_q) \qquad i = 1, 2, \ldots, m \end{aligned} \tag{2.30}$$

where,

V_T: generator terminal voltage

V_{REF}: exciter reference voltage

V_{PSS}: power system stabilizer voltage

$a = T_{Ci}/T_{Bi}$, T_{Bi} and T_{Ci} are time constants

2.3.3 Power system stabilizer model

A power system stabilizer is used to add a modulation signal to a generator's voltage reference input. The idea is to produce an electric torque at the generator proportional to speed. Since there is a phase lag between the voltage signal and the electric torque, PSS usually uses a simple phase lead compensator to adjust the input signal to give it the correct phase. Figure 2.6 shows the action of the PSS.

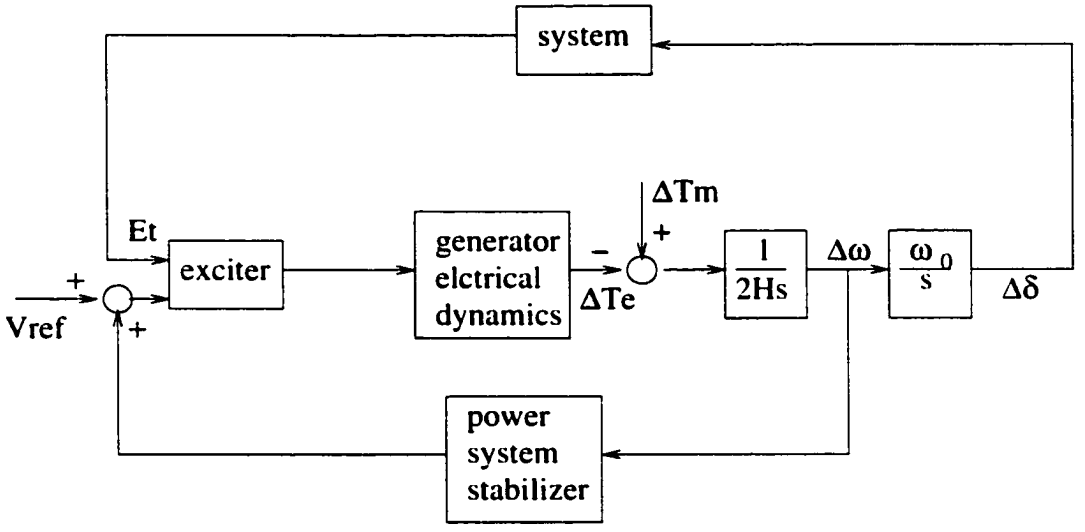

Figure 2.6 Block diagram showing stabilizer action.

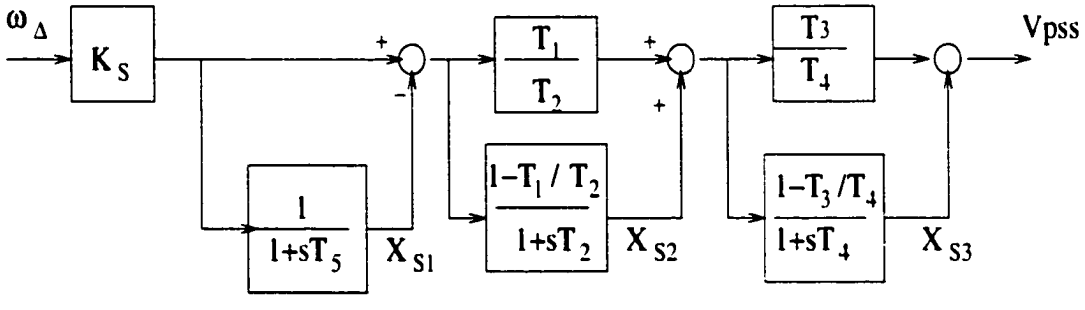

Figure 2.7 Power system stabilizer model.

When we performed the robustness analysis, we chose a conventionally designed PSS as our controller. Its block diagram is shown in Figure 2.7. The state variables are X_{S1}, X_{S2} and X_{S3}. The equations for these variables are as follows:

$$\dot{X}_{S1i} = -\frac{1}{T_{5i}}X_{S1i} + \frac{1}{T_{5i}}K_{Si}\omega_{\Delta i} \tag{2.31}$$

$$\dot{X}_{S2i} = -\frac{1}{T_{2i}}X_{S2i} + \frac{1}{T_{2i}}(1 - \frac{T_{1i}}{T_{2i}})[K_{Si}\omega_{\Delta i} - X_{S1i}] \tag{2.32}$$

$$\dot{X}_{S3i} = -\frac{1}{T_{4i}}X_{S3i} + \frac{1}{T_{4i}}(1 - \frac{T_{3i}}{T_{4i}})[X_{S2i} + \frac{T_{1i}}{T_{2i}}(K_{Si}\omega_{\Delta i} - X_{S1i})] \tag{2.33}$$

$$V_{PSSi} = -\frac{T_{1i}T_{3i}}{T_{2i}T_{4i}}X_{S1i} + \frac{T_{3i}}{T_{4i}}X_{S2i} + X_{S3i} + \frac{T_{1i}T_{3i}}{T_{2i}T_{4i}}K_{Si}\omega_{\Delta i} \tag{2.34}$$

where $\omega_{\Delta i} = \frac{\omega_i}{\omega_S} - 1$. When doing linearization of the above equations, $\Delta\omega_{\Delta i} = \frac{\partial\omega_{\Delta i}}{\partial\omega i}\Delta\omega_i = \frac{1}{\omega_S}\Delta\omega_i$

2.3.4 Network modeling

Constant impedance loads are used. By eliminating all the load nodes, the network is reduced to contain only the generator internal buses. The bus admittance matrix Y_{bus} consists of diagonal elements $Y_{ii}\angle\theta_{ij} = G_{ii} + jB_{ii}$, $Y_{ij}\angle\theta_{ij} = G_{ij} + jB_{ij}$. Based on a procedure given in Chapter 9 of [3] the generator currents are given in the following form:

$$I_{qi} = \sum_{j=1}^{m}[F_{G+B}(\delta_{ij})E'_{qj} - F_{B-G}(\delta_{ij})E'_{dj}] + \sum_{k=m+1}^{n}F_{G+B}(\delta_{ik})E_k \tag{2.35}$$

$$I_{di} = \sum_{j=1}^{m}[F_{B-G}(\delta_{ij})E'_{qj} + F_{G+B}(\delta_{ij})E'_{dj}] + \sum_{k=m+1}^{n}F_{B-G}(\delta_{ik})E_k \tag{2.36}$$

$$I_k = \sum_{j=1}^{m}[F_{G+B}(\delta_{kj})E'_{qj} - F_{B-G}(\delta_{kj})E'_{dj}] + \sum_{l=m+1}^{n}F_{G+B}(\delta_{kl})E_l \tag{2.37}$$

$$i = 1, 2, \ldots, m \qquad k, l = m+1, \ldots, n$$

where

$$F_{G+B}(\delta_{ij}) = G_{ij}\cos(\delta_{ij}) + B_{ij}\sin(\delta_{ij}) \tag{2.38}$$

$$F_{B-G}(\delta_{ij}) = B_{ij}\cos(\delta_{ij}) - G_{ij}\sin(\delta_{ij}) \tag{2.39}$$

$$\delta_{ij} = \delta_i - \delta_j \tag{2.40}$$

2.3.5 Overall system equation

The dynamic equations governing the generators, exciters, and the PSS have the following general form:

$$\dot{X} = f(X, Z, u) \tag{2.41}$$

where,

$X^T = [X_{SM}^T, X_{ES}^T, X_{PSS}^T]$, the vector of state variables

$X_{SM} = [E'_{q(1-m)}, E'_{d(1-m)}, \omega_{(1-n)}, \delta_{(2-n)1}]^T$

$X_{ES} = [E_{FD(1-m)}, X_{E1(1-m)}, X_{E2(1-m)}]^T$

$X_{PSS} = [X_{S1(1-m)}, X_{S2(1-m)}, X_{S3(1-m)}]^T$

$Z = [I_{q(1-m)}, I_{d(1-m)}, I_{[(m+1)-n]}, V_{T(1-n)}]^T$, the vector of network variables

$u = [V_{REF(1-m)}]^T$, the vector of control inputs

and **f** is the vector of nonlinear functions summarized below:

$$f_{1i} = \dot{E}'_{qi} \qquad i = 1, \ldots, m$$

$$= \frac{1}{\tau'_{d0i}}[E_{FDi} - E'_{qi} + (x_{di} - x'_{di})I_{di}] \tag{2.42}$$

$$f_{2i} = \dot{E}'_{di} \qquad i = 1, \ldots, m$$

$$= \frac{1}{\tau'_{q0i}}[-E'_{di} - (x_{qi} - x'_{qi})I_{qi}] \tag{2.43}$$

$$f_{3i} = \dot{\omega}_i \qquad i = 1, \ldots, n$$

$$= \frac{1}{M_i}[P_{mi} - (I_{di}E'_{di} + I_{qi}E'_{qi}) + (x'_{qi} - x'_{di})I_{qi}I_{di} - \frac{D_i}{\omega_S}(\omega_i - \omega_S)] \tag{2.44}$$

$$f_{4i} = \dot{\delta}_{i1} \qquad i = 2, \ldots, n$$

$$= \omega_i - \omega_1 \tag{2.45}$$

$$f_{5i} = \dot{E}_{FDi} \qquad i = 1, \ldots, m$$

$$= \frac{K_{Ai}}{T_{Ai}}X_{E2i} - \frac{1}{T_{Ai}}E_{FDi} + \frac{aK_{Ai}}{T_{Ai}}(V_{REFi} + V_{PSSi} - X_{E1i}) \tag{2.46}$$

$$
\begin{aligned}
f_{6i} &= \dot{X}_{E1i} \qquad i = 1, \ldots, m \\
&= -\frac{1}{T_{Ri}} X_{E1i} + \frac{1}{T_{Ri}} V_{Ti} \qquad (2.47) \\
f_{7i} &= \dot{X}_{E2i} \qquad i = 1, \ldots, m \\
&= -\frac{1}{T_{Bi}} X_{E2i} + \frac{1-a}{T_{Bi}} (V_{REFi} + V_{PSSi} - X_{E1i}) \qquad (2.48) \\
f_{8i} &= \dot{X}_{S1i} \qquad i = 1, \ldots, m \\
&= -\frac{1}{T_{5i}} X_{S1i} + \frac{1}{T_{5i}} \frac{K_{Si}}{\omega_S} \Delta\omega_i \qquad (2.49) \\
f_{9i} &= \dot{X}_{S2i} \qquad i = 1, \ldots, m \\
&= -\frac{1}{T_{2i}} X_{S2i} + \frac{1}{T_{2i}} (1 - \frac{T_{1i}}{T_{2i}}) [\frac{K_{Si}}{\omega_S} \Delta\omega_i - X_{S1i}] \qquad (2.50) \\
f_{10i} &= \dot{X}_{S3i} \qquad i = 1, \ldots, m \\
&= -\frac{1}{T_{4i}} X_{S3i} + \frac{1}{T_{4i}} (1 - \frac{T_{3i}}{T_{4i}}) [X_{S2i} + \frac{T_{1i}}{T_{2i}} (\frac{K_{Si}}{\omega_S} \Delta\omega_i - X_{S1i})] \qquad (2.51)
\end{aligned}
$$

Note that we use (2.44) to model generators in the two-axis model as well as in the classical model. This is true because the classical model can be viewed as a special case of the two-axis model with $E'_q = E$, $E'_d = 0$, $I_q = I$, and $I_d = 0$.

Linearization of (2.41) leads to

$$\Delta\dot{X} = \frac{\partial f}{\partial X} \Delta X + \frac{\partial f}{\partial Z} \Delta Z + \frac{\partial f}{\partial u} \Delta u \qquad (2.52)$$

We also have the network algebraic equation

$$0 = g(X, Z) \qquad (2.53)$$

This equation is linearized and organized so that all the terms related to the algebraic variables are put at one side of the equation and those related to the state variables are on the other side of the equation.

We obtain the representation of the whole system in the state space form as

$$
\begin{aligned}
\Delta\dot{X} &= A\Delta X + F\Delta Z + B\Delta u \qquad (2.54) \\
G\Delta Z &= H\Delta X \qquad (2.55)
\end{aligned}
$$

where

$$A = \frac{\partial f}{\partial X}, F = \frac{\partial f}{\partial Z}, B = \frac{\partial f}{\partial u} \tag{2.56}$$

The procedure to obtain G, H and the detailed expressions for the elements of all the coefficient matrices are given in Appendix 4.2.

2.4 Uncertainty Characterization

2.4.1 Capture the uncertainties in the linearized model

As mentioned in Chapter 2.1, we will use the state-space representation to capture the parameter uncertainties in the system matrices.

In [32], the parameter uncertainties in the system equations were characterized in the differential equations which were obtained after representing all the network variables by the state variables. A more natural way of characterizing the uncertainties was investigated in this dissertation, where the uncertainties in the algebraic equations and differential equations were considered separately.

In this research, the uncertainties considered were different operating conditions in the power system, which are represented by parameter variation, such as tie-line power flow, total generation of certain areas, etc. When the operating condition changes, some elements of the coefficient matrices of the dynamic equation (2.19) also change. Our study shows that the dependence of such a change on the parameter variation can be approximated by a low order polynomial. Results show that linear approximation achieves very good accuracy, compared to quadratic approximations in [32].

Next, we cast our problem as a robust stability problem in the canonical $M - \Delta$ framework to apply the SSV method. The range of the operating parameters within which the system can remain stable is determined. For simplicity, we only took one operating parameter p varying within the known interval $[p^{min}, p^{max}]$ (two or more varying parameters can be treated in a similar way). Those coefficients of the matrices in the

dynamic equation (2.19) which depend on p will change with the change of operating conditions. Consider the entries of the A-matrices as an example. Each element of the A-matrix in (2.19) that depends on the parameter can be expressed as follows:

$$a_{ij} = a'_{ij0} + a'_{ij1}p \tag{2.57}$$

It is desirable to normalize the range of uncertain parameter to the interval [-1,1]. Let

$$p = \frac{p^{max} + p^{min}}{2} + \frac{p^{max} - p^{min}}{2}\delta \tag{2.58}$$

where $-1 \leq \delta \leq 1$. Note that as δ varies within the interval $[-1, 1]$, p will vary within the interval $[p^{min}, p^{max}]$. Thus the variation in p is captured by the variation in δ. When substituting (2.58) into (2.57), we get a_{ij} as a polynomial of δ:

Then (2.57) can be rewritten as:

$$a_{ij} = a_{ij0} + a_{ij1}\delta \tag{2.59}$$

where δ takes the values in the interval [-1,1], and where a_{ijk} depends on a'_{ijk}, p^{min}, and p^{max}.

Based on the above representation, it is possible to write the system equations with one perturbed real parameter as follows:

$$\begin{aligned} \dot{X} &= (A_0 + \delta A_1)X + (F_0 + \delta F_1)Z \\ (G_0 + \delta G_1)Z &= (H_0 + \delta H_1)X \end{aligned} \tag{2.60}$$

where $\delta \in [-1, +1]$: $A_0 = [a_{ij0}]$ is the matrix of the constant part in equation (2.57), and $A_1 = [a_{ij1}]$ is the matrix of the coefficients of the first order part in equation (2.57): F_0, G_0, H_0 are matrices of the constant parts after linear curve fitting for F, G, H respectively while F_1, G_1 and H_1 are the respective first order part. Note that we omitted the subscript Δ, and all the variables here are the incremental variables actually.

Since G_0 is invertible(see expression for G_0 in appendix 4.2), we can rewrite the above equations as follows:

$$\begin{aligned}\begin{bmatrix} \dot{X} \\ Z \end{bmatrix} &= \begin{bmatrix} A_0 & F_0 \\ G_0^{-1}H_0 & 0 \end{bmatrix}\begin{bmatrix} X \\ Z \end{bmatrix} + \delta \begin{bmatrix} A_1 & F_1 \\ G_0^{-1}H_1 & -G_0^{-1}G_1 \end{bmatrix}\begin{bmatrix} X \\ Z \end{bmatrix} \\ &= P\begin{bmatrix} X \\ Z \end{bmatrix} + \delta R \begin{bmatrix} X \\ Z \end{bmatrix} \end{aligned} \tag{2.61}$$

where the matrices P and R are defined by

$$P = \begin{bmatrix} A_0 & F_0 \\ G_0^{-1}H_0 & 0 \end{bmatrix} \tag{2.62}$$

$$R = \begin{bmatrix} A_1 & F_1 \\ G_0^{-1}H_1 & -G_0^{-1}G_1 \end{bmatrix} \tag{2.63}$$

Singular Value Decomposition (SVD) is then used to reduce the order of the system. By using SVD factorization for R, we have

$$R = U\Sigma V^H.$$

The matrix Σ is diagonal, with the singular values in decreasing order on the diagonal. The matrices U and V are unitary matrices and the superscript H denotes the hermitian conjugate, which equals the normal transpose in the case of real matrices. The matrix R has precisely $r = rank(R)$ number of singular values that are separated from zero. If we partition the matrix U and V according to the non-zero singular values, we get

$$R = [U_1\ U_2]\begin{bmatrix} \Sigma_r & 0 \\ 0 & 0 \end{bmatrix}[V_1\ V_2]^H = U_1\Sigma_r V_1^H.$$

Now we let $R_1 = U_1$ and $R_2 = \Sigma_r V_1^H$. This allows us the possibility of reducing the order of the system.

To extract the uncertainty δ, we define the vectors v and w as

$$v = R_2 \begin{bmatrix} X \\ Z \end{bmatrix} \tag{2.64}$$

$$w = \delta v \tag{2.65}$$

We see that because of the factorization the size of the vectors v and w will be exactly $r = rank(R)$. If R is of low rank, then the order of the uncertainty block will be reduced significantly. Now,

$$\begin{bmatrix} \dot{X} \\ Z \end{bmatrix} = P \begin{bmatrix} X \\ Z \end{bmatrix} + R_1 \delta v = P \begin{bmatrix} X \\ Z \end{bmatrix} + R_1 w = P \begin{bmatrix} X \\ Z \end{bmatrix} + R_1 \begin{bmatrix} w_{\dot{X}} \\ w_Z \end{bmatrix} \tag{2.66}$$

Let us add v to the outputs and w to the inputs; hence,

$$\begin{bmatrix} v \\ \begin{bmatrix} \dot{X} \\ Z \end{bmatrix} \end{bmatrix} = \begin{bmatrix} 0 & R_2 \\ R_1 & P \end{bmatrix} \begin{bmatrix} w \\ \begin{bmatrix} X \\ Z \end{bmatrix} \end{bmatrix} \tag{2.67}$$

Partition R_1, R_2, P, let:

$$R_2 = \begin{bmatrix} R_{2.X} & R_{2.Z} \end{bmatrix} \tag{2.68}$$

$$R_1 = \begin{bmatrix} R_{1.\dot{X}} \\ R_{1.Z} \end{bmatrix} \tag{2.69}$$

$$P = \begin{bmatrix} P_{\dot{X}.X} & P_{\dot{X}.Z} \\ P_{Z.X} & P_{Z.Z} \end{bmatrix} \tag{2.70}$$

Then,

$$\begin{bmatrix} v \\ \begin{bmatrix} \dot{X} \\ Z \end{bmatrix} \end{bmatrix} = \begin{bmatrix} 0 & R_{2.X} & R_{2.Z} \\ R_{1.\dot{X}} & P_{\dot{X}.X} & P_{\dot{X}.Z} \\ R_{1.Z} & P_{Z.X} & P_{Z.Z} \end{bmatrix} \begin{bmatrix} w \\ \begin{bmatrix} X \\ Z \end{bmatrix} \end{bmatrix} \tag{2.71}$$

Rearranging the input and output, we get

$$\begin{bmatrix} Z \\ \begin{bmatrix} \dot{X} \\ v \end{bmatrix} \end{bmatrix} = \begin{bmatrix} P_{Z,Z} & P_{Z,X} & R_{1,Z} \\ P_{\dot{X},Z} & P_{\dot{X},X} & R_{1,\dot{X}} \\ R_{2,Z} & R_{2,X} & 0 \end{bmatrix} \begin{bmatrix} Z \\ \begin{bmatrix} X \\ \omega \end{bmatrix} \end{bmatrix} \tag{2.72}$$

Taking Z as an internal signal.

$$\begin{bmatrix} \dot{X} \\ v \end{bmatrix} = \Gamma \begin{bmatrix} X \\ \omega \end{bmatrix} \tag{2.73}$$

where

$$\Gamma = \begin{bmatrix} P_{\dot{X},X} & R_{1,\dot{X}} \\ R_{2,X} & 0 \end{bmatrix} + \begin{bmatrix} P_{\dot{X},Z} \\ R_{2,Z} \end{bmatrix} (I - P_{Z,Z})^{-1} \begin{bmatrix} P_{Z,X} & R_{1,Z} \end{bmatrix} \tag{2.74}$$

This process of "pulling out" and isolating the uncertainty to get the resulting interconnection of known system components and uncertain parameters is redrawn in Figure 2.8, where M is a known dynamic system, and Δ is a diagonal(structured) perturbation which accounts for the uncertainty.

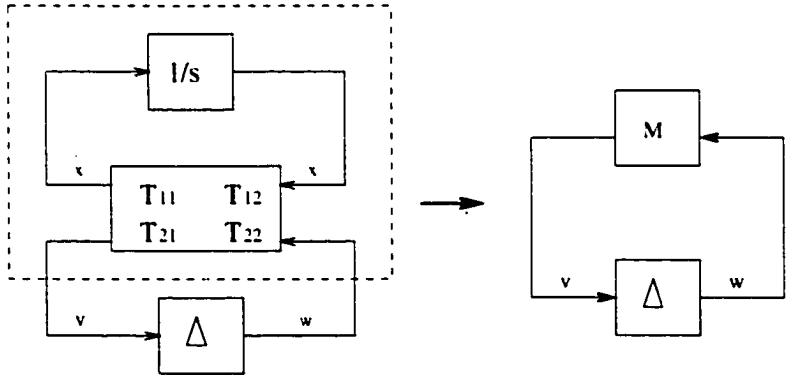

Figure 2.8 Robust stability analysis framework.

2.4.2 Numerical results for the uncertainty characterization

The robustness analysis approach was first applied to a four-machine, two-area sample system, as shown in Figure 2.9. This system was specially designed by Ontario Hydro to study the fundamental nature of inter-area oscillations [27].

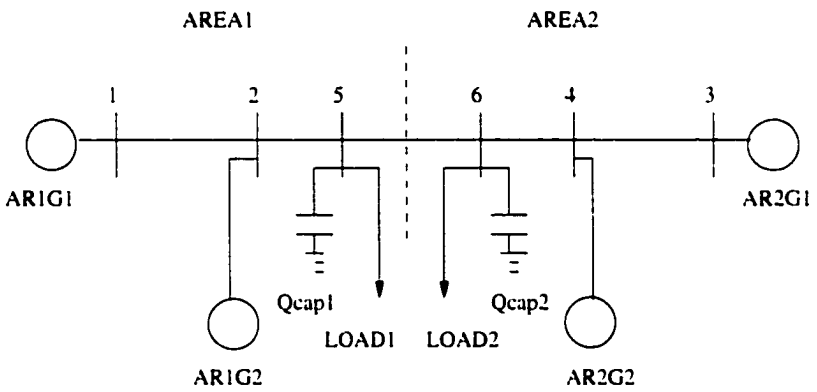

Figure 2.9 Four-machine two-area test system.

For the 4-machine, 2-area test system, the exporting power from Area1 was chosen as the uncertainty, which was allowed to vary in the range $[0 - 400]MW$. The Load 1 was varied in the range $[1140 - 1540]MW$ while Load 2 was varied in the range $[1400 - 1800]MW$.

The results are shown in Table 2.1 under symbol "DAE". The estimated exporting power was obtained from performing the eigenvalue test, by increasing the varying parameter(power export) to find the "critical" system eigenvalues. As a comparison, the robustness analysis results using the lumped differential equation(under symbol "DE") to capture uncertainties [32] are also listed. The time cost was for 50 points of μ calculation in the frequency sweep.

From Table 2.1 we see that using linear approximation in the proposed approach for uncertainty characterization can achieve accuracy comparable with that achieved by using quadratic approximation in the "DE" method. In addition, the computation time

Table 2.1 Robust Analysis Results for 4-machine System

	DAE	DE
μ upper bound	1.4913	1.4550
Estimated P_{exp}(MW)	334.1	337.5
Exact exporting power(MW)	344.5	344.5
Error(%)	3.02	2.04
size of Δ	14	22
Time cost(s)	59.15	100.19

for the former procedure is much less than that of the latter.

Another test was performed on a fifty-machine system [50]. This is a moderate sized system which includes all the modeling features and the complexity of large scale power systems. A one-line diagram of the area of interest is shown in Figure 2.10.

This test system contains 44 generators represented by the classical model with uniform damping and 6 generators represented by a two-axis model. All classical modeled machines have uniform damping $D_i/M_i = 0.1$ except machines at buses #137 and #140 which have $D_i/M_i = 0.5$. The base case power flow was characterized by setting the generation at Bus #93 and #110 to be 1250MW. This generation was treated as uncertain and was allowed to vary in the range [2*1150-2*1350]MW.

By performing an eigenvalue test, the exact critical generation was obtained as: 1320.5MW. The robust analysis results using the differential algebraic model with the changing elements in A matrix represented by linear approximation are shown in Table 2.2. The time cost is for 20 points of μ calculation for the frequency sweep.

Note that the peak of μ-plot in both cases was larger than 1.0, so the robust stability was not achieved within the given operating range. In both cases, the estimated stability limits agreed with the exact stability limits. Therefore, we can conclude that the proposed method provides a precise tool for the evaluation of power system robust stability.

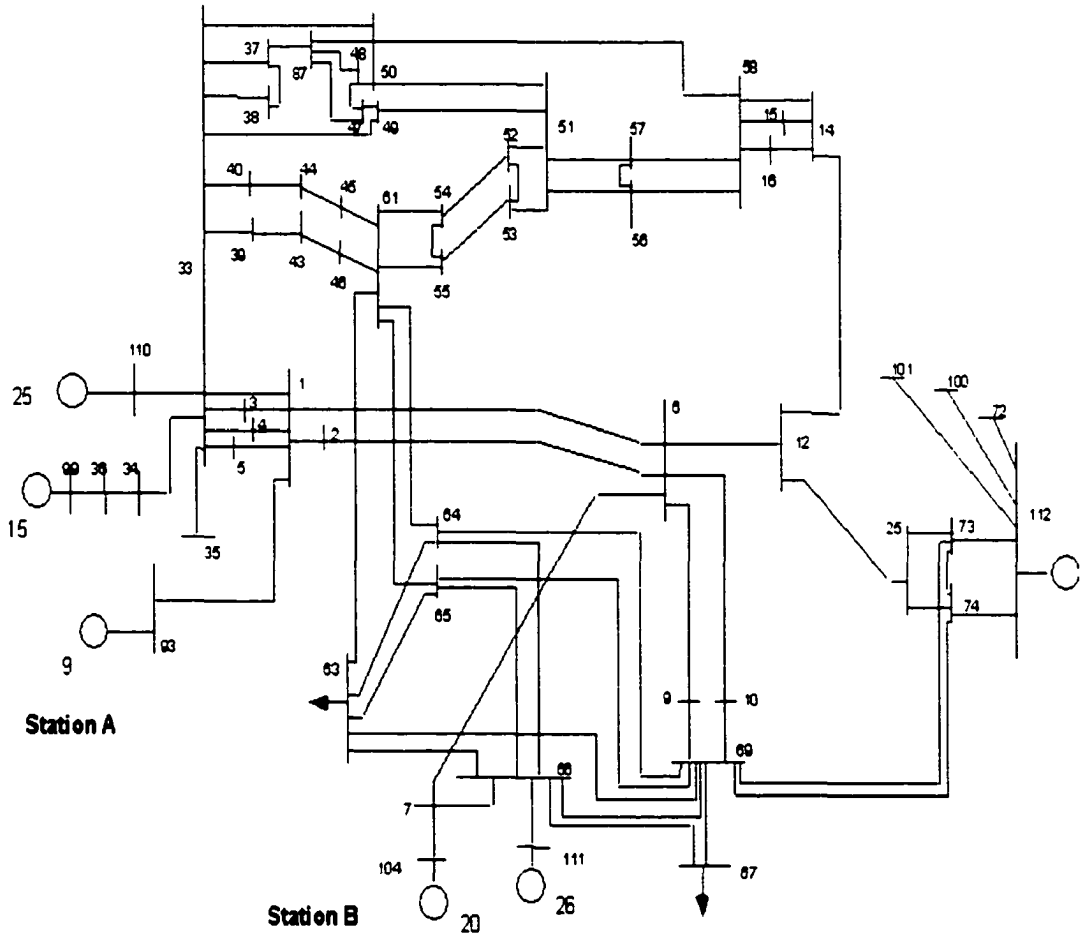

Figure 2.10 IEEE 50-generator system: a one-line diagram of the study area.

Table 2.2 Robust Analysis Results for 50-machine System

	DAE	DE
Peak of μ upper bound	1.4217	1.4436
Frequency for this peak(rad/s)	1.8299	1.8307
Estimated critical generation(MW)	1320.3	1319.3
Exact critical generation(MW)	1320.5	1320.5
Error(%)	1.5×10^{-4}	9.1×10^{-4}
Size of Δ	112	122
Time cost(s)	862.48	878.09

2.5 Robustness Analysis

2.5.1 The real spectral radius

Looking at the definition of μ in (2.3), it is not difficult to see that μ for a single repeated real scalar block reduces to the real spectral radius, i.e., when $m_r = 1, m_c = m_C = 0$, $\mu_{\mathcal{K}}(M) = \rho_R(M)$, where the real spectral radius is defined as [53]

$$\rho_R(M) := max\{|\lambda| : \lambda \text{ is a real eigenvalue of } M\},$$

with $\rho_R(M) = 0$ if M has no real eigenvalues.

Proof: Suppose $\Delta = \delta I$, where $\delta \in \mathbf{R}$.

$$\begin{aligned}
\mu_{\Delta}(M) &= [\min_{\Delta \in \mathcal{X}_{\mathcal{K}}} \{\bar{\sigma}(\Delta) : \det(I - M\Delta) = 0\}]^{-1} \\
&= [\min_{\delta \in \mathbf{R}} \{\delta : \det(I - M(\delta I)) = 0\}]^{-1} \\
&= [\min_{\delta \in \mathbf{R}} \{\delta : \delta[\det(\frac{1}{\delta} I - M)] = 0\}]^{-1} \\
&= \rho_R(M)
\end{aligned}$$

Thus, μ is the real spectral radius of M in such a special case. This provides a fast procedure to obtain exact μ since the μ calculation is reduced to a single eigenvalue computation at each frequency.

The application of this property is restricted due to lack of numerical stability. For a complex matrix M, even if it does have some real eigenvalue, a small perturbation of

its elements will cause the disappearance of the real eigenvalue. The simulation results show that we never found a real eigenvalue for the matrix $M(j\omega)$.

However, some complex eigenvalues of $M(j\omega)$ have a relatively small imaginary part, which can be ignored when compared to its real part. These eigenvalues can be approximated as real eigenvalues. Among them, we find the one which has the largest real part and take this real part as $\rho_R(M)$. This gives an approximation of μ, and the result is very close to what we get from the frequency sweep.

To obtain the peak value of μ over the frequency, we still need the frequency sweep, and the possibility of ignoring important frequency points still exists.

2.5.2 Bounded frequency test

In light of the state space test, an alternative solution is proposed [43] to transform a classical frequency dependent μ analysis problem into a bounded frequency test problem, in which the frequency ω is introduced as an additional uncertainty. Unlike the state space test, which treats the frequency variables over the whole frequency space (complex variables over the whole right half plane) as uncertainties, this test could obtain μ over a specified frequency range while the frequency is treated as a real scalar parameter.

Consider the interconnection structure $M(s)-\Delta$, where Δ is the structured perturbation. We would like to compute without frequency gridding: $\mu_{max} = \max_{\omega\in[\omega_{min},\omega_{max}]} \mu_K(M(j\omega))$

In order to do this, we need to derive an LFT model for the dynamic system $M(j\omega)$, in which the frequency is viewed as a real scalar parameter. Let (A, B, C, D) be the state-space model of the transfer function matrix $M(s)$. For a given positive ω, the matrix H satisfying $M(j\omega) = \mathcal{F}_u(H, \omega I)$ is given as follows:

$$H = \begin{bmatrix} jA^{-1} & A^{-1}B \\ -jCA^{-1} & -CA^{-1}B + D \end{bmatrix}. \tag{2.75}$$

This can be verified by the definition of the upper LFT as follows.

Proof: Let

$$H = \begin{bmatrix} jA^{-1} & A^{-1}B \\ -jCA^{-1} & -CA^{-1}B + D \end{bmatrix} = \begin{bmatrix} H_{11} & H_{12} \\ H_{21} & H_{22} \end{bmatrix} \tag{2.76}$$

where $H_{11} = jA^{-1}$, $H_{12} = A^{-1}B$, $H_{21} = -jCA^{-1}$, $H_{22} = -CA^{-1}B + D$.

By definition,

$$\begin{aligned} & \mathcal{F}_u(H, \omega I) \\ = \; & H_{22} + H_{21}(\omega I)(I - H_{11}\omega I)^{-1}H_{12} \\ = \; & -CA^{-1}B + D + (-jCA^{-1})(\omega I)(I - jA^{-1}\omega)^{-1}A^{-1}B \\ = \; & D - C[A^{-1} + A^{-1}(j\omega I)(I - A^{-1}(j\omega I))^{-1}A^{-1}]B \end{aligned}$$

Use the fact [57] that for any matrix E,

$$(E_{11} - E_{12}E_{22}^{-1}E_{21})^{-1} = E_{11}^{-1} + E_{11}^{-1}E_{12}(E_{22} - E_{21}E_{11}^{-1}E_{12})^{-1}E_{21}E_{11}^{-1}$$

$$\Rightarrow A^{-1} + A^{-1}(j\omega I)(I - A^{-1}(j\omega I))^{-1}A^{-1} = (A - j\omega I)^{-1}$$

Then the above equation can be simplified as

$$\begin{aligned} & \mathcal{F}_u(H, \omega I) \\ = \; & D - C[A^{-1} + A^{-1}(j\omega I)(I - A^{-1}(j\omega I))^{-1}A^{-1}]B \\ = \; & D - C(A - j\omega I)^{-1}B \\ = \; & D + C(j\omega I - A)^{-1}B \\ = \; & M(j\omega) \end{aligned}$$

To normalize the frequency uncertainty, let

$$\omega = \omega_0 + \omega_1 \times \delta\omega,$$

where

$$\omega_0 = (\omega_{max} + \omega_{min})/2, \omega_1 = (\omega_{max} - \omega_{min})/2$$

we have

$$\begin{aligned} M(j\omega) &= D + C(j\omega I - A)^{-1}B \\ &= D + C[j(\omega_0 + \omega_1\delta\omega)I - A]^{-1}B \\ &= D + C[j(\omega_1\delta\omega)I - (A - j\omega_0 I)]^{-1}B \end{aligned}$$

Let

$$A' = A - j\omega_0 I,\ H(\omega_0) = \begin{bmatrix} jA'^{-1} & A'^{-1}B \\ -jCA'^{-1} & -CA'^{-1}B + D \end{bmatrix}$$

then

$$M(j\omega) = \mathcal{F}_u(H(\omega_0), (\omega_1\delta\omega)I)$$

Absorb ω_1 into H and let

$$H_1(\omega_0) = \begin{bmatrix} jA'^{-1}\omega_1 & A'^{-1}B \\ -jCA'^{-1}\omega_1 & -CA'^{-1}B + D \end{bmatrix}$$

We get the normalized perturbation blocks $\bar{\Delta}$ as: $\bar{\Delta} = \begin{bmatrix} \delta\omega I & 0 \\ 0 & \Delta \end{bmatrix}$. This process is shown in Figure 2.11.

Theorem([43]) With the notation introduced before.

$$\mu_{\max} = \max_{\omega\in[\omega_{\min},\omega_{\max}]} \mu_{\Delta}(M(j\omega)) \leq 1 \text{ iff } \mu_{\bar{\Delta}}(H_1) \leq 1 \tag{2.77}$$

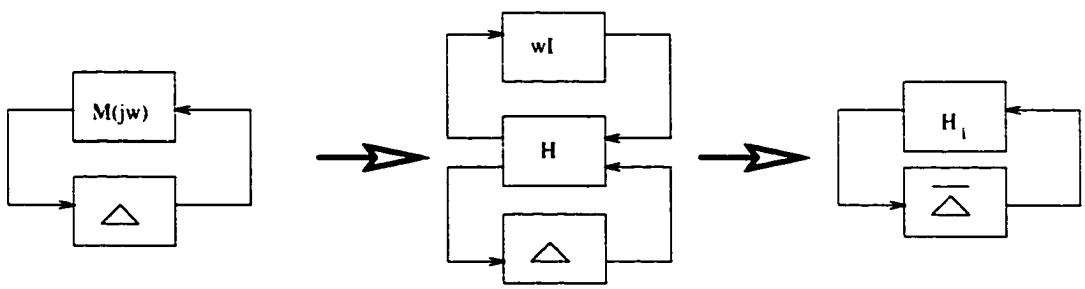

Figure 2.11 Form the bounded frequency test.

This theorem provides a reliable way to check robust stability in the sense that the potential problems with frequency discontinuities are avoided. Now we can solve the robustness analysis problem on the $H_1(\omega_0) - \tilde{\Delta}$ framework. In doing so, this bounded frequency test reduces our problem to a single constant μ problem with purely real uncertainties, thereby arriving at a very fast solution of the original problem.

Next, we need to perform a similar α searching process as in a state space test to find the maximum uncertainty size before instability occurs. The introduction of α factor is related to the concept of "skewed-μ" [42]. Skewed-μ is used when we need to check how large a particular source of uncertainty can be before the system loses stability while keeping other blocks fixed. If we have two uncertainties, say $\Delta = diag\{\Delta_1, \Delta_2\}$, and assume we have fixed $||\Delta_1|| \leq 1$, and we want to find how large Δ_2 can be before we get instability, the solution is to shrink Δ_2 by a factor of α and then find the smallest value of α which makes $\mu_{\tilde{\Delta}}(H_1) \leq 1$, where $\tilde{\Delta} = diag\{\Delta_1, \frac{1}{\alpha}\Delta_2\}$ The above idea can be restated as follows:

Theorem

$$\max_{\omega} \mu_{\Delta}(M(j\omega)) \quad = \quad \inf_{\alpha}\{\alpha | \mu_{\tilde{\Delta}}(H_1') \leq 1\} \text{ with } H_1' = \begin{bmatrix} H_{11_1} & \frac{1}{\alpha}H_{12} \\ H_{21} & \frac{1}{\alpha}H_{22} \end{bmatrix} \qquad (2.78)$$

Note that in this theorem, the shrinking factor α for the uncertainty block Δ has been absorbed into the system matrix $H_1(\omega_0)$ to form H_1'. It can be proved that $\mu_{\tilde{\Delta}}(H_1')$ is a monotonically decreasing function of α, thus allowing a systematic way of finding α, such as by a bisection procedure.

A problem with this application is that we have to use upper or lower bounds as substitutes for $\mu_{\tilde{\Delta}}(H_1')$ in the α searching procedure. Although the exact $\mu_{\tilde{\Delta}}(H_1')$ is a monotonically decreasing function with respect to α, its bounds are not necessary. This is especially true of the lower bounds; sometimes we only get poor lower bounds due to the non-convex nature of the problem. This leads to difficulty in applying the bisection algorithm. To compensate for this disadvantage, we propose to combine this

test with branch and bound schemes. By doing this, we do not need to perform the α searching, and we can take advantage of the frequency sweep without worrying about missing important frequency points.

2.5.3 Branch and bound scheme

In this branch and bound scheme, the objective is to find the frequency where the $\sup_{\omega \in R} \mu_{\mathcal{K}}(M(j\omega))$ happens. We first screen the frequency intervals using a bounded frequency test which is only a one-shot μ test at a certain frequency interval. After eliminating all the intervals with $\mu_{\bar{\Delta}}(H_1)$ less than 1, we perform a frequency sweep test on the remaining intervals. This provides an intelligent way to do a frequency sweep instead of blindly choosing the frequency interval to perform the sweep. The screening results of the branch and bound procedure gives frequency ranges small enough to indicate where the instability might happen.

We use the upper bound information to determine whether a certain frequency interval should be thrown away or not. If the upper bound of $\mu_{\bar{\Delta}}(H_1)$ is less than 1, $\mu_{\bar{\Delta}}(H_1)$ itself will definitely be less than 1. Such an interval can be eliminated. To perform faster screening, we try to use rough upper bounds whenever possible. For any $M \in \mathbf{C}^{n\times n}$, $\mu_{\Delta}(M) \leq \inf_{D\in\mathcal{D}_{\mathcal{K}}} \bar{\sigma}(DMD^{-1})$ where $\mathcal{D}_{\mathcal{K}}$ is a set of matrices commutable with all the matrices in $\mathcal{X}_{\mathcal{K}}$, see equation (2.6) for details.

The branch and bound scheme for our problem will be as follows:

branch $[\omega_{\min}, \omega_{\max}]$

while $\omega_{\max} - \omega_{\min} > tolerance$

perform the bounded frequency test over $[\omega_{\min}, \omega_{\max}]$.

Let U *= the upper bound of* $\mu_{\bar{\Delta}}(H_1)$*:*

if $U < 1$ ***break:***

else ***branch***$[\omega_{min}, (\omega_{\max} + \omega_{\min})/2]$*:*

branch$[(\omega_{\max} + \omega_{\min})/2, \omega_{max}]$;

endif

endwhile

2.5.4 Numerical results

2.5.4.1 For the real spectral radius μ calculation

For the 4-machine, 2-area test system, the exporting power from Area1 was chosen as the uncertainty, which was allowed to vary in the range $[0 - 400]MW$. The Load 1 was varied in the range $[1140 - 1540]MW$ while Load 2 was varied in the range $[1400 - 1800]MW$. Since the total load of the system remains the same, this case is one real uncertainty case.

Since now $\mu_K(M(j\omega)) = \rho_R(M(j\omega))$, in order to get $\sup_{\omega \in R} \mu_K(M(j\omega))$, we searched over the frequency space for $\sup_{\omega \in R} \rho_R(M(j\omega))$. This involved a frequency sweep, but at each frequency gridding point, the computation of eigenvalues of $M(j\omega)$ was rather simple and quick.

The following table gives the eigenvalues of $M(j\omega)$ for $\omega = 2.7316$, where the peak of $\mu_K(M(j\omega))$ appeared.

In Table 2.3, the first eigenvalue has a relatively small imaginary part compared with its real part. This small imaginary part may have been introduced by numerical error. Nevertheless, we can consider it as a real eigenvalue. So now $\rho_R(M(j2.7316)) \approx 1.5095$. Similarly, we get $\rho_R(M(j\omega))$ at each frequency gridding point. The maximal real spectral radius is achieved at approximately $\omega = 2.7316$ and its value is 1.5095. The resulting critical exporting power is $332.5MW$. The result is pretty close to $334.1MW$ from a frequency sweep for μ, compared with $344.5MW$ from a traditional eigenvalue test. For a frequency gridding of 50 points it takes only 0.79s.

Table 2.3 The Eigenvalues of $M(j\omega)$ for $\omega = 2.7316$

real part	imaginary part
1.5095	-0.0088
-0.0240	0.0920
-0.0785	0.0230
0.0189	-0.0812
0.0354	-0.0740
-0.0199	-0.0557
0.0473	0.0572
0.0104	0.0539
0.0265	0.0322
-0.0323	-0.0037
0.0116	-0.0196
-0.0047	0.0086
-0.0000	-0.0000
0.0022	0.0002

For one real uncertainty case in the fifty machine system, the scenario is also similar to the one mentioned above. We got $\rho_R \approx 1.4288$ (approximated from an eigenvalue of $M(j\omega) = 1.4288 - j0.01087$(at $\omega = 1.8301$). The resulting critical generation at bus #93 and #110 is $2 \times 1320.MW$. The result is the same for a frequency sweep for μ as compared with $1320.5MW$ from a traditional eigenvalue test. For a frequency gridding of 50 points it takes only 14.11s.

2.5.4.2 For the bounded frequency test

- One shot μ test

  This test was performed on the four-machine system. Conditions were kept the same as those in the frequency sweep test conducted above. A frequency range [2.65, 2.85], which includes the critical frequency, was selected.

  The one shot μ test gave the upper bound of $\mu_{\bar{\Delta}}(H_1)$ as 1.9527 and the lower bound as 1.5346, which indicates that the exact $\mu_{\bar{\Delta}}(H_1)$ must be greater than 1.

So we can conclude that the system is unstable within the given uncertainty range.

- Estimate the parameter range for a stable operation

Figure 2.12 gives the upper and lower bounds of $\mu_{\bar{\Delta}}(H_1')$ corresponding to the changing in α.

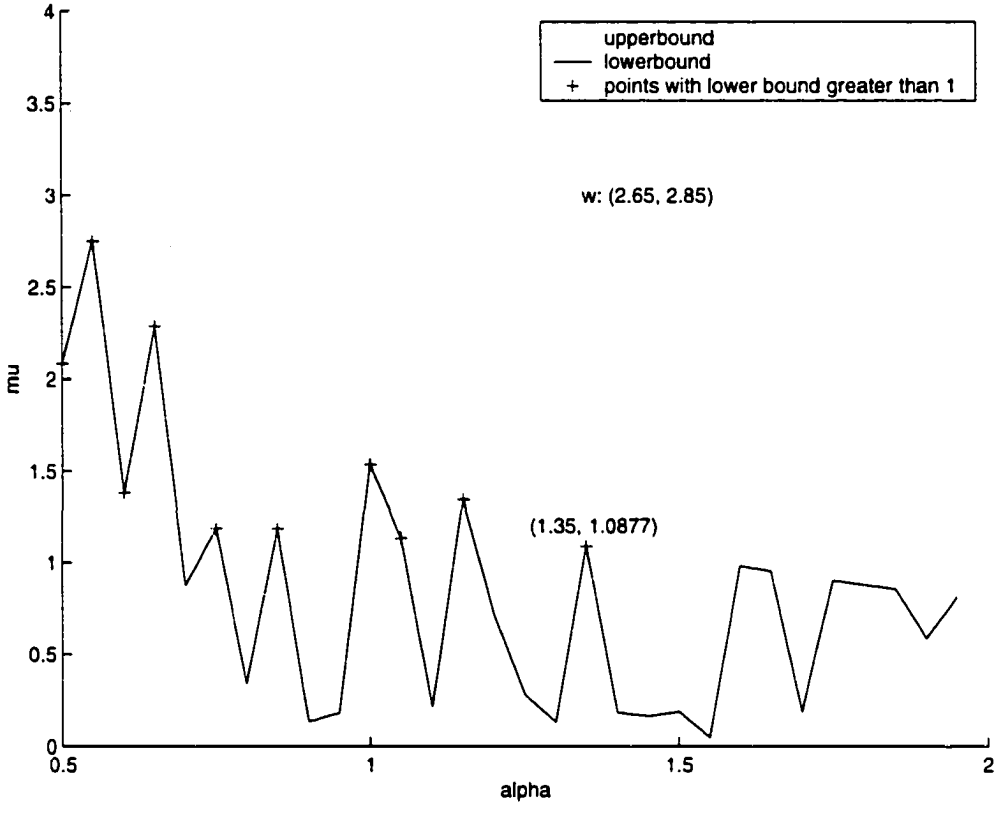

Figure 2.12 α searching to get the skewed-μ.

Since the upper bound remains above 1, it provides no information on when the exact $\mu_{\bar{\Delta}}(H_1')$ goes down through 1. But if we look at the lower bound, when $\alpha = 1.35$, the lower bound of $\mu_{\bar{\Delta}}(H_1')$ is still above 1. Thus, we can say that the exact $\mu_{\bar{\Delta}}(H_1')$ goes down through 1 at least after $\alpha = 1.35$. Since there is no point beyond $\alpha = 1.35$ that gives the value of the lower bound of $\mu_{\bar{\Delta}}(H_1')$ greater than

1, we can use 1.35 as an approximation of $\bar{\mu}$. Accordingly, we found the estimate value of the critical exporting power as $348.MW$. Compared to the results from the eigenvalue test, where the value of the critical exporting power was $344.5MW$, the error is only 0.2%.

2.5.4.3 For the branch and bound scheme

The test was performed on the four machine system with the same scenario in the previous sections. The initial frequency range was chosen as $[0, 100]rad/s$.

When the tolerance was set to $0.1s$, it only took $32.05s$ to arrive at the results. Large frequency intervals with $\bar{\mu} < 1$ were eliminated. The conclusion was that the frequency sweep test should be performed on the intervals $[0, 0.19531]rad/s$ and $[2.53906, 3.51562]rad/s$ to find the peak value of μ, see Figure 2.13.

The frequency sweep followed in this procedure immediately ruled out the former interval and determined the peak of $\mu_{\Delta}(M(j\omega))$. Figure 2.14 is the μ plot for the frequency sweep in the interval $[0, 0.19531]rad/s$, and Figure 2.15 is the μ plot for the frequency sweep in the interval $[2.53906, 3.51562]rad/s$. The peak of μ is 1.4605 at $\omega = 2.7384$.

The proposed branch and bound scheme can efficiently rule out frequency intervals where $\mu_{\Delta}(H_1) < 1$) and can narrow the frequency sweep process down to a reasonable frequency interval. This can help us intelligently select intervals for a frequency sweep and avoid missing important points.

From Figure 2.15, we see that a narrow spike appears in the μ plot. If one performs the frequency sweep test without knowing which frequency interval should pay attention to, it is very easy to miss the peak and draw wrong conclusions accordingly. Although the branch and bound scheme takes additional dozens of seconds before performing the frequency sweep, it not only saves time for blindly trying frequency interval to sweep on but also avoids missing important frequency range.

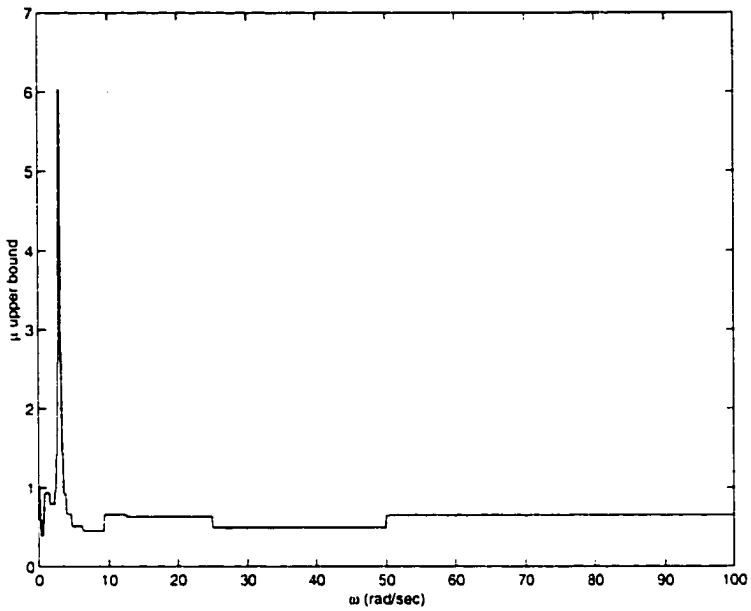

Figure 2.13 μ upper bound from the branch and bound scheme.

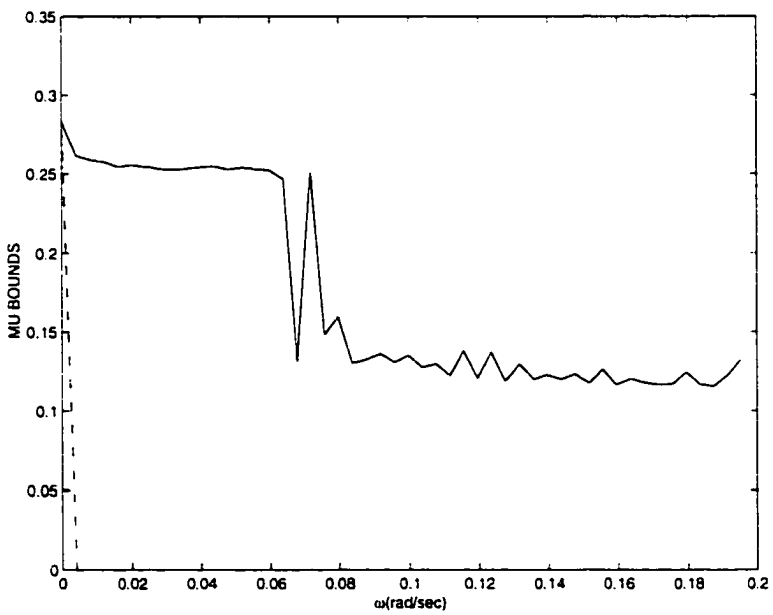

Figure 2.14 Frequency sweep for $[0.0.19531] rad/s$.

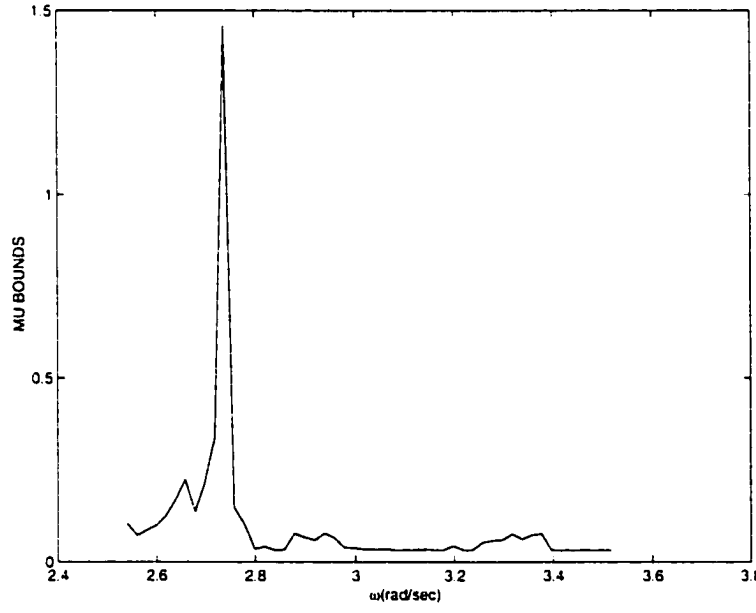

Figure 2.15 Frequency sweep for $[2.53906, 3.51562] rad/s$.

3 ν GAP METRIC BASED ROBUTNESS ANALYSIS

3.1 From the Structured Singular Value to the Gap Metric

The structured singular value μ is a very powerful tool for the evaluation of robustness with a given controller. It is natural for one to try to use it for controller design. For complex perturbations a method known as DK-iteration is available [7, 14]. It has several applications in literature [51, 52]. Let's take a brief look at the DK-iteration.

The standard framework for μ-synthesis is given in Figure 3.1. The system labeled P is the open-loop interconnection and contains all of the the known elements including the nominal plant model and appropriate weighting functions, and Δ is the uncertainty block from the set $\mathbf{\Delta}_S$. The set of uncertain systems to be controlled is described by the LFT

$$\{F_u(P, \Delta) : \Delta \in \mathbf{\Delta}_S, \bar{\sigma}(\Delta) \leq 1\}$$

The design objective is to find a controller K that belongs to the class K_s of all rational proper controllers such that for all uncertainty $\Delta \in \mathbf{\Delta}_S$, $\bar{\sigma}(\Delta) \leq 1$, , the closed-loop system is stable and satisfies

$$\|F_l[F_u(P, \Delta), K]\|_\infty < 1 \tag{3.1}$$

It is clear from Figure 3.1 that

$$F_l[F_u(P, \Delta), K] = F_u[F_l(P, K), \Delta]$$

Therefore, the performance requirement in (3.1) becomes:

$$\|F_u[F_l(P, K), \Delta]\|_\infty < 1 \tag{3.2}$$

Since the robust performance problem can be treated as an "augmented" robust stability problem, and K achieves robust performance if and only if

$$\max_{\omega} \mu_{\mathbf{\Delta}_P}(F_l(P, K)(j\omega)) < 1 \tag{3.3}$$

so the μ-synthesis is equivalent to minimizing the peak value of $\mu_{\mathbf{\Delta_P}}(.)$ of the closed-loop transfer function $F_l(P, K)$ over all stabilizing controllers K, i.e.,

$$\min_{K} \max_{\omega} \mu_{\mathbf{\Delta_P}}(F_l(P, K)(j\omega)) \tag{3.4}$$

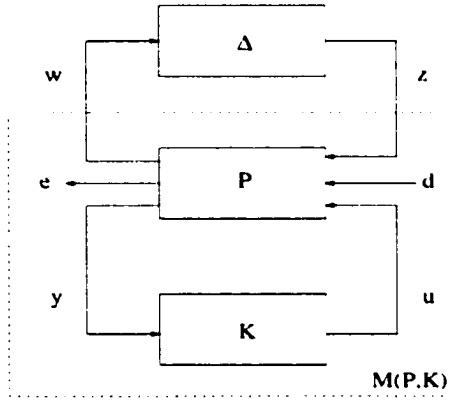

Figure 3.1 μ synthesis framework.

Since

$$\mu_{\mathbf{\Delta_P}}(F_l(P, K)(j\omega)) \leq \min_{D \in \mathcal{D}} \bar{\sigma}(DF_l(P, K)(j\omega)D^{-1}).$$

(3.4) is equivalent to finding the controller that minimizes the peak value of μ upper bound over frequency instead, namely

$$\min_{K} \max_{\omega} \min_{D \in \mathcal{D}} \bar{\sigma}(DF_l(P, K)(j\omega)D^{-1})$$

by alternating between minimizing $\bar{\sigma}(DF_l(P, K)(j\omega)D^{-1})$ with respect to either K or D (while holding the other fixed). The DK-iteration proceeds as follows:

1. **K-step.** Synthesize an H_∞ controller for the scaled problem, $\min_{D\in\mathcal{D}} \bar{\sigma}(DF_l(P,K)(j\omega)D^{-1})$ with fixed $D(s)$.

2. **D-step.** Find $D(j\omega)$ to minimize at each frequency $\bar{\sigma}(DF_l(P,K)(j\omega)D^{-1}$ with fixed K.

3. Fit the magnitude of each element of $D(j\omega)$ to a stable and minimum phase transfer function $D(s)$ and go to step 1.

The iteration may continue until satisfactory performance is achieved, $\bar{\sigma}(DF_l(P,K)(j\omega)D^{-1}) < 1$, or until the H_∞ norm no longer decrease.

One major problem with this approach is that although each of the minimization steps (K-step and D-step) are convex, joint convexity is not guaranteed. Therefore, the iterations may converge to a local optimum. The other problem is the high order of the resulting controller. The order of the controller resulting from each iteration is equal to the number of states in the plant $P(s)$ plus the number of states in the weights plus twice the number of states in $D(s)$. Besides, the DK-iteration depends heavily on optimal solutions for steps 1 and 2, and also on good fits in step3. Furthermore, in some cases, the iterations may converge slowly, and it may be difficult to judge whether the iterations are converging or not. One may even experience the μ-value increasing. This may be caused by numerical problems or inaccuracies, or by a poor fit of the D-scales. In any case, if the iteration converge slowly, one may have to consider going back to the initial problem and rescaling the inputs and outputs.

For the design problems which arise with real or mixed real and complex perturbations, there is a corresponding DGK-iteration procedure proposed by Young. It is related to the tighter upper bound for the mixed μ problem. See [53] for details. The practical implementation for this algorithm is even difficult, and a very high order fit may be required for the G-scales.

For all these problems associating with the μ synthesis, we would seek a more practical and easily implementable alternative for robust controller design. The normalized coprime factor uncertainty provides a good general class of uncertianty, and the associated Glover-McFarlane H_∞ design procedure has proved itself very useful in applications. The resulting controller from this design is guaranteed to stabilize a plant set within an uncertainty ball captured by the coprime perturbations. The ball is proved to equivalent to a ball of the same radius in terms of the gap metric. This promotes us to study the application of the gap metrics in robust analysis as well as controller design. In the following sections, related mathematical background will be presented. After that, the gap based analysis an synthesis procedure will follow in the next two sections.

3.2 Gap Metric Related Concepts

3.2.1 Mathematical preliminaries

3.2.1.1 Function spaces and signal spaces

The most important objective of a control system is to achieve certain performance specifications in addition to providing internal stability. One way to describe the performance specifications of a control system is in terms of the size of certain signals of interest. For this purpose, we introduce the Hardy spaces $\mathcal{H}_2$ and $\mathcal{H}_\infty$.

The $\mathcal{H}_2$ space is a Hilbert space. A *Hilbert space* is a complete inner product space with the norm induced by its inner product. For example, $\mathcal{C}^n$ with the usual inner product is a (finite dimensional) Hilbert space.

The signal spaces $\mathcal{L}_2$ and $\mathcal{H}_2$. In the context of this research, $\mathcal{L}_2$ is the space of all signals, or vectors of signals, with bounded energy. It is a Hilbert space with inner product

$$< x, y >= \int_{-\infty}^{\infty} x^*(t)y(t)dt$$

and norm

$$\|x\|_{\mathcal{L}_2^t} = \sqrt{< x, x >}$$

Alternatively, $\mathcal{L}_2$ can be thought of as a frequency domain space, with inner product

$$< \tilde{x}, \tilde{y} >= \frac{1}{2\pi} \int_{-\infty}^{\infty} \tilde{x}^*(j\omega)\tilde{y}(j\omega)d\omega$$

and norm

$$\|\tilde{x}\|_{\mathcal{L}_2^f} = \sqrt{< \tilde{x}, \tilde{x} >}.$$

where $\tilde{x}$ is the Fourier transform of x.

In the time domain, $\mathcal{L}_2$ can be decomposed into $\mathcal{L}_{2+}$ and $\mathcal{L}_{2-}$, where $\mathcal{L}_{2+}$ is the space of signals defined for positive time and zero for negative time. Similarly, $\mathcal{L}_{2-}$ is the space of signals defined for negative time and zero for positive time. In the frequency domain, $\mathcal{L}_2$ can be decomposed into $\mathcal{H}_2$ and $\mathcal{H}_2^\perp$, where $\mathcal{H}_2$ is the space of Fourier transformations of signals in $\mathcal{L}_{2+}$ and $\mathcal{H}_2^\perp$ is the space of Fourier transformations of signals in $\mathcal{L}_{2-}$. Thus, when we say x is in $\mathcal{H}_2$, we mean that x is a signal of bounded energy which, when considered in the time domain, is zero for negative time. For such signals, the Fourier transformation is identical to the Laplace transformation with the Laplace variable s replaced by $j\omega$.

The real rational subspace of $\mathcal{H}_2$, which consists of all proper and real rational stable transfer matrices, is denoted by $\mathcal{RH}_2$.

The function spaces $\mathcal{L}_\infty$ and $\mathcal{H}_\infty$. A system P is stable if, for any input in $\mathcal{H}_2$, the output is also in $\mathcal{H}_2$. That is, a stable system maps bounded energy inputs onto bounded energy outputs. If a system is unstable then its output can have infinite energy in response to a finite energy input. $\mathcal{H}_\infty$ is defined as the space of functions of the complex variable s analytic for all s in the open right half plane with a finite norm defined as

$$\|P\|_{\mathcal{H}_\infty} = \sup_{s:\mathcal{R}(s)>0} \bar{\sigma}(P(s)).$$

$\mathcal{RH}_\infty$ is defined as the subspace of $\mathcal{H}_\infty$ which consists of all proper and real rational stable transfer matrices. For such systems, the supremum is attained on the boundary $s = j\omega$, (for possibly infinite ω),*ie*

$$\|P\|_{\mathcal{RH}_\infty} = \max_{\omega \in \mathbf{R} \cup \infty} \bar{\sigma}(P(j\omega)).$$

$\mathcal{L}_\infty$ is the space of all functions essentially bounded on the imaginary axis with norm

$$\|P\|_{\mathcal{L}_\infty} := ess\sup_{\omega} \bar{\sigma}(P(j\omega)).$$

$\mathcal{H}_\infty$ is a subspace of $\mathcal{L}_\infty$. Any proper rational transfer function matrix is in $\mathcal{L}_\infty$ provided it has no imaginary axis poles.

3.2.1.2 Internal stability of the feedback system

For the standard feedback configuration shown in Figure 3.2, the transfer function

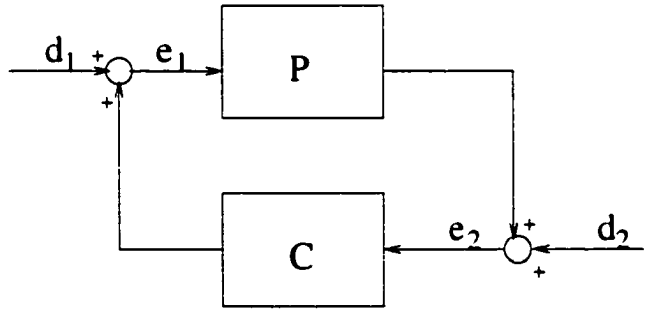

Figure 3.2 Standard feedback configuration.

we are interested in is that from $\begin{bmatrix} d_1 \\ d_2 \end{bmatrix}$ to $\begin{bmatrix} e_1 \\ e_2 \end{bmatrix}$, i.e. the transfer function between the plant input and output to the input and output to the controller denoted as $H(P,C)$. The system in Figure 3.2 is said to be *internally stable* if $H(P,C)$ belongs to $\mathcal{RH}_\infty$.

Internal stability is a basic requirement for a practical feedback system. Because all interconnected systems may be unavoidably subject to some nonzero initial conditions

and some errors, in practice such errors at some locations should not lead to unbounded signals at some other locations in the closed-loop system. Internal stability guarantees that all signals in a system are bounded provided that the injected signals(at any locations) are bounded.

We define a generalized stability margin in terms of this transfer function as:

$$b_{P,C} := \begin{cases} \left\| \begin{bmatrix} I \\ C \end{bmatrix} (I - PC)^{-1} [P \; I] \right\|_{\infty}^{-1}, & \text{if } [P,C] \text{ is stable} \\ 0, & \text{otherwise.} \end{cases} \tag{3.5}$$

$$= \|H(P,C)\|_{\infty}^{-1} \tag{3.6}$$

Here $[P,C]$ denotes the feedback combination of the standard feedback system. In order for $H(P,C)$ to exist, $[P,C]$ must be well posed. Besides, $[P,C]$ is stable if each element of this closed-loop transfer function is in $\mathcal{H}_\infty$.

3.2.1.3 Coprime factors

Right coprime factorization. Let P be a proper real rational matrix. A *right coprime factorization(rcf)* of P is a facorization $P = NM^{-1}$, where N and M are right coprime over $\mathcal{RH}_\infty$. That is, M and N have the same number of columns and there exist matrices X_r and Y_r in $\mathcal{RH}_\infty$ such that

$$[X_r \; Y_r] \begin{bmatrix} M \\ N \end{bmatrix} = X_r M + Y_r N = I.$$

Given $\{N, M\}$ a *rcf* of P, all possible *rcfs* may be generated as $\{NQ, MQ\}, Q, Q^{-1} \in \mathcal{RH}_\infty$. The *normalized right coprime factorization* of P is defined as an ordered pair $\{N, M\}$ such that $\{N, M\}$ is an *rcf* of P and

$$M^* M + N^* N = I.$$

Left coprime factorization. Similarly, a *left coprime factorization(rcf)* of P is a facorization $P = \tilde{M}^{-1}\tilde{N}$, where $\tilde{N}$ and $\tilde{M}$ are left coprime over $\mathcal{RH}_\infty$. That is, $\tilde{M}$ and

$\tilde{N}$ have the same number of rows and there exist matrices X_l and Y_l in $\mathcal{RH}_\infty$ such that

$$[\tilde{M}\ \tilde{N}]\begin{bmatrix} X_l \\ Y_l \end{bmatrix} = X_r M + Y_r N = I.$$

The *normalized left coprime factorization* of P is defined as an ordered pair $\{\tilde{N}, \tilde{M}\}$ such that $\{\tilde{N}, \tilde{M}\}$ is an *lcf* of P and

$$\tilde{M}\tilde{M}^* + \tilde{N}\tilde{N}^* = I.$$

3.2.1.4 Metric and the graph topology

Metric. Let X be a set and let ρ be a function: $X \times X \to \mathbf{R}$. If ρ satisfies the following conditions, then we can say that ρ is a *metric* on X and call the pair (X, ρ) a metric space.

1. $\rho(x, y) \geq 0$ for all $x, y \in X$
2. $\rho(x, y) = 0$ iff $x = y$
3. $\rho(x, y) = \rho(y, x)$ for all $x, y \in X$
4. $\rho(x, z) \leq \rho(x, y) + \rho(y, z)$ for all $x, y, z \in X$(triangle inequality)

Topology. A topology on a space $\mathcal{S}$ is the collection $\mathcal{T}$ of all sets $\mathcal{T}_i \subset \mathcal{S}$ regarded as being *open* in the space, provided this collection satisfies the following axioms:

1. Both the entire space $\mathcal{S}$, and the empty set $\emptyset$ are elements of $\mathcal{T}$.
2. Any arbitrary union or finite intersection of sets in $\mathcal{T}$ is also an element of $\mathcal{T}$.

Any space may be equipped with a number of different topologies. If we have a metric on a space, then we can define a set $\mathcal{U} \in \mathcal{S}$ to be open if, for every $x \in \mathcal{U}$, there exists an ϵ such that the set $\{y : delta(x, y) < \epsilon\}$ is also contained in $\mathcal{U}$. The collection of all such sets is guaranteed to satisfy the properties in the definition of the topology and is called the topology induced by the metric δ.

- **The norm topology.** The norm topology is the natural topology induced by $\|\bullet\|_\infty$ consisting of open balls given by

$$\mathcal{B}(P_0, \epsilon) := \{P : \|P - P_0\|_\infty < \epsilon\}.$$

- **The graph topology.** Given an LTI system P, let $[N, M]$ be an rcf of P over $\mathcal{RH}_\infty$. It is well known [46] that there exists a positive constant $\mu(N, M)$ such that given $[N_1, M_1]$ of compatible dimension, $[N_1, M_1]$ are also right coprime whenever $\|(N_1 - N)^T, (M_1 - M)^T)^T\|_\infty < \mu(N, M)$. Thus, given an LTI plant P, it is possible to define a basic neighborhood of $P = NM^{-1}$ consisting of the set

$$\mathbf{N}(N, M; \epsilon) := \left\{ P_1 = N_1 M_1^{-1} : \left\| \begin{pmatrix} N - N_1 \\ M - M_1 \end{pmatrix} \right\|_\infty < \epsilon < \mu(N, M) \right\}.$$

Thus a basic neighborhood of P consists of all plants P_1 which have an rcf $[N_1, M_1]$ that is "close" to an rcf of P. Or we can obtain a basic neighborhood of P starting with some rcf $[N, M]$ of P and making a "small" perturbation of $[N, M]$ to $[N_1, M_1]$, then taking the ratio $N_1 M_1^{-1}$. By varying ϵ over all positive numbers less than $\mu(N, M)$, or by varying $[N, M]$ over all possible right coprime factorizations of P and by varying P over all finite-dimensional LTI systems, we can obtain a collection of neighborhoods that form a base of the graph topology.

The fundamental importance of this topology is captured in the following proposition.

Proposition [46] *Suppose that $\lambda \mapsto P_\lambda, \lambda \mapsto C_\lambda$ are functions mapping a first countable topological space Λ into the set of finite-dimensional LTI systems; suppose that the pair $(P_{\lambda_0}, C_{\lambda_0})$ is stable.*

1. *Suppose the function $\lambda \mapsto P_\lambda, \lambda \mapsto C_\lambda$ are continuous at λ_0 in the graph topology. Then there exists a neighborhood $\mathbf{N}$ of λ_0 such that (P_λ, C_λ) is*

stable for all $\lambda \in \mathbf{N}$, *and in addition* $H(P_\lambda, C_\lambda)$ *is continuous at* λ_0 *in the norm topology.*

2. *Conversely, suppose there is a neighborhood* $\mathbf{N}$ *of* λ_0 *such that* (P_λ, C_λ) *is stable for all* $\lambda \in \mathbf{N}$, *and such that* $H(P_\lambda, C_\lambda)$ *is continuous at* λ_0 *in the norm topology. Then the functions* $\lambda \mapsto P_\lambda, \lambda \mapsto C_\lambda$ *are continuous at* λ_0 *in the graph topology.*

This proposition shows that the graph topology is a suitable topology for capturing the perturbations to the nominal plant that can be stabilized by feedback and for which the mapping $\lambda \mapsto H(P_\lambda, C)$ is continuous. The continuity in $H(P_\lambda, C_\lambda)$ is very important. Because of this property, as long as the perturbation is small enough, (P_{λ_0}, C) is stable, and $H(P_{\lambda_0}, C)$ meets the nominal performance objectives, the interconnection (P_λ, C) will be stable.

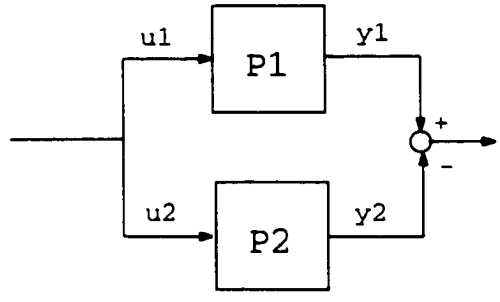

Figure 3.3 Measuring open loop uncertainty.

We can see the difference between the uncertainty measured by norm and those measured by the gap notation through the following two figures: Figure 3.3 and Figure 3.4.

Let's apply the same, bounded energy, input to the nominal and perturbed plants and look at the energy of the difference between their outputs as in Figure 3.3.

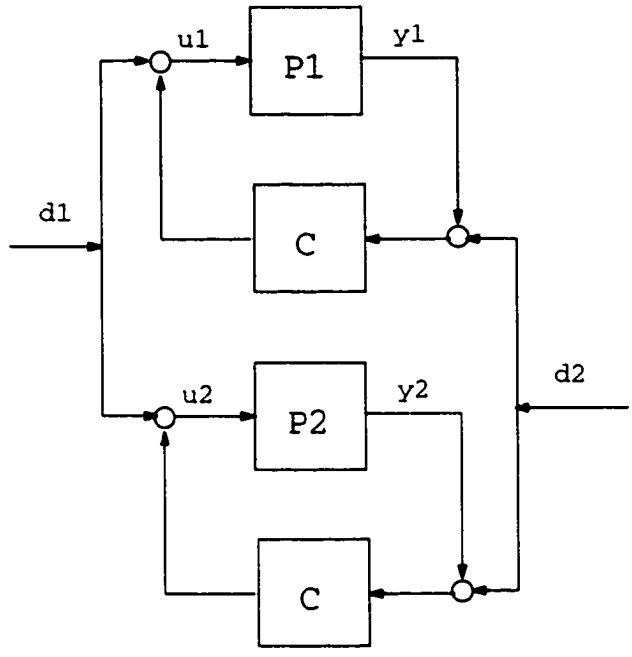

Figure 3.4 Closed loop uncertainty.

We call the two systems P_1 and P_2 "close" if the difference is small, provided that both P_1 and P_2 are transfer functions in $\mathcal{H}_\infty$. The main attraction of this notion of uncertainty is that it is easily measured. In the scalar case, we can simply plot the Nyquist diagram of the two plants and measure the distance between them frequency by frequency. The "difference" is then the maximum of this distance over frequency. However, such a notion of uncertainty takes no account of the special structure of the feedback problem. We are really interested in comparing the closed loop behavior of different plants in conjunction with the same feedback compensator, as depicted in Figure 3.4.

If we apply the same input $\begin{bmatrix} d_1 \\ d_2 \end{bmatrix}$ to the two loops, then the signals at the plant inputs will be different, i.e. u_1 will be different from u_2; whereas uncertainty in the norm topology, as discussed above, is related to the difference in the outputs

of the two plants when each receives the same input. A more appropriate notion would allow for uncertainty in both the inputs and the outputs: two systems might be deemed close if, given any input u_1 to P_1, there is input u_2 to P_2 that makes

$$\frac{\left\| \begin{bmatrix} y_1 \\ u_1 \end{bmatrix} - \begin{bmatrix} y_2 \\ u_2 \end{bmatrix} \right\|_2}{\left\| \begin{bmatrix} y_1 \\ u_1 \end{bmatrix} \right\|_2}$$

small, where $y_1 = P_1 u_1$ and $y_2 = P_2 u_2$. That is to say, if their graphs are close. We will introduce the graph representation of LTI system in section 3.2.2.1. It is important to note that this notion also makes sense for unstable plants.

3.2.2 The gap and the ν gap metrics

The graph topology represents the correct setting for the study of robust control in the presence of plant and/or controller uncertainty since it captures all perturbations that can be stabilized by feedback while causing gradual degradation in performance.

To study the stability of uncertain systems, we need a metric in the space of the systems under consideration to provide a mechanism to measure the size of the uncertainty. A desired property of the metric is to ensure the continuity of the function $(P, C) \rightarrow H(P, C)$. That is, if $[P_0, C_0]$ is well posed and $H[P_0, C_0]$ is stable, then $[P, C]$ is also well posed and $H[P, C]$ is stable for $[P, C]$ close to $[P_0, C_0]$ in the sense of the metric. We also want to use this metric to determine how much uncertainty can be tolerated on a pair $[P_0, C_0]$ which is well posed with stable $H(P_0, C_0)$. This requires that the metric should have certain desirable quantitative properties so that the question above can be easily answered in terms of the size of uncertainty measured by the metric.

A number of metrics having this property have been introduced: these include the graph metric [47], the gap metric [15, 20, 55], the pointwise gap metric [41], and more

recently, the ν-gap metric [48]. All these metrics induce the same topology, namely graph topology, and have the desired qualitative properties for the study of stability robustness. But only two, the gap metric and the ν-gap metric, are amenable to computation [21, 48] and consequently have practical application. In the following section, we will discuss the gap and the ν-gap metrics, stating important robust stability results.

3.2.2.1 The gap metric

The gap metric was first introduced into the control literature by Zames and El-Sakkary [55, 15] as being appropriate for the study of uncertainty in feedback systems. A computable formula of the gap metric is given by Georgiou [20]; several authors have obtained *sufficient* conditions for the closed-loop stability robustness in terms of the radius of the gap metric ball centered at the nominal plant or the nominal controller. It has application in a number of area of applied mathematics.

To define the gap metric, we must first introduce the definition of the graph of LTI system.

The graph representation of LTI system. The graph of a finite-dimensional LTI system is defined as all stable input-output pairs

$$\mathcal{G}(P) := \left\{ \begin{pmatrix} Pu \\ u \end{pmatrix} : u \in \mathcal{D}(P) \right\}$$

considered as a subspace of $\mathcal{H}_2 \oplus \mathcal{H}_2$, where $\mathcal{D}(P)$ represents the domain of P.

The graph of a given system can be generated through the use of coprime factors. Let $P = NM^{-1}$ be a right coprime facorization of the LTI plant with transfer function P, then its graph $\mathcal{G}(P)$ is given by

$$\mathcal{G}(P) = \begin{bmatrix} N \\ M \end{bmatrix} q, q \in \mathcal{H}_2$$

The **gap** between two systems P_1 and P_2 is defined by

$$\delta_g(P_1, P_2) := \left\| \Pi_{\begin{bmatrix} M_1 \\ N_1 \end{bmatrix} \mathcal{H}_2} - \Pi_{\begin{bmatrix} M_2 \\ N_2 \end{bmatrix} \mathcal{H}_2} \right\|$$

where Π_K denotes the orthogonal projection onto K and $P_1 = N_1 M_1^{-1}$, and $P_2 = N_2 M_2^{-1}$ are normalized right coprime factorizations.

The properties of the gap metric [20].

- $\delta_g(P_1, P_2) = \max\{\vec{\delta}_g(P_1, P_2), \vec{\delta}_g(P_2, P_1)\}$

  where $\vec{\delta}_g(P_1, P_2)$ is the *directed gap* and can be computed by

$$\vec{\delta}_g(P_1, P_2) = \inf_{Q \in \mathcal{H}_\infty} \left\| \begin{bmatrix} M_1 \\ N_1 \end{bmatrix} - \begin{bmatrix} M_2 \\ N_2 \end{bmatrix} Q \right\|_\infty$$

- $\delta_g(\bullet, \bullet)$ is a metric.

- $0 \leq \delta_g(P_1, P_2) \leq 1$

- If $\delta_g(P_1, P_2) < 1$, then $\delta_g(P_1, P_2) = \vec{\delta}_g(P_1, P_2) = \vec{\delta}_g(P_2, P_1)$.

- Let P have a normalized coprime factorization $P = NM^{-1}$. Then for all $0 < b \leq 1$,

$$\{P_1 \ : \ \vec{\delta}_g(P, P_1) < b\}$$
$$= \left\{ P_1 : P_1 = (N + \Delta_N)(M + \Delta_M)^{-1}, \Delta_N, \Delta_M \in \mathcal{H}_\infty, \left\| \begin{bmatrix} \Delta_N \\ \Delta_M \end{bmatrix} \right\|_\infty < b \right\}.$$

  This property shows that a ball of uncertainty in the gap metric of a given radius is equal to a ball of uncertainty of the same radius defined by perturbations of a normalized right coprime faction, provided the radius is smaller than a certain quantity.

- Consider a system P with normalized coprime faction $P = NM^{-1}$ and consider a controller C which stabilizes P. Take a real number b with $0 < b \leq 1$. Then the following statements are equivalent.

  1. $[P_1, C]$ is stable for all P_1 with transfer function $P_1 = (N + \Delta_N)(M + \Delta_M)^{-1}$ where $\Delta_M, \Delta_N \in \mathcal{RH}_\infty$ and $\left\| \begin{bmatrix} \Delta_N \\ \Delta_M \end{bmatrix} \right\|_\infty < b$.
  2. $[P_1, C]$ is stable for all P_1 with $\vec{\delta}(P, P_1) < b$.
  3. $[P_1, C]$ is stable for all P_1 with $\delta_g(P, P_1) < b$.

3.2.2.2 The ν gap metric

Unlike other metrics, the ν gap metric has a clear frequency response interpretation. It can be estimated directly from the frequency response measurements and is easy to compute. Furthermore, it is the smallest metric that satisfies certain robustness properties. Therefore, it gives less conservative results in assessing the stability robustness.

Let P_i be a $p \times q$ rational transfer matrix and let $[N_i, M_i]$ denote a normalized right coprime factorization(rcf), and $[\tilde{N}_i, \tilde{M}_i]$ a normalized left coprime factorization(lcf) of P_i. We write:

$$G_i := \begin{bmatrix} N_i \\ M_i \end{bmatrix}, \quad \tilde{G}_i := [-\tilde{M}_i, \tilde{N}_i] \tag{3.7}$$

Recall that $[N_i, M_i]$ is a normalized rcf of P_i if and only if a) $P_i = N_i M_i^{-1}$, b) $G_i \in \mathcal{H}_\infty$, c) there exists an $X \in \mathcal{H}_\infty : XG_i = I$(the coprimeness condition), and d) $G_i^* G_i = I$(the normalized condition). Similarly, $[\tilde{N}_i, \tilde{M}_i]$ is a normalized lcf of P_i if and only if a) $P_i = \tilde{M}_i^{-1} \tilde{N}_i$, b) $\tilde{G}_i \in \mathcal{H}_\infty$, c) there exists an $Y \in \mathcal{H}_\infty : \tilde{G}_i Y = I$, and d) $\tilde{G}_i \tilde{G}_i^* = I$.

The function $\delta_\nu(\bullet, \bullet)$ is defined as:

$$\delta_\nu(P_1, P_2) = \begin{cases} \|\tilde{G}_2 G_1\|_\infty, & \text{if } det(G_2^* G_1)(j\omega) \neq 0 \forall \omega \text{ and } wno\ det(G_2^* G_1) = 0 \\ 1, & \text{otherwise} \end{cases} \tag{3.8}$$

where *wno* denotes the winding number of a scalar transfer function $g(s)$ about the origin as s follows the standard Nyquist contour.

An alternative definition of δ_ν is given as:

$$\delta_\nu(P_1, P_2) = \begin{cases} \|\Psi(P_1, P_2)\|_\infty, & \text{if } det(I + P_2^* P_1)(j\omega) \neq 0 \forall \omega \\ & \text{and } wno\ det(I + P_2^* P_1) + \eta(P_1) - \eta_0(P_2) = 0 \\ 1, & \text{otherwise} \end{cases} \quad (3.9)$$

where $\Psi(P_1, P_2) := (I + P_2^* P_1)^{-1/2}(P_1 - P_2)(I + P_2^* P_1)^{-1/2}$, $\eta(P)$ and $\eta_0(P)$ denotes the number of open right-half plane and imaginary axis poles of $P(s)$ respectively. This definition is useful when doing hand calculation or when computing from the frequency response of the plants.

The following proposition was proved to be true by Vinnicombe [48].

Theorem(Robustness in terms of the ν-gap metric) Given a nominal plant $P_1 \in \mathcal{P}^{p \times q}$ and a compensator $C \in \mathcal{P}^{q \times p}$ then:

$[P_2, C]$ is stable for all plants, P_2, satisfying $\delta_\nu(P_1, P_2) \leq \beta$ if and only if $b_{P_1,C} > \beta$.

3.2.2.3 Comparison between the gap metric and the ν gap metric

Vinnicombe [48] showed that the topology induced by δ_ν and the gap metric are identical, and that the following inequality holds:

$$\delta_g(P_1, P_2) b_{opt}(P_1) \leq \delta_\nu(P_1, P_2) \leq \delta_g(P_1, P_2)$$

where $b_{opt}(P_1) := sup_C b_{P,C}$.

The second inequality shows that any set that is δ_ν-open is also δ_g-open as, for any P and any b, $\mathcal{B}_g(P, b) \subseteq \mathcal{B}_\nu(P, b)$, where

$$\mathcal{B}_g(P, b) = \{\hat{P} : \delta_g(P, \hat{P}) < b\} \text{ and } \mathcal{B}_\nu(P, b) = \{\hat{P} : \delta_\nu(P, \hat{P}) < b\}.$$

That is to say, if we use the criteria $b > \delta(P, \hat{P})$ as an indicator of stability, using δ_g will always be more conservative than using δ_ν.

3.2.2.4 The gap metric in robust design

For controller design, the objectives include optimizing stability robustness as well as achieving a specified level of performance. In this regard, McFarlane and Glover [35] have introduced a design procedure which incorporates loop shaping methods to obtain performance/robust stability tradeoffs.

By McFarlane and Glover, the resulting controller can stabilize all plants within an uncertainty ball captured by coprime perturbations. That is, if the nominal plant is

$$G = \tilde{M}^{-1}\tilde{N}$$

and the perturbed plant is given as

$$G_\Delta = (\tilde{M} + \Delta_M)^{-1}(\tilde{N} + \Delta_N).$$

where $\tilde{M}, \tilde{N}$ is a left coprime factorization(LCF) of G. Δ_M, Δ_N are stable, unknown transfer functions representing the uncertainty and satisfying $\|[\Delta_M, \Delta_N]\| < \epsilon$, and if the designed controller could achieve a stability margin of at least the value of ϵ, then all the controllers can stabilize all the perturbed plants.

Furthermore, according to Georgiou, the ball of uncertainty in the gap metric is equal to a ball of uncertainty of the same radius defined by the normalized coprime factorization. Thus, in terms of the gap metric, all G_Δ with $\delta_g(G, G_\Delta) < \epsilon$ can be stabilized by this controller.

We will briefly introduce the design procedures here. In the loop shaping stage, frequency weights are introduced to shape the open-loop frequency response of the nominal plant. A designer specifies closed-loop objectives in terms of requirements on the open-loop singular values of the compensated system. For example, given a plant G and a controller K, at frequencies where $\underline{\sigma}(GK) \gg 1$, where $\underline{\sigma}(\cdot)$ denotes the minimum singular value, then the loop gain is large, and we can make the approximations

$$\bar{\sigma}((I - GK)^{-1}) \approx 1/\underline{\sigma}(GK)$$

$$\bar{\sigma}((I - GK)^{-1}G) \approx 1/\underline{\sigma}(K)$$

Generally speaking, a weighting function is selected so as to achieve sufficiently high loop gain at low frequency for disturbance attenuation and low loop gain at high frequency for good noise rejection. See Figure 3.5 for an illustration.

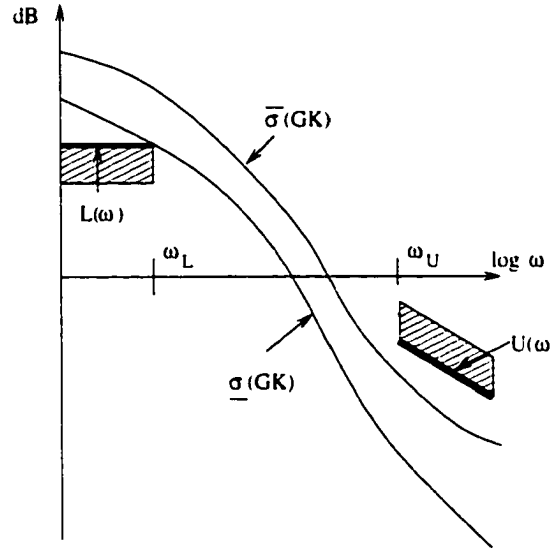

Figure 3.5 Open loop singular value shaping.

After that, a normalized coprime factor H_∞ problem is used to robustly stabilize the shaped plant.

The H_∞ loop shaping design procedure

1. *Loop shaping:* Using a precompensator W_1 and/or a postcompensator W_2, the singular value of the nominal plant are shaped to give a desired open-loop shape. The nominal plant G and the shaping functions W_1, W_2 are combined to form the shaped plant, G_s where $G_s = W_2GW_1$. We assume that W_1 and W_2 are such that G_s contains no hidden modes.

2. *Robust Stabilization:* Select $\epsilon \leq \epsilon_{max}$, then synthesize a stabilizing controller K_∞, which satisfies

$$\left\| \begin{bmatrix} I \\ K_\infty \end{bmatrix} (I - G_s K_\infty)^{-1} M_s^{-1} \right\|_\infty \leq \epsilon^{-1}$$

3. The final feedback controller $K = W_1 K_\infty W_2$, see Figure 3.6.

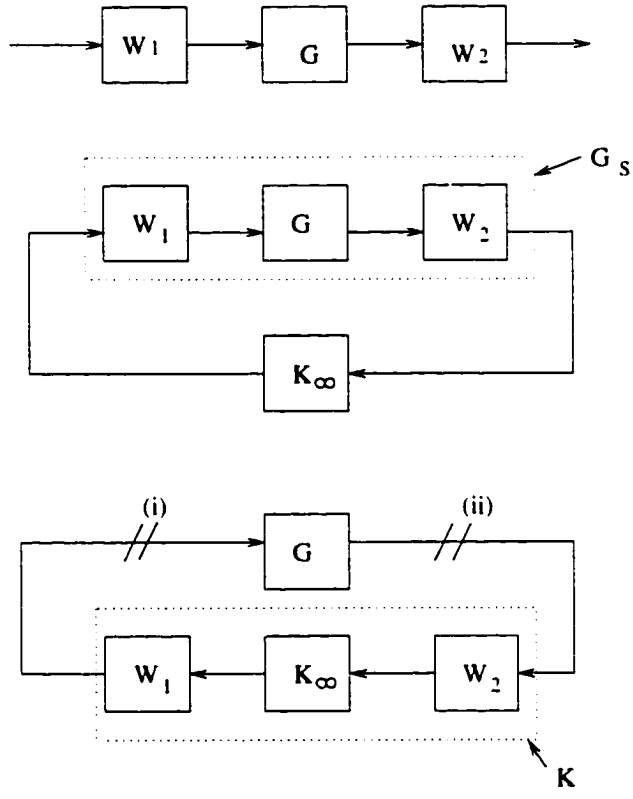

Figure 3.6 The loop shaping design procedure.

3.3 Literature Review

We are about to perform a robust stability assessment based on the ν gap metric concepts. Given a controller, using the gap metric based theory to assess its robustness

is a new topic in power system. The ν gap has a definite interpretation in frequency domain, this paper provides some examples of performing the analysis making use of the frequency response of the ν gap metric. In addition, the weighted ν gap is also investigated.

A power system stabilizer using H_∞ loop shaping procedure to stabilize a set of plants is designed. Here we will give a brief literature review on PSS design.

Power system stabilizers have been used for many years to add damping to electromechanical oscillations. They were developed to extend stability limits by modulating the generator excitation to provide additional damping to the oscillations of synchronous machine rotors [30]. Many methods have been used in the design of appropriate PSS, such as tuning the gain and time constants of the PSS, which are mostly lead-lag compensators, using a combination of modal frequency technique, root locus and sensitivity analysis [30, 27], pole placement [38], adaptive control [31], etc.

Recently, design of PSS using H_∞ optimal control has received considerably attention [56, 25, 19]. The resulting PSS achieves good robustness, meaning the controller has the ability to maintain the stability and the performance of the system under a wide range of operating conditions in spite of uncertainties in the system model. A common H_∞ design procedure involves uncertainty characterization and a mixed sensitivity optimization problem. Usually, the uncertainties are represented in additive and/or multiplicative ways with respect to the nominal plant. After that, the performance requirements are incorporated to form a mixed-sensitivity H_∞ problem to be optimized. The solution of the H_∞ problem consists of iterative adjustments of the weighting function and solving two set of Riccati equations.

The H_∞ robust stabilization combined with the classical loop shaping design procedure brought out by McFarlane and Glover [35] is a nice design process. A summary of the advantages it provides are as follows [42]:

- It is easy to apply and works very well in practice,
- It does not require iteration for its solution. and explicit formulas for the corresponding controllers are available,
- For a selected nominal plant. there is a closed formula for the maximum stability margin.
- Except for special systems. ones with all-pass factors. there are no pole-zero cancellations between the plant and controller. Pole-zeros cancellations are common in many H_∞ control problems and are a problem when the plant has lightly damped modes.

Ever since this design procedure was proposed. there have been many applications in industry. For power systems. Ambos [2].Pannett [40] *et al* used the procedure to design a controller for generator control. Graham [22] has designed robust controllers for FACTS devices to damp low frequency oscillations. In light of these successful applications. we introduce this design procedure to PSS design. and provide some basic guidelines for loop shaping weighting selection and controller design paradigm formulation.

The H_∞ loop shaping design procedure guarantees the stabilization of a plant set within a ball of certain radius in terms of the gap metric. It is naturally tied with the concept of gap metric and is an elegant approach to synthesize controllers.

3.4 Robust Stability Analysis in terms of the ν Gap in Power Systems

3.4.1 Robustness assessment using the ν gap metric

3.4.1.1 Robust stabilization theorem

A major concern in controller design in power systems is the robustness of the controller. In practice this translates into the ability of the controller to perform satisfactorily under a broad range of operating conditions. If we model the nominal plant as P_0, and when the operating condition changes, model the changed or perturbed plant as P, then the distance between P and P_0 can be measured either by the gap metric or the ν gap metric. From Chapter 3.2, we know that what the gap metric captured was the coprime factor type uncertainties.

Given a set of plants resulting from different operating conditions, we would like to first select a plant as the nominal plant in order to constrain all the other plants in a ball of the gap. To some extent, the stability margin $b_{P,C}$ provides the ability of the controller to stabilize a plant set. It is guaranteed that any plant within a distance of the value of $b_{P,C}$ from the nominal plant will be stabilized by the same controller. But the theorem does not exclude the possibility that a plant beyond this distance is stabilized by this controller. We will investigate the relationship between the stability margin and the ball of the ν gap metric.

We performed the robustness analysis test on both the four-machine system and the 50 machine system. The following steps were followed:

1. Set the standard feedback configuration:

2. When operating conditions change, the plant P varies to form a set of systems $\mathcal{P}$:

3. Calculate $\delta_\nu(P_1, P_2)$ for all $P_1, P_2 \in \mathcal{P}$. Choose a nominal plant P_0 accordingly and get the radius of a ball in the ν gap metric(β) that covers all the other plants.

4. Check if $b_{P_0,C} > \beta$ for the nominal plant P_0 to make conclusions on the robustness of the controller.

But the requirement of $b_{P_0,C} > \delta_\nu(P_0, P)$ for all $P \in \mathcal{P}$ is too strong. The theorem guarantees the stabilization of the plant set satisfying this condition with the controller, but didn't exclude the possibility that the same controller could stabilize plants outside this plant set. A looser conclusion is drawn by using the frequency response of the ν gap.

The following theorem is from [57]:

Theorem Suppose (P_0, C) is stable and $\delta_\nu(P_0, P_1) < 1$. Then (P_1, C) is stable if

$$b_{P_0,C}(\omega) > \psi(P_0(j\omega), P_1(j\omega)), \forall\omega.$$

Where $b_{P_0,C}(\omega)$ and $\psi(P_0(j\omega), P_1(j\omega))$ are defined as follows:

$$\begin{aligned} \frac{1}{b_{P_0,C}(\omega)} &:= \bar{\sigma}\left(\begin{bmatrix} I \\ C(j\omega) \end{bmatrix}(I - P(j\omega)C(j\omega))^{-1}[P(j\omega)\ I]\right) \\ \psi(P_0(j\omega), P_1(j\omega)) &:= \bar{\sigma}(\Psi(P_0(j\omega), P_1(j\omega))) \end{aligned}$$

and $\Psi(P_0(j\omega), P_1(j\omega)) := (I+P_1(j\omega)^* P_0(j\omega))^{-1/2}(P_0(j\omega)-P_1(j\omega))(I+P_1(j\omega)^* P_0(j\omega))^{-1/2}$ as in the definition of the ν-gap.

By generating the frequency response of $b_{P_0,C}(\omega)$, whose infimum over the frequency is the value of stability margin $b_{P_0,C}$, and that of $\psi(P_0(j\omega), P_1(j\omega))$, whose supremum over frequency is the value of $\delta_\nu(P_0, P)$, we only need the value of $b_{P_0,C}(\omega)$ when it is greater than $\psi(P_0(j\omega), P_1(j\omega))$ at each corresponding frequency points by the above theorem. While the previous condition $b_{P_0,C} > \delta_\nu(P_0, P)$ requires $b_{P_0,C} = \inf_\omega b_{P_0,C}(\omega) > \psi(P_0(j\omega), P_1(j\omega))$ for all frequencies, the condition is relaxed to a great extent.

3.4.1.2 Test on four machine system

In the four machine system, we selected five plants by varying the exporting power on the tie line:

$$P_1 : P_{exp} = 0.MW;$$

$$P_2 : P_{exp} = 100.MW;$$

$$P_3 : P_{exp} = 200.MW;$$

$$P_4 : P_{exp} = 300.MW;$$

$$P_5 : P_{exp} = 400.MW;$$

All the five plants are equipped with ETMSP type 30 excitation system and are stable. If we use a PSS at machine AR2G2 as controller, all the five systems will still be stable with the PSS.

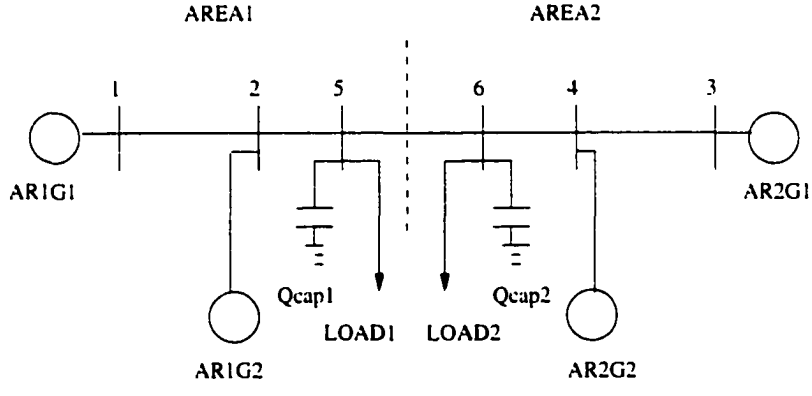

Figure 3.7 Four-machine two-area test system.

Calculate the ν-gap between these plants. The i-jth entry in table 3.1 represents $\delta_{\nu ij}$.

If we choose plant P_1 as the nominal plant, then the radius of the ν gap ball that can cover all the plants is 0.3704. Next we calculate the stability margin and continue to take P_1 as nominal plant, $b_{P_1,C} = 0.0211$. Now $b_{P_1,C} < \delta_\nu$, so no conclusions can be drawn on the stability of the inter-connection of the plants and the controllers.

Table 3.1 The ν-gap between the plants

δ_ν	1	2	3	4	5
1	0	0.0371	0.1102	0.1883	0.3704
2	0.0371	0	0.1021	0.1890	0.3713
3	0.1102	0.1021	0	0.1862	0.3719
4	0.1883	0.1890	0.1862	0	0.3715
5	0.3704	0.3713	0.3719	0.3715	0

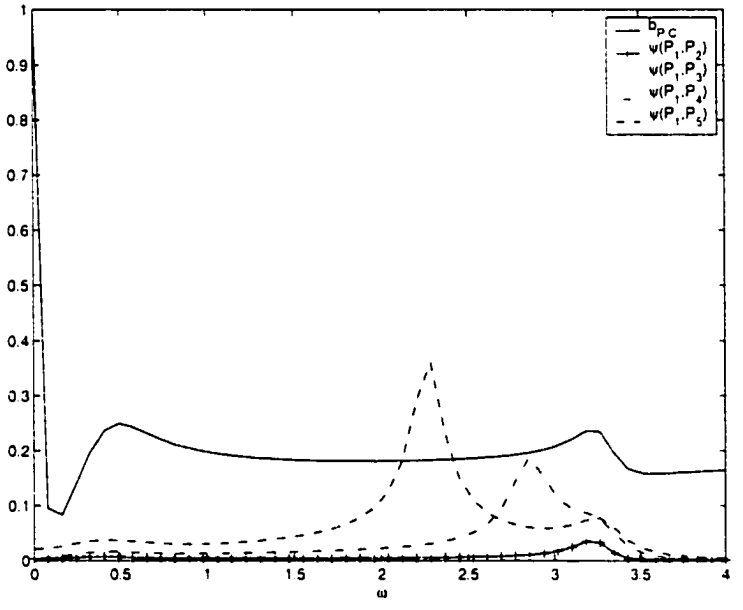

Figure 3.8 Frequency responses of $b_{P_1C}(\omega)$ and $\psi(P_1, P_i)$.

Now we choose P_1 as the nominal plant and draw the frequency responses of $b_{P_1,C}(\omega)$ and $\psi(P_1(j\omega), P_i(j\omega))$, for $i = 2, \cdots, 5$

From the figure, we may use Theorem 3.4.1.1 to conclude that plant P_2 and P_3 can be stabilized by the controller. But we observe that at some frequencies, $\psi(P_1(j\omega), P_4(j\omega))$ and $\psi(P_1(j\omega), P_5(j\omega))$ exceed $b_{P_1,C}(\omega)$ while in fact, the controller can stabilize both P_4 and P_5. This happens because Theorem 3.4.1.1 only gives the sufficient condition for (P_i, C) to be stable.

Different plants other than P_1 have been tested as nominal plant, and the fre-

quency responses of $\psi(P_0(j\omega), P_i(j\omega))$ and $b_{P_0,C}(\omega)$ were drawn. Similar curves are obtained (there exist some frequencies where $\psi(P_0(j\omega), P_i(j\omega))$ exceeds $b_{P_0,C}(\omega)$ for some plant P_i).

3.4.1.3 Test on the 50-machine system

The one-line diagram of the area of interest for for the 50 machine system is shown in Figure 2.10. Vary the operating condition to select three plants as follows:

P_0 : under stressed operating condition;

P_1 : remove one of the lines between bus 12 and 14 in P_0;

P_2 : remove one of the lines between bus 12 and 25 in P_0;

all three plants are unstable plants.

Next, calculate the ν-gap between these plants:

$$\delta_\nu(P_0, P_1) = 0.0320$$

$$\delta_\nu(P_0, P_2) = 0.0324$$

$$\delta_\nu(P_1, P_2) = 0.0223$$

Four PSS's are equipped at bus 93, 104, 110, 111 respectively as controllers. With the set of controllers, all three plants are stable(verified both by MASS and by MATLAB program).

If P_1 is chosen as nominal plant, $b_{P_1,C} = 0.00353 \Rightarrow b_{P_1,C} < \delta_\nu(P_i, P_j), \forall i, j, i \neq j$. Thus, by the sizes of $b_{P_1,C}$ and δ_ν, no conclusions can be drawn on the stability of the inter-connection of the plants and the controllers.

Now we choose P_2 as the nominal plant and draw the frequency responses of $b_{P_2,C}(\omega)$ and $\psi(P_2(j\omega), P_i(j\omega))$, for $i = 1, 3$

From the figure, we can see that at all the frequencies the curves of $\psi(P_2(j\omega), P_1(j\omega))$ and $\psi(P_2(j\omega), P_3(j\omega))$ are strictly under that of $b_{P_2,C}(\omega)$, even though the supremum of

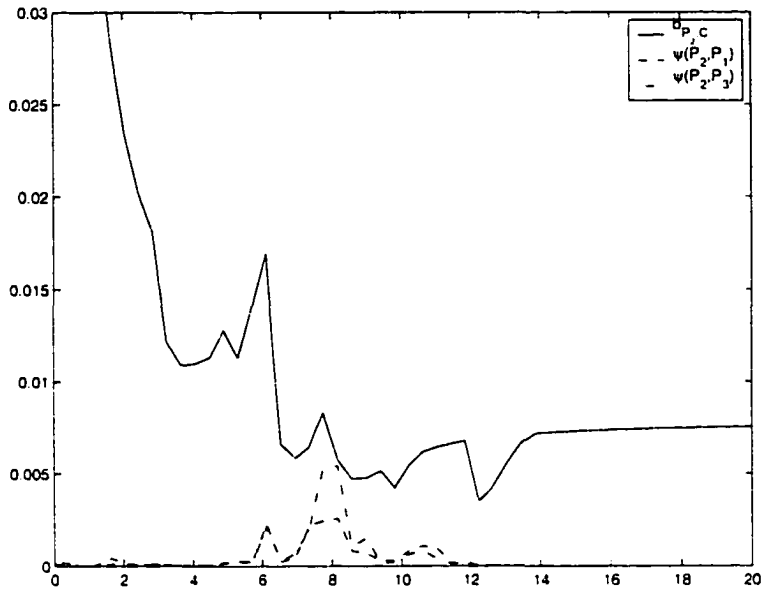

Figure 3.9 Frequency responses of $b_{P_2,C}(\omega)$ and $\psi(P_2, P_i)$.

the former is greater that the infimum of the latter. By Theorem 3.4.1.1, we conclude that the controller can stabilize both P_1 and P_3.

The results from the tests show that the robust stability criteria in terms of the ν gap metric sometimes is too conservative to make conclusions on the robustness of the controller. However the ν gap metric has an explicit frequency domain interpretation which helps to reduce the conservatism.

To further reduce the conservatism, the weighted ν gap metric is introduced to include the frequency domain "scaling" for the spaces of inputs and outputs. Now it is possible to scale each input and output channel in different factors. By introducing the scale factors, we treat the distance between two systems in different "direction" by different weights. Instead of using the unify weighting to measure the perturbation in a ball, this weighted ν gap allows to put more weights at the direction where large distance exists. Note that the weighting itself is a stable system, this allows to scale each input or output channel in the frequency domain. One may decide the frequency response of the

weighting from the comparison of the original frequency response of the ν gap metric with that of the stability margin. For those frequency range where the two are closer, more works need to be done. In the following section, the concepts of weighted ν gap metric is introduced and examples of using it are given.

3.4.2 Weighted ν gap metric

3.4.2.1 Robust stability theorem

First we define the weighted ν gap

$$\delta_\nu(P_1, P_2; W_o, W_i) := \delta_\nu(W_o P_1 W_i, W_o P_2 W_i;).$$

Using the fact that $[P, C]$ is stable if and only if $[W_o P W_i, W_i^{-1} C W_o^{-1}]$ is stable(as illustrated in Figure 3.10), similar property for the frequency responses of the original ν gap in the theorem also holds for the weighted ν gap.

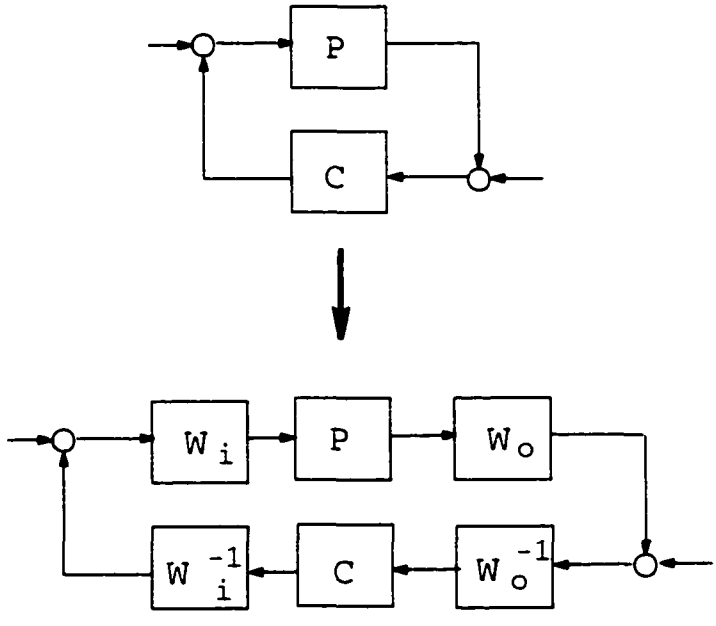

Figure 3.10 The equivalent feedback configurations.

Corollary Suppose(P_0, C) is stable and $\delta_\nu(P_0, P_1; W_o, W_i) < 1$. Then (P_1, C) is stable if

$$b_{W_o P_0 W_i, W_i^{-1} C W_o^{-1}}(\omega) > \psi(W_o P_0 W_i(j\omega), W_o P_1 W_i(j\omega)), \forall \omega.$$

The advantage of using the weighted ν gap is, by choosing input and output weighting functions W_i and W_o, the distances between systems are measured after having scaled their domain and range spaces. It is possible to further reduce conservatism when assessing the stability of the interconnected systems.

3.4.2.2 Test on the frequency responses of the weighted inter-connection

In the four machine system, we chose the same five plants by varying the exporting power on the tie line from $0MW$ to $400MW$.

As in the previous case, all the five plants are equipped with ETMSP type 30 excitation system and are stable. Suppose we use a PSS at machine AR2G2 as controller. All the five systems are known to be stable with the PSS.

Notice that in Figure 3.8 the peak of the distance between P_5 and P_1 happens at around $\omega = 2.0408 rad/s$. So we focus on working at approximately this frequency. If we choose $W_o = I$, $W_i = 30\frac{(0.1s+4)^2}{(s+4)^2}$ then the frequency response of $b_{W_o P_0 W_i, W_i^{-1} C W_o^{-1}}(\omega)$ and $\psi(W_o P_0 W_i(j\omega), W_o P_1 W_i(j\omega))$ will look like figure 3.11.

According to the Corollary, we can conclude that P_5 can be stabilized by the same controller. This gives a less conservative conclusion compared to that of Theorem 3.4.1.1.

The above tests show that it is possible to deal with the conservatism problem by appropriately selecting the weighting functions to shape the input and output channels. But the weighting selection invloves trial and error, and there is no gurantee that a weighting can always be found for the stable case. Thus we suggest only for rough estimation the ν gap metric tool be used. If it gives too conservative results, use the μ analysis instead.

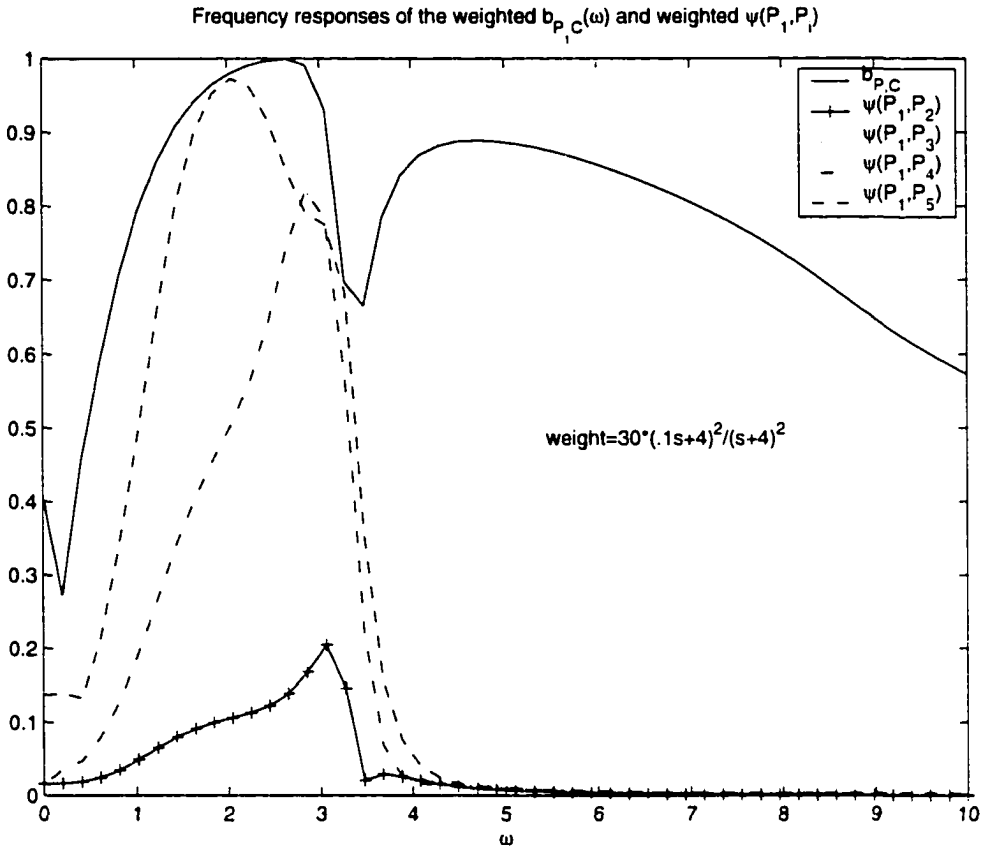

Figure 3.11 Frequency response of weighted ν gap.

3.5 Robust Controller Design

3.5.1 H_∞ Loop shaping controller design

In previous research, the μ synthesis approach has been used to design PSS [32, 33, 34, 51]. The design procedure invloves "D-K" iteration, which is computationally intensive and the resulting controller is of high order. In this chapter, we will design a robust PSS using the H_∞ loop shaping procedure. It is an easily implementable method, and the design gurantees a controller that can stabilize a plant set within a gap metric ball with a certain radius.

Although the details of the design procedure can be found in Section 3.2, here we form

the specific feedback structure for our problem. As shown in Fig 3.12, the weighting function W_a is chosen to shape the open-loop system to make to closed-loop system achieve good disturbance attenuation. The shaping objective is to make the output $y = \Delta\omega$(the generator speed variation) as small as possible in the presence of the disturbance signal $d = \Delta V_{ref}$. Since the frequency of the inter-area mode oscillation is around $3rad/sec$, the performance objective has been translated to increase the open-loop gain around that frequency so as to make the transfer function between d and y, which is $P(I - PW_a)^{-1}$, as small as possible.

An H_∞ controller was then synthesized to ensure the robust stability of the closed-loop system. Finally the H_∞ controller, K_∞ was cascaded with the shaping function W_a to form the final controller $K = K_\infty W_a$.

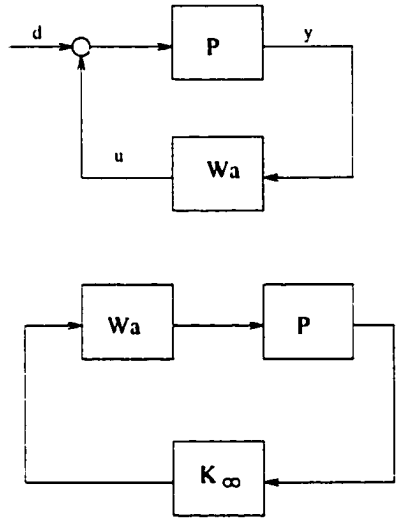

Figure 3.12 The H_∞ loop shaping design.
(Above: Step 1 - Loop shaping;
Below: Step2 - H_∞ synthesis.)

3.5.2 Simulation results

In the four machine system. we selected five plants by varying the exporting power on the tie line:

$$\begin{aligned} P_1 : P_{exp} &= 0MW; \\ P_2 : P_{exp} &= 100MW; \\ P_3 : P_{exp} &= 200MW; \\ P_4 : P_{exp} &= 300MW; \\ P_5 : P_{exp} &= 400MW; \end{aligned}$$

All the five plants are equipped with ETMSP type 30 excitation system. and all five plants are stable but have poorly damped inter-area modes. As studied in [27]. different location of the PSS will result in different damping effect. As has been shown. the case when only 1 PSS is installed at the machine close to the tie line in the sending area has the worst performance and stability behavior. It even destabilizes the most stressed plant. We would choose this case to design our controller. The resulting controller not only stabilizes all the plants but also demonstrates very good damping ability.

3.5.2.1 Loop shaping

We chose the weighting function by shaping the nominal plant according to our performance objective. The weighting function was chosen as

$$W_a = \frac{186.5 \times 10s(1 + 0.33s)}{(1 + 10s)(1 + 0.1852s)}.$$

There was a washout filter block in W_a with time constant 10s to ensure the controller only works in a transient state. The selection of the pole at $\frac{1}{0.1852}$ and the zero at $\frac{1}{0.33}$ increased the gain around the frequency of interest so that the disturbance with frequency around that range can be attenuated effectively.

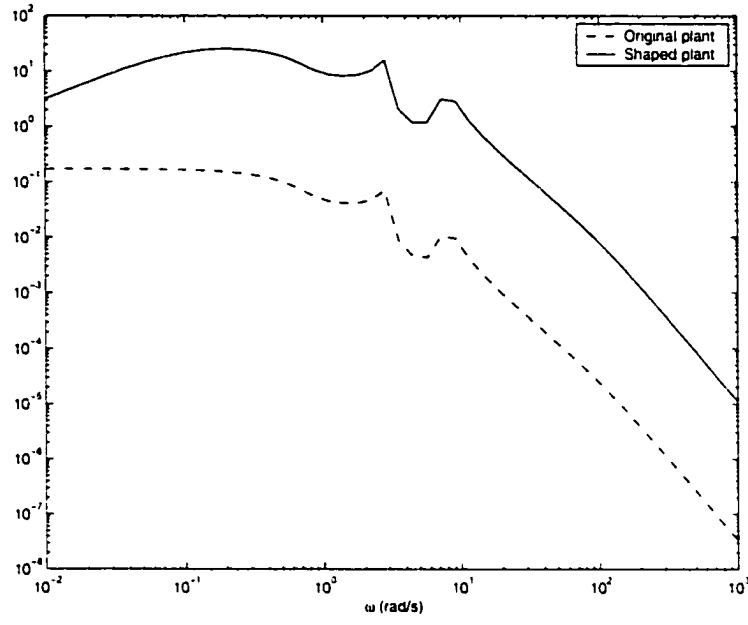

Figure 3.13 Comparison of the open-loop gains between the original plant and the shaped plant.

The resulting open-loop gain from the reference voltage variation to the generator speed variation is shown in Fig 3.13.

3.5.2.2 H_∞ synthesis

Next, we synthesized a K_∞ to achieve robust stability for the nominal plant. The maximum stability margin of this controller is 0.4975, which is large enough and indicates the feasibility of our loop shaping design. According to McFarlane and Glover [35], given the normalized LCF of the nominal plant as $P_0 = \tilde{M}^{-1}\tilde{N}$, this controller can stabilize all $P = (\tilde{M} + \Delta_M)^{-1}(\tilde{N} + \Delta_N)$ satisfying $\|[\Delta_M, \Delta_N]\| < 0.4975$. Furthermore, according to Georgiou [20], the ball of uncertainty in the gap metric is equal to a ball of uncertainty of the same radius defined by the normalized coprime factorization. Thus, in terms of the gap metric, all P with $\delta_g(P, P_0) < 0.4975$ can be stabilized by this controller.

We listed the gap between the weighted plants($P_{si} = P_i W_i, i = 1, \cdots, 5$) in Table 3.2.

Table 3.2 The Gap Between the Weighted Plants

$\delta_g(P_{s4}, P_{s1})$	$\delta_g(P_{s4}, P_{s2})$	$\delta_g(P_{s4}, P_{s3})$	$\delta_g(P_{s4}, P_{s5})$
0.3463	0.2615	0.1698	0.2215

Thus all the plants can be stabilized by this controller, or the controller achieves robust stability.

The final controller is the combination of W_a with K_∞, that is $W_a K_\infty$. To check the performance of this controller, the frequency response of the closed-loop singular values are given in Fig 3.14.

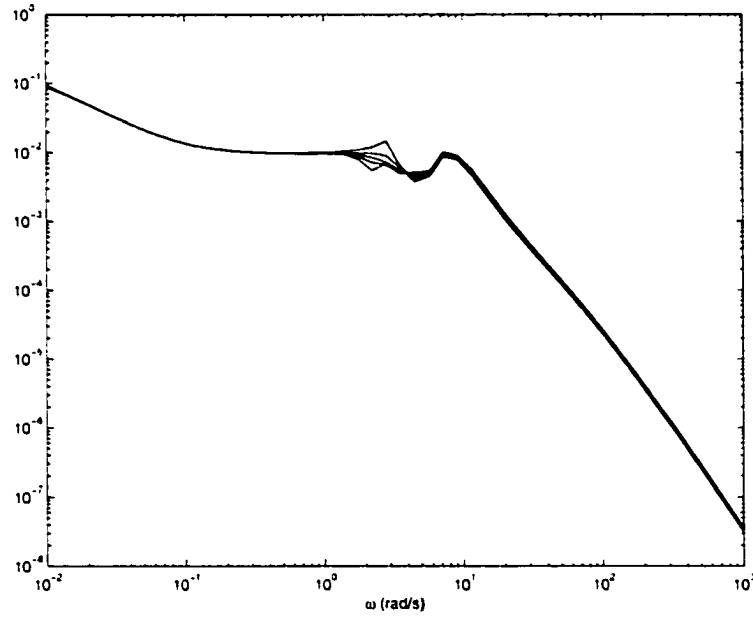

Figure 3.14 Singular values of closed-loop transfer functions: $\bar{\sigma}((I - PK)^{-1}P)$ for five plants.

The frequency response of the singular value for all five closed-loop transfer functions (from the voltage disturbance to the generator speed variation) are shown in Fig 3.14. The gains around 3 *rad/sec* are small which shows good disturbance attenuation for oscillations with such frequency. The minimum damping ratio for the nominal plant is

only 0.0246. After adding the designed controller, the nominal and perturbed closed-loop systems have a minimum damping ratio of 0.1449 for the nominal system, and 0.1245 for the perturbed system.

We would also like to see how much the open-loop shape has been changed because of the inclusion of K_∞. Comparing the curves in Fig 3.15, it can be seen that the robust stabilization stage has not significantly altered the desired loop shape.

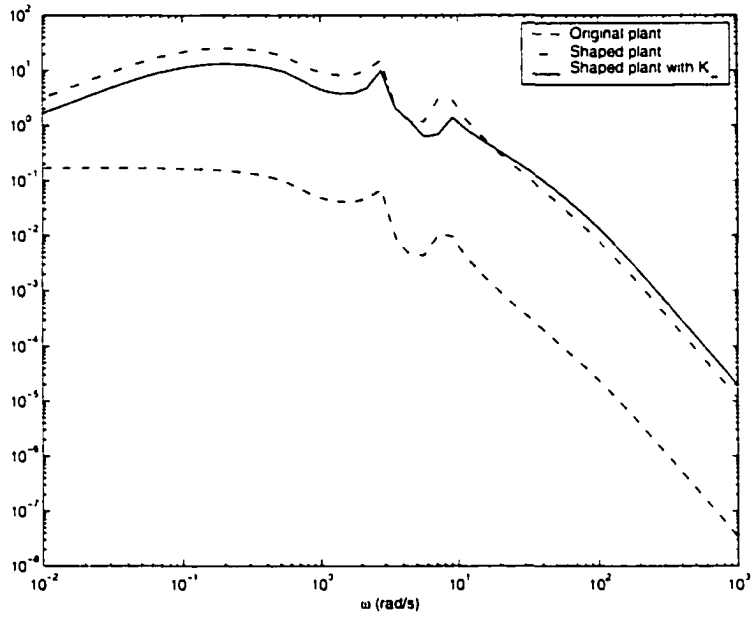

Figure 3.15 Comparison of open loop singular values.

3.5.2.3 Controller model reduction

We want to conduct a nonlinear simulation using ETMSP to see the performance of the designed controller. The resulting controller has a high order($27th$) while ETMSP can only handle a user defined model up to the $8th$ order. The controller is reduced to a 7 order controller using the Hankel Norm reduction.

The state space representation of the reduced order controller is as follows.

$$A = \begin{bmatrix} -24.2384 & -6.5548 & 8.5212 & 2.6300 & 1.5281 & 5.3913 & -0.9227 \\ 7.5266 & -13.7842 & -2.2902 & -4.5975 & -1.7136 & 5.4652 & -1.2115 \\ 0 & 0 & -1.0422 & -5.7732 & -0.2795 & -0.7951 & 0.2044 \\ 0 & 0 & 4.9026 & -0.7908 & -0.4977 & 1.1849 & -0.3540 \\ 0 & 0 & 0 & 0 & -0.1202 & -2.8912 & -0.1562 \\ 0 & 0 & 0 & 0 & 3.2674 & -1.2369 & 0.6295 \\ 0 & 0 & 0 & 0 & 0 & 0 & -0.0888 \end{bmatrix}$$

$$B = \begin{bmatrix} 113.8980 & -17.6032 & -17.4600 & 0.1204 & -3.2935 & -11.8868 & 2.9512 \end{bmatrix}^T$$

$$C = \begin{bmatrix} -111.4803 & -9.4906 & 27.1835 & 4.4597 & 1.9801 & 20.0392 & -5.0941 \end{bmatrix}$$

$$D = 583.3225$$

The transfer function of the reduced order controller is given below:

$$G_k(s) = \frac{583.3s^7 + 10828s^6 + 82531s^5 + 588160s^4 + 2.49 \times 10^6 s^3 + 4.97 \times 10^6 s^2 + 1.03 \times 10^7 s - 36500}{s^7 + 41.3s^6 + 549.6s^5 + 2895.8s^4 + 18506s^3 + 34149s^2 + 1.1 \times 10^5 s + 9516.6}$$

The bode plots of the full-order controller and the reduced-order controller are shown in Fig 3.16 to verify the accuracy of the model reduction.

3.5.2.4 Nonlinear simulation

Nonlinear simulation is performed using ETMSP to test the efficacy of the designed controller. A three-phase short circuit fault is applied at bus 6 for $10ms$: the tie line real power flow is monitored.

The performance of the designed controller is compared with that of a conventional PSS, which has been tuned using the procedure described in [29]. The conventional PSS is designed for the case where the tie line exporting power is 0MW. It works well and has a good damping effect under this specific operating condition. But when the operating point changes and the system becomes more stressed, the improperly tuned PSS even

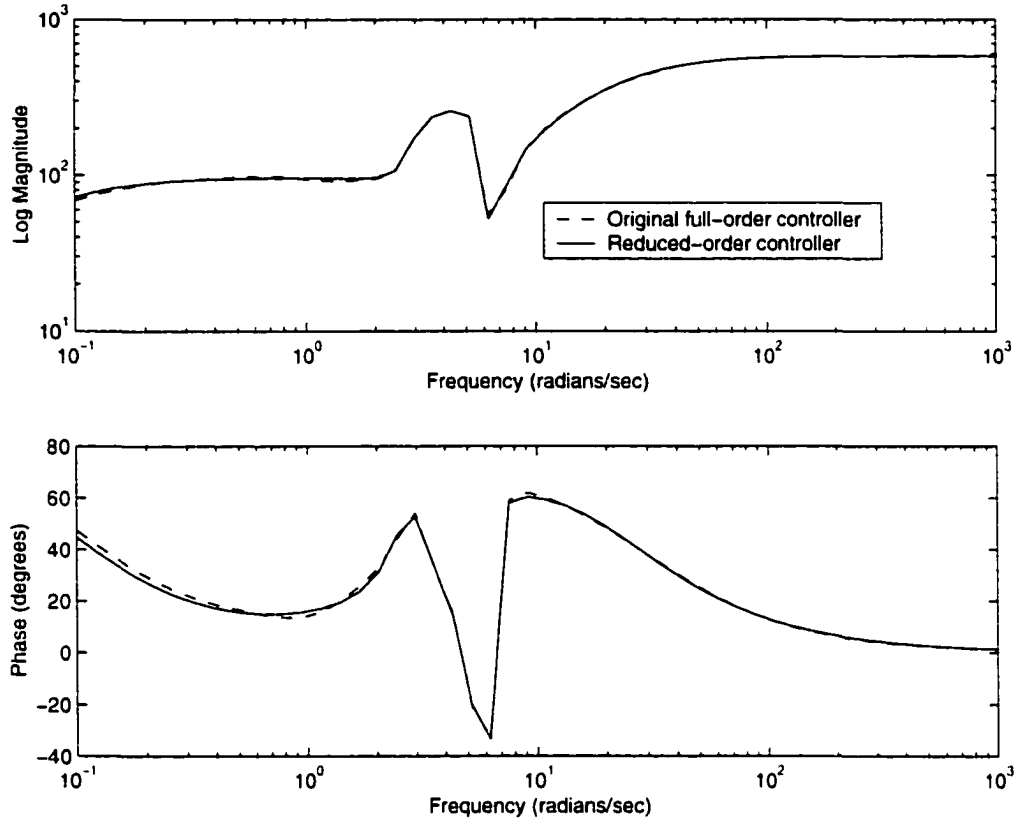

Figure 3.16 Bode plots comparison of full-order controller and the reduced-order controller.

destabilizes the system. It is observed that the PSS designed using the loop shaping procedure and the H_∞ approach provides good damping in the entire range of operating conditions.

In this case, if we tune the conventional PSS properly at the operating point where the exporting power is 400MW, it should work well and stabilize the plant at this operating point. And since it works for a stressed operating condition, it might also work for the less stressed operating condition when the exporting power is 0MW. But such design approach is not a systematic way and cannot guarantee robustness. We chose 0MW case to tune the PSS and make comparison just want to emphasis on this point.

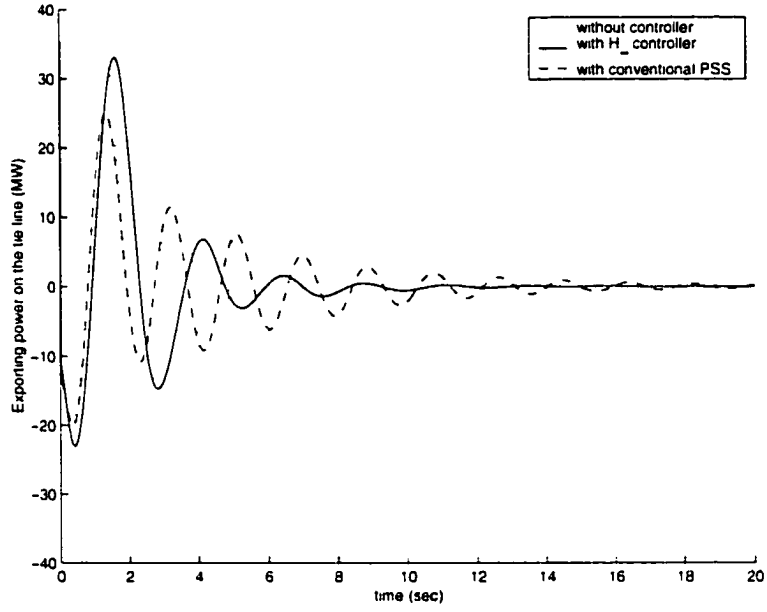

Figure 3.17 Comparison between the H_∞ loop shaping controller and the conventional PSS ($0.MW$ case).

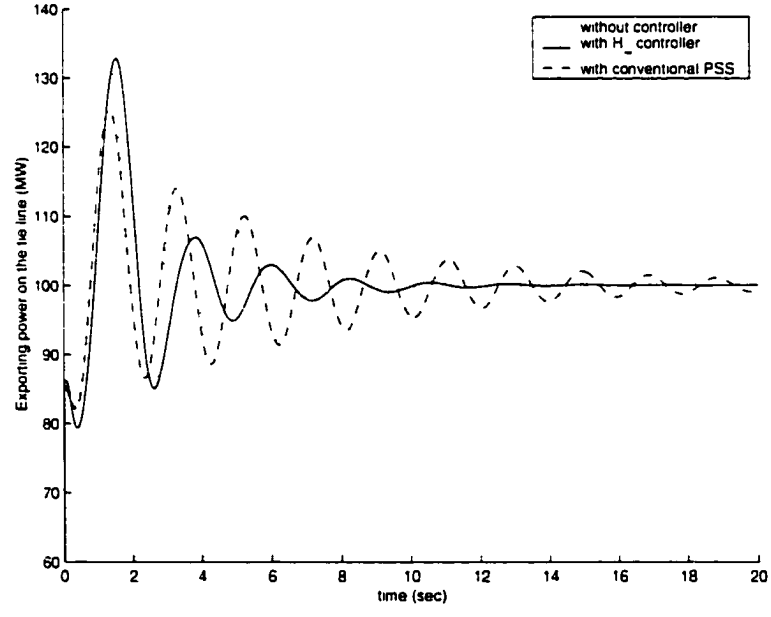

Figure 3.18 Comparison between the H_∞ loop shaping controller and the conventional PSS ($100.MW$ case).

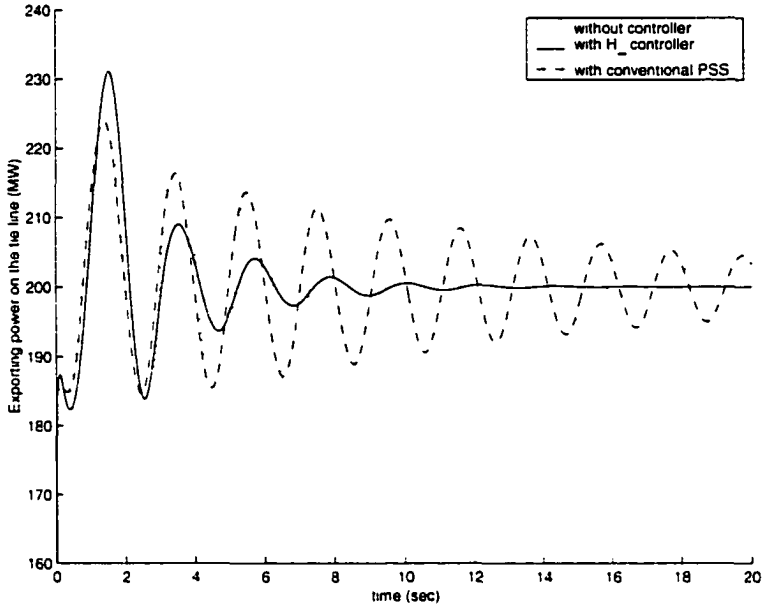

Figure 3.19 Comparison between the H_∞ loop shaping controller and the conventional PSS ($200MW$ case).

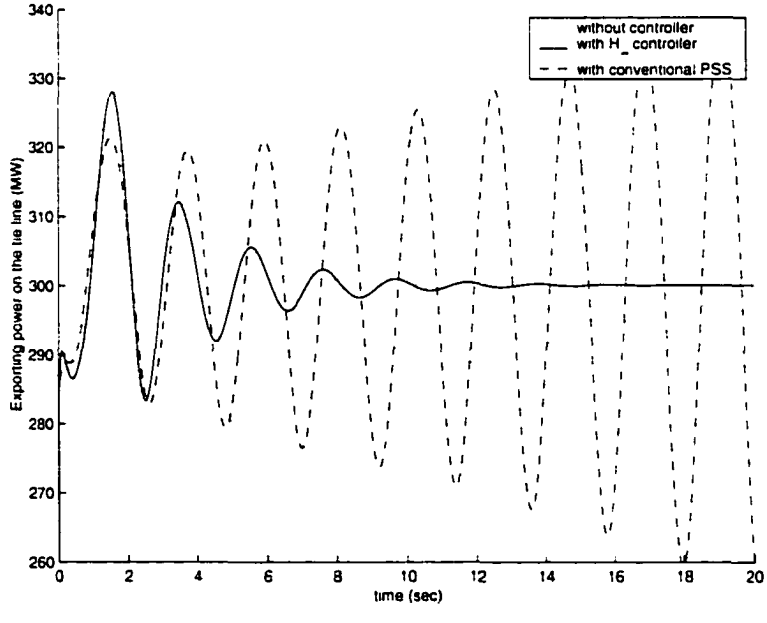

Figure 3.20 Comparison between the H_∞ loop shaping controller and the conventional PSS ($300MW$ case).

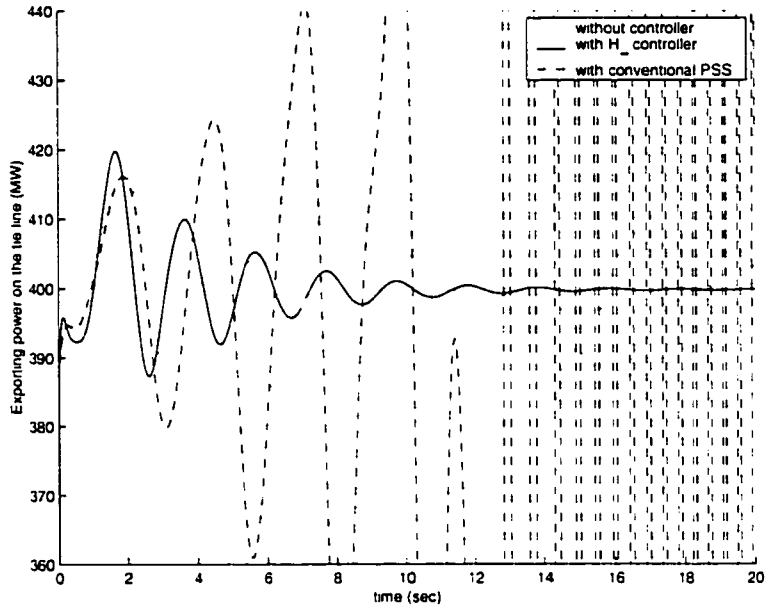

Figure 3.21 Comparison between the H_∞ loop shaping controller and the conventional PSS ($400MW$ case).

The comparison is also made between the H_∞ loop shaping controller and the μ controller. From the simulation results shown in Figure 3.22 to Figure 3.26, we see that both controllers achieve robust performance and damp the oscillations for the whole operation range very well. However, the design procedure for the μ controller is more complex than the H_∞ loop shaping. Besides the selection of the weighting function, it involves DK-iterations and will generate a controller with a much larger order than the H_∞ loop shaping controller. Moreover, sometimes it even has convergence problem (see the discussion at the beginning of this chapter).

3.5.2.5 Robustness validation by SSV approach

To further validate the robustness of the designed H_∞ loop shaping controller, the branch and bound scheme proposed in Part 2 based on the Structured Singular Value calculation is performed on the system equipped with the designed controller.

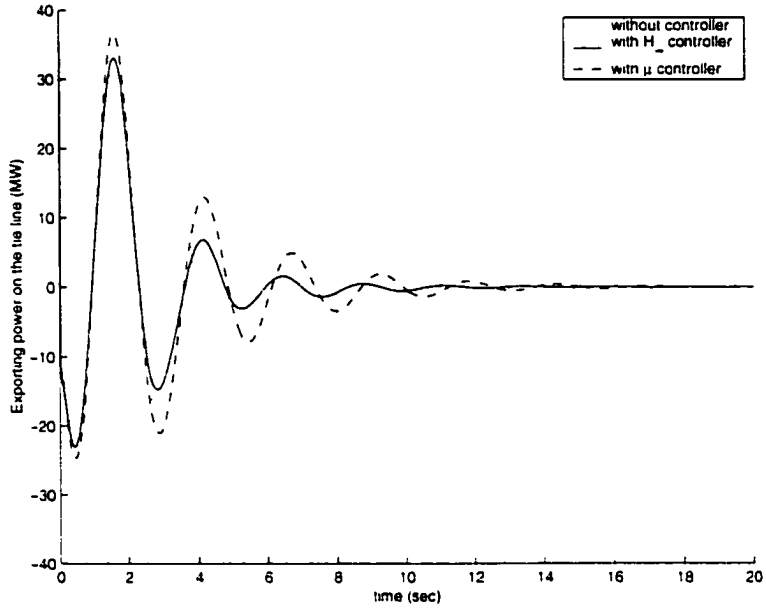

Figure 3.22 Comparison between the H_∞ loop shaping controller and the μ controller ($0MW$ case).

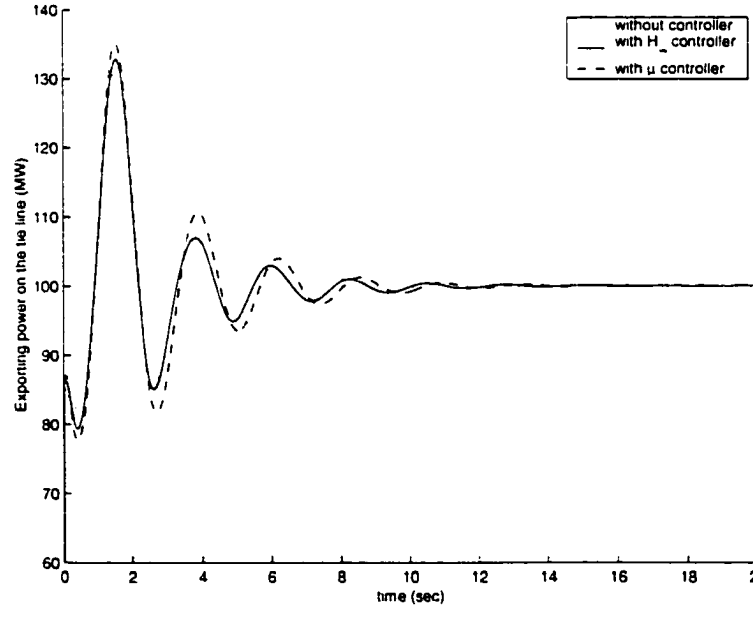

Figure 3.23 Comparison between the H_∞ loop shaping controller and the μ controller ($100MW$ case).

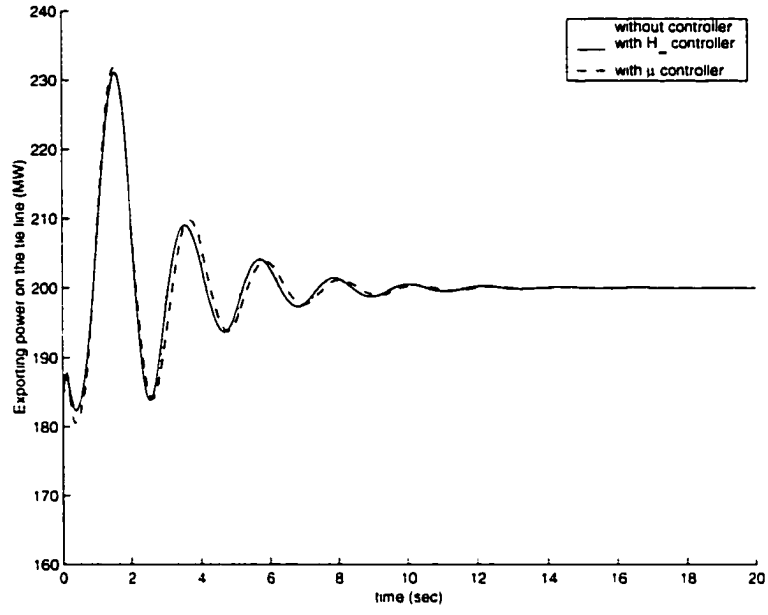

Figure 3.24 Comparison between the H_∞ loop shaping controller and the μ controller ($200MW$ case).

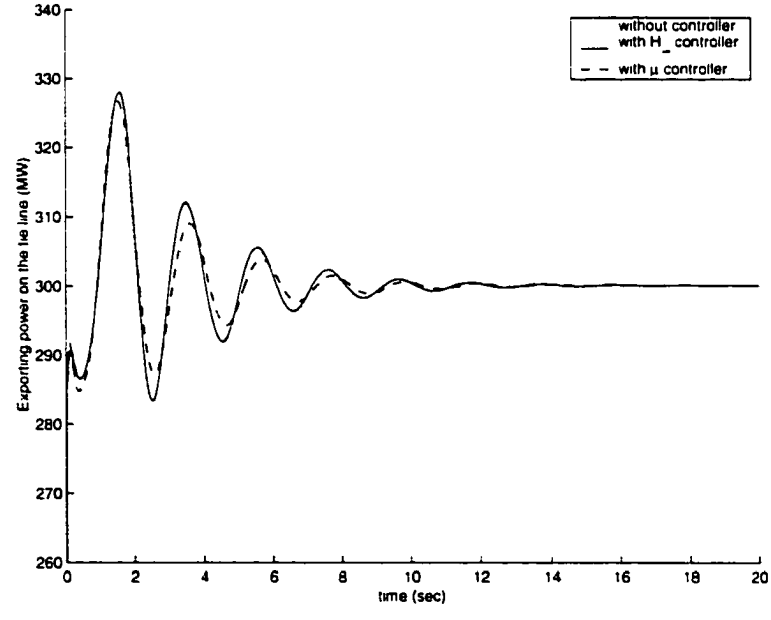

Figure 3.25 Comparison between the H_∞ loop shaping controller and the μ controller ($300MW$ case).

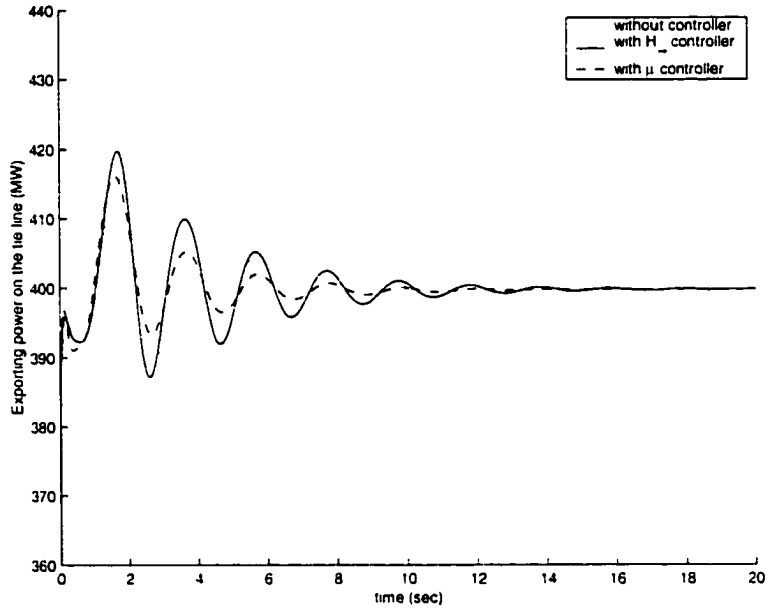

Figure 3.26 Comparison between the H_∞ loop shaping controller and the μ controller ($400MW$ case).

The initial frequency range is chosen as $[0, 100] rad/s$ and the tolerance is set to $0.1s$. Bounded frequency tests are performed at each frequency subintervals. Large frequency intervals with $\bar{\mu} < 1$ are eliminated. Finally, only within the interval range $[0, 0.19531] rad/s$, we have $\bar{\mu} > 1$. The upper bound of μ is shown in Figure 3.27.

The followed frequency sweep test performed on the interval $[0, 0.19531] rad/s$ immediately excludes the existence of instability points: see Figure 3.28. Besides, the frequency sweep test is also performed over the interval $[2.53, 3.52] rad/s$ which is the frequency interval where oscillations might occur. The resulting μ plot is shown in Figure 3.29. The peak value of the μ upper bound is 0.6193, indicating good robustness of the designed controller.

As a comparison, we also include the branch and bound frequency test results for the convensional PSS (Figure 3.30 and Figure 3.31) and the μ controller (Figure 3.32 and Figure 3.33). The peak value of the μ for the conventional PSS and the μ con-

troller are 3.0 and 0.422 respectively. These results show that the μ controller also has good robustness while the conventional PSS cannot achieve robustness. The results are consistent with the nonlinear simulation.

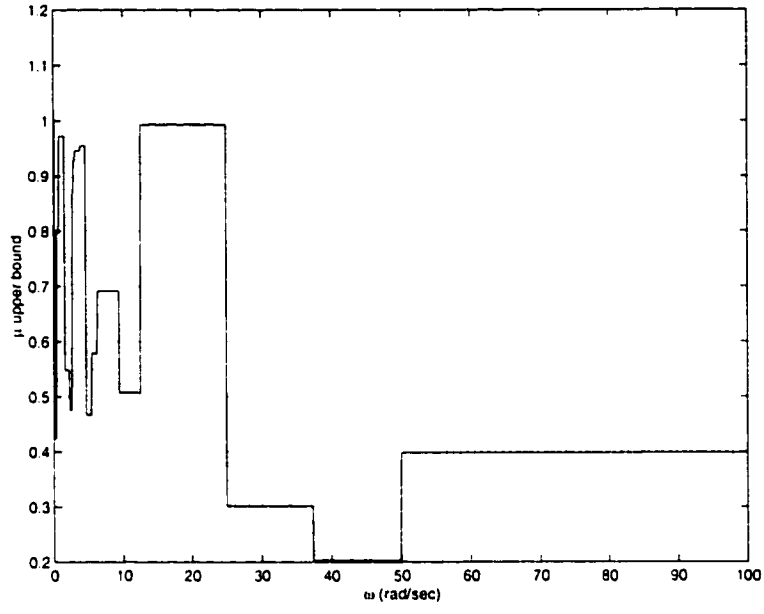

Figure 3.27 Branch and bound scheme result for the H_∞ controller.

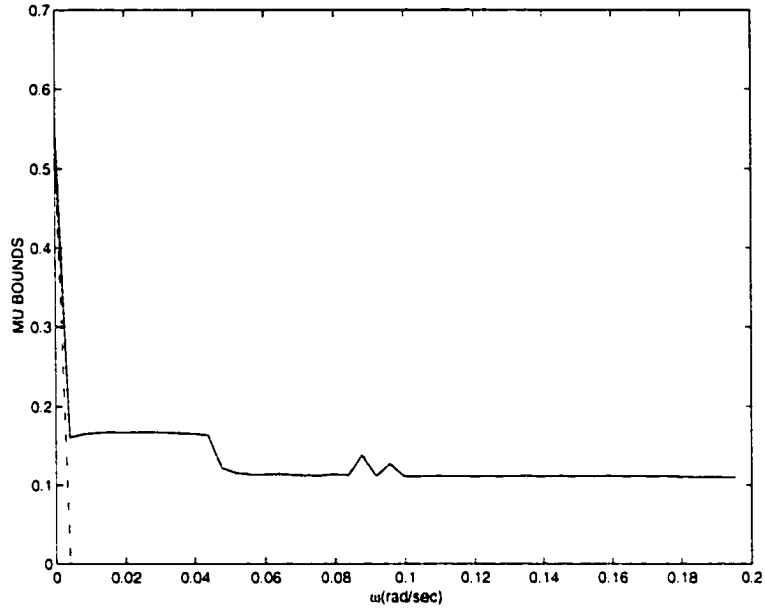

Figure 3.28 Frequency sweep test for $[0.0.19531]rad/s$.

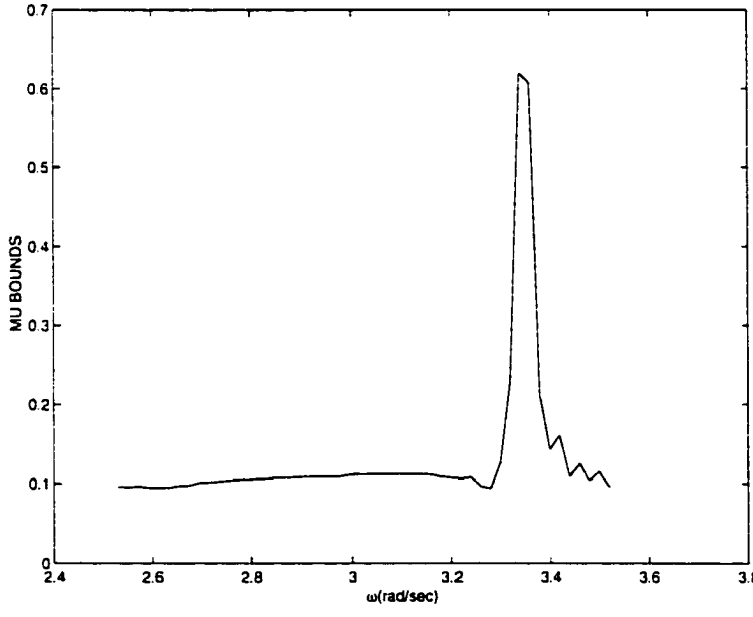

Figure 3.29 Frequency sweep test for $[2.53.3.52]rad/s$.

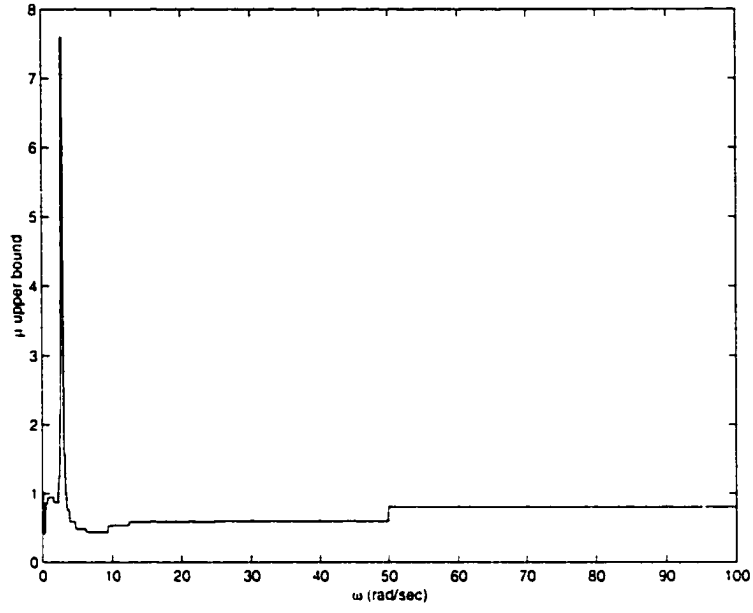

Figure 3.30 Branch and bound test result for the conventional PSS.

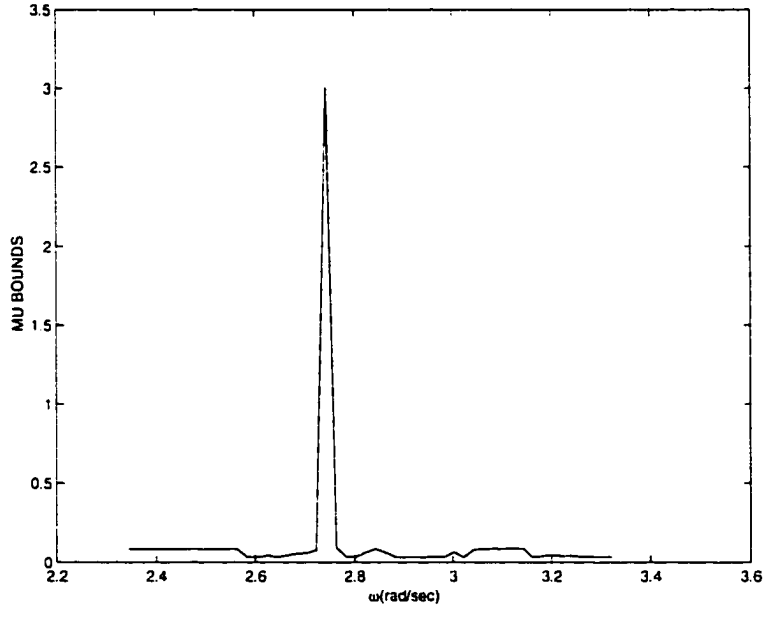

Figure 3.31 Frequency sweep test for the conventional PSS over $[2.34, 3.32] rad/s$.

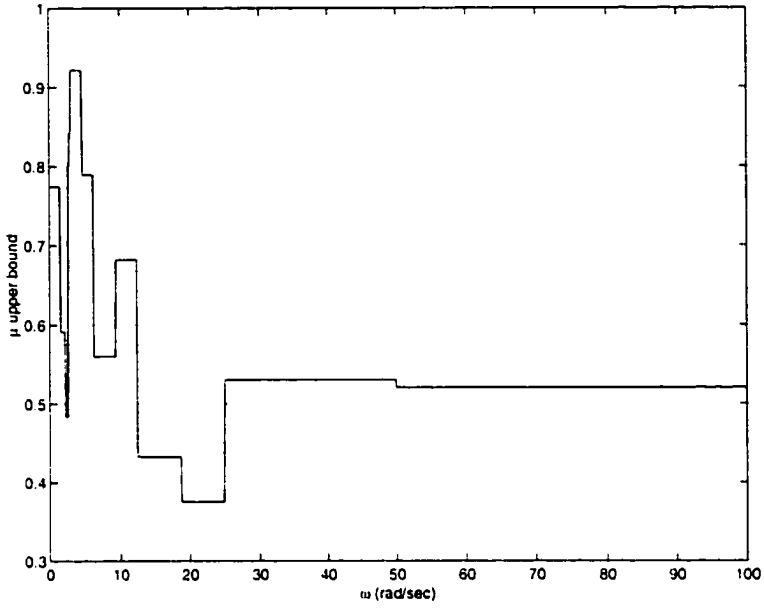

Figure 3.32 Branch and bound test result for the μ controller.

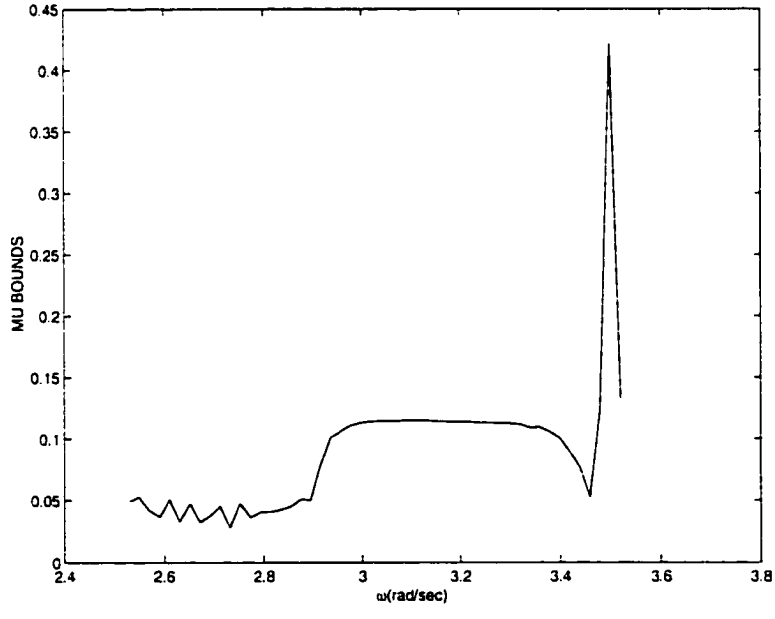

Figure 3.33 Frequency sweep test for the μ controller over $[2.53, 3.52] rad/s$.

4 CONCLUDING REMARKS

4.1 Conclusions

Two kinds of analysis tools were investigated to evaluate the power system robustness. The main work completed in this research is summarized as follows:

For the structured singular value part.

1. The linearized model of power system including PSS was developed. Based on this model, a new way to characterize the uncertainty was proposed. Various operating conditions were model as parametric uncertainties, and were captured by the polynomial approximation. In order to convey more information from the algebraic equation and achieves more accurate results, the uncertainties in the algebraic equations and the differential equations were extracted separately. The general framework for the robust stability of the power system under different operating conditions was formulated.

2. For the case of one parameter uncertainty, the spectral radius was calculated as the exact value of μ. This proved to be very quick approach to obtain the worst case parameter.

3. By extracting the frequency variable as an additional uncertainty, the bounded frequency test can be performed on a certain frequency interval to determine whether instability points exist over that interval. Based on the bounded frequency test, the branch and bound scheme proposed can effectively select frequency intervals

where instability might happen. This provides an intelligent way to perform the frequency sweep test to generate μ plots and obtain the parameter range for the system to maintain stability. Since the frequency range has been mapped inclusively, no frequency points will be ignored even if discontinuities exist on the μ plot.

For the ν gap metric part,

1. Ways to apply the robust stability assessment in terms of the ν gap metric to power systems were established. The frequency response explanation of ν gap metric was explored based on the power system plant set with parametric uncertainties.

2. The McFarlane and Glover [35] H_∞ loop shaping design procedure was implemented for power system stabilizer design. A systematic way to design H_∞ loop shaping controller was presented by constructing the feedback structure and selecting proper loop shaping weighting functions. The resulting controller can stabilize all the plants with perturbations within a gap metric ball with respect to the nominal plant. Nonlinear simulations proved the good damping performance of the designed controller.

3. The proposed branch and bound scheme has been used to verify the robustness of the designed controller.

The two robustness analysis tools were studied based on the same test systems and scenarios so that comparisons can be made easily. Both methods can give a yes or no answer to the robust stability of the problem under investigation. But because of the differences in uncertainty characterization, analysis framework, and the underlying theory background, the results obtained and the efforts made for the results are quite different.

1. The structured singular value based analysis tool characterizes the parametric uncertainty in a structured manner. It utilizes as much as possible the known information about the uncertainty; thus, it can reduce conservatism to a great extent. The gap metric based analysis tool characterizes the normalized coprime factorization type uncertainty, a kind of additive uncertainty. It is more conservative than the former one. Although the frequency domain interpretation of the ν gap metric and the weighted ν gap metric help to reduce the conservatism, the results are not as promising as those based on the SSV theory. Besides, the structured singular value based approach can give the range of parameter that can maintain the system stability while the ν gap metric based approach doesn't provide such indicators. Thus for robust analysis, μ approach is better than the ν gap metric based approach.

2. For the controller synthesis, the μ synthesis involves $D - K$ iteration, it is much more complicated and time consuming than the H_∞ loop shaping design. The H_∞ loop shaping design is tightly related to the gap metric based robust stability theory in that the resulting controller can stabilize a plant set within a ball with respect to the nominal plant in terms of the gap metric. It proved to be an easily implementable and effective design tool. It involves a trial and error process in choosing the weighting functions for loop shaping. After properly selecting the weights, the followed procedure for H_∞ optimization controller synthesis is very straightforward.

Based on the above observations, we suggest using the H_∞ loop shaping procedure for controller synthesis while using the μ analysis combined with efficient bound calculation algorithms for robust analysis.

4.2 Suggestions for Future Work

The robustness problems of power system have just been investigated and there are a lot of topics in robust control area can be explored. For future research, the following directions are attractive and efforts can be made to solve the problems.

For the μ analysis, several questions have been left unanswered.

Power System Characteristics Investigation: For large power systems, there are some characteristics that haven't been exploited and might provide helpful information for reducing the computation burden in μ calculation. These characteristics include, for example, the sparsity of the system matrices, the model reduction techniques for very large systems, etc. Further efforts can be made by combining those nicely developed techniques in the power system area with robust control theory.

More General Uncertainty Types: More complicated uncertainty blocks can be included in the uncertainty characterization. Currently, we consider parametric uncertainties that are within a certain range. The approach also works for discontinuous parameters with conservatism. Nonlinear and/or time varying uncertainties could be studied. It would be useful to allow for more general uncertainties.

Branch and Bound: The present Branch and Bound scheme is fairly simple. It works well, but there are a number of areas where one may consider possibilities for improvement. These include a better chopping criterion, and use of rough bounds.

Model Reduction: For simplicity of the problem, one may consider to reduce the order of the system. Beck [4, 5] has investigated the model reduction of uncertain systems represented by linear fractional transformations on structured uncertainty sets. The methods used are extensions of the well-known method of balanced truncation, with provably good properties in the induced-norm. It may be possible to combine the results with the work presented here, to save the expensive computation.

As to the controller synthesis, Vinnicombe's discussion [49] of using the frequency re-

sponse explanation of the ν gap metric for controller design requires further investigation to determine its feasibility for controller design in power systems.

APPENDIX DETAILS OF SYSTEM LINEARIZATION

Power System Formulation

The mathematical model of power system can be represented by two set of equations: one set of differential equations and one set of algebriac equations.

$$\begin{aligned} \dot{X} &= f(X, Z, u) \\ &= [f_{1i}, f_{2i}, \cdots, f_{9i}, f_{10i}]^T \qquad (A.1) \\ Z &= g(X, Z) \\ &= [g_{1i}, g_{2i}, g_{3i}]^T \qquad (A.2) \end{aligned}$$

where, if we consider the dynamics of synchronous machine, excitation systems, and the power system stabilizer,

$X^T = [X_{SM}^T, X_{ES}^T, X_{PSS}^T]$, the vector of state variables

$X_{SM} = [E'_{q(1-m)}, E'_{d(1-m)}, \omega_{(1-n)}, \delta_{(2-n)1}]^T$

$X_{ES} = [E_{FD(1-m)}, X_{E1(1-m)}, X_{E2(1-m)}]^T$

$X_{PSS} = [X_{S1(1-m)}, X_{S2(1-m)}, X_{S3(1-m)}]^T$

$Z = [I_{q(1-m)}, I_{d(1-m)}, I_{[(m+1)-n]}, V_{T(1-n)}]^T$, the vector of network variables

$u = [V_{REF(1-m)}]^T$, the vector of control inputs

and **f** is the vector of nonlinear functions summarized below:

$$\begin{aligned} f_{1i} &= \dot{E}'_{qi} \qquad i = 1, \ldots, m \\ &= \frac{1}{\tau'_{d0i}}[E_{FDi} - E'_{qi} + (x_{di} - x'_{di})I_{di}] \qquad (A.3) \end{aligned}$$

$$
\begin{aligned}
f_{2i} &= \dot{E}'_{di} \qquad i = 1, \ldots, m \\
&= \frac{1}{\tau'_{q0i}}[-E'_{di} - (x_{qi} - x'_{qi})I_{qi}] && \text{(A.4)} \\
f_{3i} &= \dot{\omega}_i \qquad i = 1, \ldots, n \\
&= \frac{1}{M_i}[P_{mi} - (I_{di}E'_{di} + I_{qi}E'_{qi}) + (x'_{qi} - x'_{di})I_{qi}I_{di} - \frac{D_i}{\omega_S}(\omega_i - \omega_S)] && \text{(A.5)} \\
f_{4i} &= \dot{\delta}_{i1} \qquad i = 2, \ldots, n \\
&= \omega_i - \omega_1 && \text{(A.6)} \\
f_{5i} &= \dot{E}_{FDi} \qquad i = 1, \ldots, m \\
&= \frac{K_{Ai}}{T_{Ai}}X_{E2i} - \frac{1}{T_{Ai}}E_{FDi} + \frac{aK_{Ai}}{T_{Ai}}(V_{REFi} + V_{PSSi} - X_{E1i}) && \text{(A.7)} \\
f_{6i} &= \dot{X}_{E1i} \qquad i = 1, \ldots, m \\
&= -\frac{1}{T_{Ri}}X_{E1i} + \frac{1}{T_{Ri}}V_{Ti} && \text{(A.8)} \\
f_{7i} &= \dot{X}_{E2i} \qquad i = 1, \ldots, m \\
&= -\frac{1}{T_{Bi}}X_{E2i} + \frac{1-a}{T_{Bi}}(V_{REFi} + V_{PSSi} - X_{E1i}) && \text{(A.9)} \\
f_{8i} &= \dot{X}_{S1i} \qquad i = 1, \ldots, m \\
&= -\frac{1}{T_{5i}}X_{S1i} + \frac{1}{T_{5i}}\frac{K_{Si}}{\omega_S}\Delta\omega_i && \text{(A.10)} \\
f_{9i} &= \dot{X}_{S2i} \qquad i = 1, \ldots, m \\
&= -\frac{1}{T_{2i}}X_{S2i} + \frac{1}{T_{2i}}(1 - \frac{T_{1i}}{T_{2i}})[\frac{K_{Si}}{\omega_S}\Delta\omega_i - X_{S1i}] && \text{(A.11)} \\
f_{10i} &= \dot{X}_{S3i} \qquad i = 1, \ldots, m \\
&= -\frac{1}{T_{4i}}X_{S3i} + \frac{1}{T_{4i}}(1 - \frac{T_{3i}}{T_{4i}})[X_{S2i} + \frac{T_{1i}}{T_{2i}}(\frac{K_{Si}}{\omega_S}\Delta\omega_i - X_{S1i})] && \text{(A.12)} \\
g_{1_i} &= I_{qi} \\
&= \sum_{j=1}^{n}[F_{G+B}(\delta_{ij})E'_{qj} - F_{B-G}(\delta_{ij})E'_{dj}] && \text{(A.13)} \\
g_{2_i} &= I_{di} \\
&= \sum_{j=1}^{n}[F_{B-G}(\delta_{ij})E'_{qj} + F_{G+B}(\delta_{ij})E'_{dj}] && \text{(A.14)} \\
g_{3_i} &= V_{Ti} \\
&= \sqrt{V_{Tqi}^2 + V_{Tdi}^2}
\end{aligned}
$$

$$= \sqrt{(E'_{qi} + x'_{di}I_{di} - rI_{qi})^2 + (E'_{di} - x'_{qi}I_{qi} - rI_{di})^2} \quad (A.15)$$

Linearized Model

Linearize the model equations at the operating point and use the relative rotor angles with respect to the first Machine as state variables.

$$\begin{aligned}
\Delta\dot{E}'_{qi} &= \frac{\partial f_{1i}}{\partial E_{FDi}}\Delta E_{FDi} + \frac{\partial f_{1i}}{\partial E'_{qi}}\Delta E'_{qi} + \frac{\partial f_{1i}}{\partial I'_{di}}\Delta I_{di} \\
&= \frac{1}{\tau'_{d0i}}[\Delta E_{FDi} - \Delta E'_{qi} + (x_{di} - x'_{di})\Delta I_{di}] && (A.16) \\
\Delta\dot{E}'_{di} &= \frac{\partial f_{2i}}{\partial E'_{di}}\Delta E'_{di} + \frac{\partial f_{2i}}{\partial I'_{qi}}\Delta I_{qi} \\
&= \frac{1}{\tau'_{q0i}}[-\Delta E'_{di} - (x_{qi} - x'_{qi})\Delta I_{qi}] && (A.17) \\
\Delta\dot{\omega}_i &= \frac{\partial f_{3i}}{\partial E'_{di}}\Delta E'_{di} + \frac{\partial f_{3i}}{\partial E'_{qi}}\Delta E'_{qi} + \frac{\partial f_{3i}}{\partial I_{qi}}\Delta I_{qi} + \frac{\partial f_{3i}}{\partial I_{di}}\Delta I_{di} + \frac{\partial f_{3i}}{\partial \omega_i}\Delta\omega_i \\
&= \frac{1}{M_i}[-I_{di0}\Delta E'_{di} - I_{qi0}\Delta E'_{qi} + (-E'_{qi0} + (x'_{qi} - x'_{di})I_{di0})\Delta I_{qi} \\
&\quad +(-E'_{di0} + (x'_{qi} - x'_{di})I_{qi0})\Delta I_{di} - \frac{D_i}{\omega_S}\Delta\omega_i] && (A.18) \\
\Delta\dot{\delta}_i &= \frac{\partial f_{4i}}{\partial \omega_i}\Delta\omega_i = \Delta\omega_i \\
\Longrightarrow \Delta\dot{\delta}_{i1} &= \Delta\omega_i - \Delta\omega_1 && (A.19) \\
\Delta\dot{E}_{FDi} &= \frac{\partial f_{5i}}{\partial X_{E2i}}\Delta X_{E2i} + \frac{\partial f_{5i}}{\partial V_{REFi}}\Delta V_{REFi} + \frac{\partial f_{5i}}{\partial V_{PSSi}}\Delta V_{PSSi} + \frac{\partial f_{5i}}{\partial X_{E1i}}\Delta X_{E1i} \\
&\quad +\frac{\partial f_{5i}}{\partial E_{FDi}}\Delta E_{FDi} \\
&= \frac{K_{Ai}}{T_{Ai}}[\Delta X_{E2i} + \frac{T_{Ci}}{T_{Bi}}(\Delta V_{REFi} + \Delta V_{PSSi} - \Delta X_{E1i})] - \frac{1}{T_{Ai}}\Delta E_{FDi} && (A.20) \\
\Delta\dot{X}_{E1i} &= \frac{\partial f_{6i}}{\partial X_{E1i}}\Delta X_{E1i} + \frac{\partial f_{6i}}{\partial V_{Ti}}\Delta V_{Ti} \\
&= -\frac{1}{T_{Ri}}\Delta X_{E1i} + \frac{1}{T_{Ri}}\Delta V_{Ti} && (A.21) \\
\Delta\dot{X}_{E2i} &= \frac{\partial f_{7i}}{\partial X_{E1i}}\Delta X_{E1i} + \frac{\partial f_{7i}}{\partial X_{E2i}}\Delta X_{E2i} + \frac{\partial f_{7i}}{\partial V_{PSSi}}\Delta V_{PSSi} + \frac{\partial f_{7i}}{\partial V_{REFi}}\Delta V_{REFi} \\
&= -\frac{1}{T_{Bi}}\Delta X_{E2i} + \frac{1}{T_{Bi}}(1 - \frac{T_{Ci}}{T_{Bi}})[\Delta V_{REFi} + \Delta V_{PSSi} - \Delta X_{E1i}] && (A.22) \\
&\quad where\ \ \Delta V_{PSSi} = 0\ \ for\ \ i \neq 2 && (A.23)
\end{aligned}$$

$$\begin{aligned}
\Delta\dot{X}_{S1i} &= \frac{\partial f_{8i}}{\partial X_{S1i}}\Delta X_{S1i} + \frac{\partial f_{8i}}{\partial \omega_i}\Delta\omega_i \\
&= -\frac{1}{T_{5i}}\Delta X_{S1i} + \frac{1}{T_{5i}}\frac{K_{Si}}{\omega_S}\Delta\omega_i \qquad (A.24) \\
\Delta\dot{X}_{S2i} &= \frac{\partial f_{9i}}{\partial X_{S1i}}\Delta X_{S1i} + \frac{\partial f_{9i}}{\partial X_{S2i}}\Delta X_{S2i} + \frac{\partial f_{9i}}{\partial \omega_i}\Delta\omega_i \\
&= -\frac{1}{T_{2i}}\Delta X_{S2i} + \frac{1}{T_{2i}}(1 - \frac{T_{1i}}{T_{2i}})[\frac{K_{Si}}{\omega_S}\Delta\omega_i - \Delta X_{S1i}] \qquad (A.25) \\
\Delta\dot{X}_{S3i} &= \frac{\partial f_{10i}}{\partial X_{S1i}}\Delta X_{S1i} + \frac{\partial f_{10i}}{\partial X_{S2i}}\Delta X_{S2i} + \frac{\partial f_{10i}}{\partial X_{S3i}}\Delta X_{S3i} + \frac{\partial f_{10i}}{\partial \omega_i}\Delta\omega_i \\
&= -\frac{1}{T_{4i}}\Delta X_{S3i} + \frac{1}{T_{4i}}(1 - \frac{T_{3i}}{T_{4i}})[\Delta X_{S2i} + \frac{T_{1i}}{T_{2i}}(\frac{K_{Si}}{\omega_S}\Delta\omega_i - \Delta X_{S1i})] \qquad (A.26)
\end{aligned}$$

Linearize equation (A.13), (A.14) and (A.15):

$$\begin{aligned}
\Delta I_{qi} &= \sum_{j=1}^{n}[\frac{\partial g_{1i}}{\partial \delta_{ij}}\Delta\delta_{ij} + \frac{\partial g_{1i}}{\partial E'_{qj}}\Delta E'_{qj} + \frac{\partial g_{1i}}{\partial E'_{dj}}\Delta E'_{dj}] \\
&= \sum_{j=1}^{n}[(F_{G+B}(\delta_{ij0})E'_{dj0} + F_{B-G}(\delta_{ij0})E'_{qj0})\Delta\delta_{ij} + F_{G+B}(\delta_{ij0})\Delta E'_{qj} - F_{B-G}(\delta_{ij0})\Delta E'_{dj}] \\
&= \sum_{j=1}^{n}[(F_{G+B}(\delta_{ij0})E'_{dj0} + F_{B-G}(\delta_{ij0})E'_{qj0})(\Delta\delta_{i1} - \Delta\delta_{j1}) \\
&\quad + F_{G+B}(\delta_{ij0})\Delta E'_{qj} - F_{B-G}(\delta_{ij0})\Delta E'_{dj}] \\
&= \Delta\delta_{i1}\sum_{j=1}^{n}[F_{G+B}(\delta_{ij0})E'_{dj0} + F_{B-G}(\delta_{ij0})E'_{qj0}] \\
&\quad + \sum_{j=1}^{n}[-(F_{G+B}(\delta_{ij0})E'_{dj0} + F_{B-G}(\delta_{ij0})E'_{qj0})\Delta\delta_{j1} \\
&\quad + F_{G+B}(\delta_{ij0})\Delta E'_{qj} - F_{B-G}(\delta_{ij0})\Delta E'_{dj}] \qquad (A.27) \\
\Delta I_{di} &= \sum_{j=1}^{n}[\frac{\partial g_{2i}}{\partial \delta_{ij}}\Delta\delta_{ij} + \frac{\partial g_{2i}}{\partial E'_{qj}}\Delta E'_{qj} + \frac{\partial g_{2i}}{\partial E'_{dj}}\Delta E'_{dj}] \\
&= \sum_{j=1}^{n}[(F_{B-G}(\delta_{ij0})E'_{dj0} - F_{G+B}(\delta_{ij0})E'_{qj0})\Delta\delta_{ij} + F_{B-G}(\delta_{ij0})\Delta E'_{qj} + F_{G+B}(\delta_{ij0})\Delta E'_{dj}] \\
&= \sum_{j=1}^{n}[(F_{B-G}(\delta_{ij0})E'_{dj0} - F_{G+B}(\delta_{ij0})E'_{qj0})(\Delta\delta_{i1} - \Delta\delta_{j1}) \\
&\quad + F_{B-G}(\delta_{ij0})\Delta E'_{qj} + F_{G+B}(\delta_{ij0})\Delta E'_{dj}] \\
&= \Delta\delta_{i1}\sum_{j=1}^{n}[(F_{B-G}(\delta_{ij0})E'_{dj0} - F_{G+B}(\delta_{ij0})E'_{qj0}] \\
&\quad + \sum_{j=1}^{n}[-(F_{B-G}(\delta_{ij0})E'_{dj0} - F_{G+B}(\delta_{ij0})E'_{qj0})\Delta\delta_{j1}
\end{aligned}$$

$$+F_{B-G}(\delta_{ij0})\Delta E'_{qj} + F_{G+B}(\delta_{ij0})\Delta E'_{dj}] \tag{A.28}$$

$$\begin{aligned}\Delta V_{Ti} &= \frac{\partial g_{3_i}}{\partial E'_{qi}}\Delta E'_{qi} + \frac{\partial g_{3_i}}{\partial E'_{di}}\Delta E'_{di} + \frac{\partial g_{3_i}}{\partial I_{qi}}\Delta I_{qi} + \frac{\partial g_{3_i}}{\partial I_{di}}\Delta I_{di} \\ &= \frac{V_{qi0}}{V_{Ti0}}\Delta E'_{qi} + \frac{V_{di0}}{V_{Ti0}}\Delta E'_{di} + \frac{1}{V_{Ti0}}(-V_{di0}x'_{qi} - rV_{qi0})\Delta I_{qi} \\ &\quad + \frac{1}{V_{Ti0}}(V_{qi0}x'_{di} - rV_{di0})\Delta I_{di} \qquad \text{(A.29)} \\ \Rightarrow\ & -\frac{1}{V_{Ti0}}(-V_{di0}x'_{qi} - rV_{qi0})\Delta I_{qi} - \frac{1}{V_{Ti0}}(V_{qi0}x'_{di} - rV_{di0})\Delta I_{di} + \Delta V_{Ti} \\ &= \frac{V_{qi0}}{V_{Ti0}}\Delta E'_{qi} + \frac{V_{di0}}{V_{Ti0}}\Delta E'_{di} \qquad \text{(A.30)}\end{aligned}$$

The Linearized power system formulation can be represented as follows:

$$\dot{X} = AX + Bu + FZ \tag{A.31}$$

$$GZ = HX \tag{A.32}$$

where,

$X^T = [\Delta X_{SM}^T, \Delta X_{ES}^T, \Delta X_{PSS}^T]$, the vector of state variables

$\Delta X_{SM} = [\Delta E'_{q(1-m)}, \Delta E'_{d(1-m)}, \Delta\omega_{(1-n)}, \Delta\delta_{(2-n)1}]^T$

$\Delta X_{ES} = [\Delta E_{FD(1-m)}, \Delta X_{E1(1-m)}, \Delta X_{E2(1-m)}]^T$

$\Delta X_{PSS} = [\Delta X_{S1(1-m)}, \Delta X_{S2(1-m)}, \Delta X_{S3(1-m)}]^T$

$Z = [\Delta I_{q(1-m)}, \Delta I_{d(1-m)}, \Delta I_{[(m+1)-n]}, \Delta V_{T(1-n)}]^T$, the vector of network variables

$u = [\Delta V_{REF(1-m)}]^T$, the vector of control inputs

and

$$A = \left[\frac{\partial f}{\partial X}\right]$$

$$
\begin{bmatrix}
\dot{E}'_{q(1-n)} \\ \dot{E}'_{d(1-n)} \\ \dot{\omega}_{(1-n)} \\ \dot{\delta}_{(21-n1)} \\ \dot{E}_{FD(1-n)} \\ \dot{X}_{E1(1-n)} \\ \dot{X}_{E2(1-n)} \\ \dot{X}_{S12} \\ \dot{X}_{S22} \\ \dot{X}_{S32}
\end{bmatrix}
=
\begin{bmatrix}
\frac{\partial f_{1i}}{\partial E'_{qj}} & 0 & 0 & 0 & \frac{\partial f_{1i}}{\partial E_{FDj}} & 0 & 0 & 0 & 0 & 0 \\
0 & \frac{\partial f_{2i}}{\partial E'_{dj}} & 0 & 0 & 0 & 0 & 0 & 0 & 0 & 0 \\
\frac{\partial f_{3i}}{\partial E'_{qj}} & \frac{\partial f_{3i}}{\partial E'_{dj}} & \frac{\partial f_{3i}}{\partial \omega_j} & 0 & 0 & 0 & 0 & 0 & 0 & 0 \\
0 & 0 & \frac{\partial f_{4i}}{\partial \omega_j} & 0 & 0 & 0 & 0 & 0 & 0 & 0 \\
0 & 0 & \frac{\partial f_{5i}}{\partial \omega_j} & 0 & \frac{\partial f_{5i}}{\partial E_{FDj}} & \frac{\partial f_{5i}}{\partial X_{E1j}} & \frac{\partial f_{5i}}{\partial X_{E2j}} & \frac{\partial f_{5i}}{\partial X_{S1j}} & \frac{\partial f_{5i}}{\partial X_{S2j}} & \frac{\partial f_{5i}}{\partial X_{S3j}} \\
0 & 0 & 0 & 0 & 0 & \frac{\partial f_{6i}}{\partial X_{E1j}} & 0 & 0 & 0 & 0 \\
0 & 0 & \frac{\partial f_{7i}}{\partial \omega_j} & 0 & 0 & \frac{\partial f_{7i}}{\partial X_{E1j}} & \frac{\partial f_{7i}}{\partial X_{E2j}} & \frac{\partial f_{7i}}{\partial X_{S1j}} & \frac{\partial f_{7i}}{\partial X_{S2j}} & \frac{\partial f_{7i}}{\partial X_{S3j}} \\
0 & 0 & \frac{\partial f_{8i}}{\partial \omega_j} & 0 & 0 & 0 & 0 & \frac{\partial f_{8i}}{\partial X_{S1j}} & 0 & 0 \\
0 & 0 & \frac{\partial f_{9i}}{\partial \omega_j} & 0 & 0 & 0 & 0 & \frac{\partial f_{9i}}{\partial X_{S1j}} & \frac{\partial f_{9i}}{\partial X_{S2j}} & 0 \\
0 & 0 & \frac{\partial f_{10i}}{\partial \omega_j} & 0 & 0 & 0 & 0 & \frac{\partial f_{10i}}{\partial X_{S1j}} & \frac{\partial f_{10i}}{\partial X_{S2j}} & \frac{\partial f_{10i}}{\partial X_{S3j}}
\end{bmatrix}
$$

for function f_{1i} :

$$
\frac{\partial f_{1i}}{\partial E'_{qj}} = \begin{cases} 0 & \text{for j} \neq i \\ -\dfrac{1}{\tau'_{d0i}} & \text{for j=i} \quad j = 1, \cdots, n \end{cases} \tag{A.33}
$$

$$
\frac{\partial f_{1i}}{\partial E_{FDj}} = \begin{cases} 0 & \text{for j} \neq i \\ \dfrac{1}{\tau'_{d0i}} & \text{for j=i} \quad j = 1, \cdots, n \end{cases} \tag{A.34}
$$

for function f_{2i} :

$$
\frac{\partial f_{2i}}{\partial E'_{dj}} = \begin{cases} 0 & \text{for j} \neq i \\ -\dfrac{1}{\tau'_{q0i}} & \text{for j=i} \quad j = 1, \cdots, n \end{cases} \tag{A.35}
$$

for function f_{3i} :

$$
\frac{\partial f_{3i}}{\partial E'_{qj}} = \begin{cases} 0 & \text{for j} \neq i \\ -\dfrac{I_{qi0}}{M_i} & \text{for j=i} \quad j = 1, \cdots, n \end{cases} \tag{A.36}
$$

$$
\frac{\partial f_{3i}}{\partial E'_{dj}} = \begin{cases} 0 & \text{for j} \neq i \\ -\dfrac{I_{di0}}{M_i} & \text{for j=i} \quad j = 1, \cdots, n \end{cases} \tag{A.37}
$$

$$\frac{\partial f_{3i}}{\partial \omega_j} = \begin{cases} 0 & \text{for j} \neq i \\ -\dfrac{D_i}{M_i \omega_S} & \text{for j=i} \quad j = 1, \cdots, n \end{cases} \tag{A.38}$$

for function f_{4_i} :

$$\frac{\partial f_{4i}}{\partial \omega_j} = \begin{cases} -1 & \text{for j=1} \\ 1 & \text{for j=i. j} \neq 1 \quad j = 1, \cdots, n \\ 0 & \text{otherwise} \end{cases} \tag{A.39}$$

for function f_{5_i} :

$$\frac{\partial f_{5i}}{\partial \omega_j} = \begin{cases} 0 & \text{for j} \neq 2 \\ a_i a_{2i} a_{3i} \dfrac{K_{Ai}}{T_{Ai}} \dfrac{K_{Si}}{\omega_S} & \text{for j=i} \quad j = 1, \cdots, n \end{cases} \tag{A.40}$$

where $a_i = T_{Ci}/T_{Bi}$ $a_{2i} = T_{1i}/T_{2i}$ $a_{3i} = T_{3i}/T_{4i}$

$$\frac{\partial f_{5i}}{\partial E_{FDj}} = \begin{cases} 0 & \text{for j} \neq i \\ -\dfrac{1}{T_{Ai}} & \text{for j=i} \quad j = 1, \cdots, n \end{cases} \tag{A.41}$$

$$\frac{\partial f_{5i}}{\partial X_{E1j}} = \begin{cases} 0 & \text{for j} \neq i \\ -a_i \dfrac{K_{Ai}}{T_{Ai}} & \text{for j=i} \quad j = 1, \cdots, n \end{cases} \tag{A.42}$$

$$\frac{\partial f_{5i}}{\partial X_{E2j}} = \begin{cases} 0 & \text{for j} \neq i \\ \dfrac{K_{Ai}}{T_{Ai}} & \text{for j=i} \quad j = 1, \cdots, n \end{cases} \tag{A.43}$$

$$\frac{\partial f_{5i}}{\partial X_{S1j}} = \begin{cases} 0 & \text{otherwise} \\ -a_i a_{2i} a_{3i} \dfrac{K_{Ai}}{T_{Ai}} & \text{for i=j} \end{cases} \tag{A.44}$$

$$\frac{\partial f_{5i}}{\partial X_{S2j}} = \begin{cases} 0 & \text{otherwise} \\ a_i a_{3i} \dfrac{K_{Ai}}{T_{Ai}} & \text{for i=j} \end{cases} \tag{A.45}$$

$$\frac{\partial f_{5i}}{\partial X_{S3j}} = \begin{cases} 0 & \text{otherwise} \\ a_i \dfrac{K_{Ai}}{T_{Ai}} & \text{for i=j} \end{cases} \tag{A.46}$$

for function f_{6_i} :

$$\frac{\partial f_{6i}}{\partial X_{E1j}} = \begin{cases} 0 & \text{for j} \neq i \\ -\dfrac{1}{T_{Ri}} & \text{for j=i} \quad j = 1, \cdots, n \end{cases} \tag{A.47}$$

for function f_{7i} :

$$\frac{\partial f_{7i}}{\partial \omega_j} = \begin{cases} 0 & \text{otherwise} \\ a_{2i}a_{3i}\dfrac{1-a_i}{T_{Bi}}\dfrac{K_{Si}}{\omega_S} & \text{for i=j} \end{cases} \tag{A.48}$$

$$\frac{\partial f_{7i}}{\partial X_{E1j}} = \begin{cases} 0 & \text{for } j \neq i \\ -\dfrac{1-a_i}{T_{Bi}} & \text{for j=i} \quad j = 1, \cdots, n \end{cases} \tag{A.49}$$

$$\frac{\partial f_{7i}}{\partial X_{E2j}} = \begin{cases} 0 & \text{for } j \neq i \\ -\dfrac{1}{T_{Bi}} & \text{for j=i} \quad j = 1, \cdots, n \end{cases} \tag{A.50}$$

$$\frac{\partial f_{7i}}{\partial X_{S1j}} = \begin{cases} 0 & \text{otherwise} \\ -a_{2i}a_{3i}\dfrac{1-a_i}{T_{Bi}} & \text{for i=j} \end{cases} \tag{A.51}$$

$$\frac{\partial f_{7i}}{\partial X_{S2j}} = \begin{cases} 0 & \text{otherwise} \\ a_{3i}\dfrac{1-a_i}{T_{Bi}} & \text{for i=j} \end{cases} \tag{A.52}$$

$$\frac{\partial f_{7i}}{\partial X_{S3j}} = \begin{cases} 0 & \text{otherwise} \\ \dfrac{1-a_i}{T_{Bi}} & \text{for i=j} \end{cases} \tag{A.53}$$

for function f_{8i} :

$$\frac{\partial f_{8i}}{\partial \omega_j} = \begin{cases} 0 & \text{for } j \neq i \quad j = 1, \cdots, n \\ \dfrac{K_{Sj}}{\omega_S T_{5i}} & \text{for j=i} \end{cases} \tag{A.54}$$

$$\frac{\partial f_{8i}}{\partial X_{S1j}} = \begin{cases} 0 & \text{for } j \neq i \quad j = 1, \cdots, n \\ -\dfrac{1}{T_{5i}} & \text{for j=i} \end{cases} \tag{A.55}$$

for function f_{9i} :

$$\frac{\partial f_{9i}}{\partial \omega_j} = \begin{cases} 0 & \text{for } j \neq i \quad j = 1, \cdots, n \\ \dfrac{(1-a_{2i})K_{Si}}{T_{2i}} & \text{for j=2} \end{cases} \tag{A.56}$$

$$\frac{\partial f_{9i}}{\partial X_{S1i}} = \begin{cases} 0 & \text{for } j \neq i \quad j = 1, \cdots, n \\ -\dfrac{(1-a_{2i})}{T_{2i}} & \text{for j=i} \end{cases} \tag{A.57}$$

$$\frac{\partial f_{9i}}{\partial X_{S2i}} = \begin{cases} 0 & \text{for j} \neq i \quad j = 1, \cdots, n \\ -\dfrac{1}{T_{2i}} & \text{for j=i} \end{cases} \tag{A.58}$$

for function f_{10i} :

$$\frac{\partial f_{10i}}{\partial \omega_j} = \begin{cases} 0 & \text{for j} \neq i \quad j = 1, \cdots, n \\ a_{2i}(1 - a_{3i})\dfrac{K_S}{T_{4i}} & \text{for j=2} \end{cases} \tag{A.59}$$

$$\frac{\partial f_{10i}}{\partial X_{S1i}} = \begin{cases} 0 & \text{for j} \neq i \quad j = 1, \cdots, n \\ -a_{2i}(1 - a_{3i})\dfrac{1}{T_{4i}} & \text{for j=i} \end{cases} \tag{A.60}$$

$$\frac{\partial f_{10i}}{\partial X_{S2i}} = \begin{cases} 0 & \text{for j} \neq i \quad j = 1, \cdots, n \\ (1 - a_{3i})\dfrac{1}{T_{4i}} & \text{for j=i} \end{cases} \tag{A.61}$$

$$\frac{\partial f_{10i}}{\partial X_{S3i}} = \begin{cases} 0 & \text{for j} \neq i \quad j = 1, \cdots, n \\ -\dfrac{1}{T_{4i}} & \text{for j=i} \end{cases} \tag{A.62}$$

$$B = \left[\frac{\partial f}{\partial u}\right] = \begin{matrix} \dot{E}'_{q(1-n)} \\ \dot{E}'_{d(1-n)} \\ \dot{\omega}_{(1-n)} \\ \dot{\delta}_{(21-n1)} \\ \dot{E}_{FD(1-n)} \\ \dot{X}_{E1(1-n)} \\ \dot{X}_{E2(1-n)} \\ \dot{X}_{S12} \\ \dot{X}_{S22} \\ \dot{X}_{S32} \end{matrix} \begin{bmatrix} 0 \\ 0 \\ 0 \\ 0 \\ \dfrac{\partial f_{5i}}{\partial V_{REFj}} \\ 0 \\ \dfrac{\partial f_{7i}}{\partial V_{REFj}} \\ 0 \\ 0 \\ 0 \end{bmatrix} \tag{A.63}$$

$$\text{where } \frac{\partial f_{5i}}{\partial V_{REFj}} = \begin{cases} 0 & \text{for j} \neq i \quad j = 1, \cdots, n \\ a_i \dfrac{K_{Ai}}{T_{Aj}} & \text{for j=i} \end{cases} \tag{A.64}$$

$$\frac{\partial f_{7i}}{\partial V_{REFj}} = \begin{cases} 0 & \text{for j} \neq i \quad j = 1, \cdots, n \\ (1 - a_i)\dfrac{1}{T_{Bj}} & \text{for j=i} \end{cases} \tag{A.65}$$

$$F = \left[\frac{\partial f}{\partial Z}\right] = \begin{array}{c} \\ \dot{E}'_{q(1-n)} \\ \dot{E}'_{d(1-n)} \\ \dot{\omega}_{(1-n)} \\ \dot{\delta}_{(21-n1)} \\ \dot{E}_{FD(1-n)} \\ \dot{X}_{E1(1-n)} \\ \dot{X}_{E2(1-n)} \\ \dot{X}_{S12} \\ \dot{X}_{S22} \\ \dot{X}_{S32} \end{array} \begin{bmatrix} & & \\ 0 & \dfrac{\partial f_{1_i}}{\partial I_{dj}} & 0 \\ \dfrac{\partial f_{2_i}}{\partial I_{qj}} & 0 & 0 \\ \dfrac{\partial f_{3_i}}{\partial I_{qj}} & \dfrac{\partial f_{3_i}}{\partial I_{dj}} & 0 \\ 0 & 0 & 0 \\ 0 & 0 & 0 \\ 0 & 0 & \dfrac{\partial f_{6_i}}{\partial V_{Tj}} \\ 0 & 0 & 0 \\ 0 & 0 & 0 \\ 0 & 0 & 0 \\ 0 & 0 & 0 \end{bmatrix} \tag{A.66}$$

for function f_{1_i} :

$$\frac{\partial f_{1_i}}{\partial I_{dj}} = \begin{cases} 0 & \text{for j} \neq i \quad j = 1, \cdots, n \\ \dfrac{1}{\tau'_{d0i}}(x_{di} - x'_{di}) & \text{for j=i} \end{cases} \tag{A.67}$$

for function f_{2_i} :

$$\frac{\partial f_{2_i}}{\partial I_{qj}} = \begin{cases} 0 & \text{for j} \neq i \quad j = 1, \cdots, n \\ -\dfrac{1}{\tau'_{q0i}}(x_{qi} - x'_{qi}) & \text{for j=i} \end{cases} \tag{A.68}$$

for function f_{3_i} :

$$\frac{\partial f_{3_i}}{\partial I_{qj}} = \begin{cases} 0 & \text{for j} \neq i \quad j = 1, \cdots, n \\ \dfrac{1}{M_i}[-E'_{qi0} + (x'_{qi} - x'_{di})I_{di0}] & \text{for j=i} \end{cases} \tag{A.69}$$

$$\frac{\partial f_{3_i}}{\partial I_{di}} = \begin{cases} 0 & \text{for j} \neq i \quad j = 1, \cdots, n \\ \dfrac{1}{M_i}[-E'_{di0} + (x'_{qi} - x'_{di})I_{qi0}] & \text{for j=i} \end{cases} \tag{A.70}$$

for function f_{6_i} :

$$\frac{\partial f_{6_i}}{\partial V_{Tj}} = \begin{cases} 0 & \text{for j} \neq i \quad j = 1, \cdots, n \\ \dfrac{1}{T_{Ri}} & \text{for j=i} \end{cases} \tag{A.71}$$

$$G = \begin{matrix} I_{q(1-n)} \\ I_{d(1-n)} \\ V_{T(1-n)} \end{matrix} \begin{bmatrix} \dfrac{\partial I_{qi}}{\partial I_{qj}} & 0 & 0 \\ 0 & \dfrac{\partial I_{di}}{\partial I_{dj}} & 0 \\ \dfrac{\partial V_{Ti}}{\partial I_{qj}} & \dfrac{\partial V_{Ti}}{\partial I_{dj}} & \dfrac{\partial V_{Ti}}{\partial V_{Tj}} \end{bmatrix} \tag{A.72}$$

where,

$$\frac{\partial I_{qi}}{\partial I_{qj}} = \begin{cases} 0 & \text{for j} \neq i \quad j = 1, \cdots, n \\ 1 & \text{for j=i} \end{cases} \tag{A.73}$$

$$\frac{\partial I_{di}}{\partial I_{dj}} = \begin{cases} 0 & \text{for j} \neq i \quad j = 1, \cdots, n \\ 1 & \text{for j=i} \end{cases} \tag{A.74}$$

$$\frac{\partial V_{Ti}}{\partial I_{qj}} = \begin{cases} 0 & \text{for j} \neq i \quad j = 1, \cdots, n \\ -\dfrac{1}{V_{Ti0}}(-V_{di0}x'_{qi} - rV_{qi0}) & \text{for j=i} \end{cases} \tag{A.75}$$

$$\frac{\partial V_{Ti}}{\partial I_{dj}} = \begin{cases} 0 & \text{for j} \neq i \quad j = 1, \cdots, n \\ -\dfrac{1}{V_{Ti0}}(V_{qi0}x'_{di} - rV_{di0}) & \text{for j=i} \end{cases} \tag{A.76}$$

$$\frac{\partial V_{Ti}}{\partial V_{Tj}} = \begin{cases} 0 & \text{for j} \neq i \quad j = 1, \cdots, n \\ 1 & \text{for j=i} \end{cases} \tag{A.77}$$

$$H = \left[\frac{\partial g}{\partial X}\right] = \begin{matrix} I_{q(1-n)} \\ I_{d(1-n)} \\ V_{T(1-n)} \end{matrix} \begin{bmatrix} \dfrac{\partial I_{qi}}{\partial E'_{qj}} & \dfrac{\partial I_{qi}}{\partial E'_{dj}} & 0 & \dfrac{\partial I_{qi}}{\partial \delta_{k1}} & 0 & 0 & 0 & 0 & 0 & 0 \\ \dfrac{\partial I_{di}}{\partial E'_{qj}} & \dfrac{\partial I_{di}}{\partial E'_{dj}} & 0 & \dfrac{\partial I_{di}}{\partial \delta_{k1}} & 0 & 0 & 0 & 0 & 0 & 0 \\ \dfrac{\partial V_{Ti}}{\partial E'_{qj}} & \dfrac{\partial V_{Ti}}{\partial E'_{dj}} & 0 & 0 & 0 & 0 & 0 & 0 & 0 & 0 \end{bmatrix} \tag{A.78}$$

where,

$$\frac{\partial I_{qi}}{\partial E_{qj}'} = F_{G+B}(\delta_{ij0}) \tag{A.79}$$

$$\frac{\partial I_{qi}}{\partial E_{dj}'} = -F_{B-G}(\delta_{ij0}) \tag{A.80}$$

$$\frac{\partial I_{qi}}{\partial \delta_{k1}} = \sum_{j=1}^{n} \frac{\partial \delta_{ij}}{\partial \delta_{k1}} [F_{G+B}(\delta_{ij0}) E'_{dj0} + F_{B-G}(\delta_{ij0}) E'_{qj0}] \qquad (A.81)$$

$$i, j = 1, \cdots, n \qquad k = 2, \cdots, n$$

$$\frac{\partial I_{di}}{\partial E_{qj}'} = F_{B-G}(\delta_{ij0}) \qquad (A.82)$$

$$\frac{\partial I_{di}}{\partial E_{dj}'} = F_{G+B}(\delta_{ij0}) \qquad (A.83)$$

$$\frac{\partial I_{qi}}{\partial \delta_{i1}} = \sum_{j=1}^{n} \frac{\partial \delta_{ij}}{\partial \delta_{k1}} [F_{B-G}(\delta_{ij0}) E'_{dj0} - F_{G+B}(\delta_{ij0}) E'_{qj0}] \qquad (A.84)$$

$$i, j = 1, \cdots, n \qquad k = 2, \cdots, n$$

$$\frac{\partial V_{Ti}}{\partial E'_{qj}} = \begin{cases} 0 & \text{for j} \neq i \quad j = 1, \cdots, n \\ \dfrac{V_{qi0}}{V_{Ti0}} & \text{for j=i} \end{cases} \qquad (A.85)$$

$$\frac{\partial V_{Ti}}{\partial E'_{dj}} = \begin{cases} 0 & \text{for j} \neq i \quad j = 1, \cdots, n \\ \dfrac{V_{di0}}{V_{Ti0}} & \text{for j=i} \end{cases} \qquad (A.86)$$

BIBLIOGRAPHY

[1] S.S. Ahmed, L. Chen, and A. Petroianu, "Design of Suboptimal H_∞ Excitation Controllers", *IEEE Trans. on Power Systems*, vol. 11, no. 1, Feburary 1996, pp312-318.

[2] P.Ambos,G.Duc and CM.Falinower, "Loop Shaping H_∞ Design Applied to the Steam Generator Level Control in EDF Nuclear Power Plant", *Proc. of the 1996 IEEE Int. Conf. on Control App.*, Dearborn, MI, September 15018, 1996.

[3] P.M.Anderson and A.A.Fouad, "Power System Control and Stability", *IEEE Press*, 1994.

[4] C.Beck, R. D'Andrea, "Computational Study and Comparisons of LFT Reducibility Methods Model reduction of multidimensional and uncertain systems", *Proc. of the American Control Conference*, vol. 2, 1998.

[5] C.L.Beck, J.Doyle, K.Glover, "Model reduction of multidimensional and uncertain systems", *IEEE Trans. Automatic Control*, vol.41, pp 1466-1477, Oct.1996.

[6] R. Asgharian, and S.A. Tavakoli, "Systematic Approach to Performance Weights Selection in Design of Robust H_∞ PSS Using Genetic Algorithms," *IEEE Trans. on Energy Conversion*, vol. 11, no. 1, March 1996, pp. 111-117.

[7] G.J.Balas, J.C.Doyle, K.Glover, A.Packard and R.Smith, " μ Analysis and Synthesis Toolbox User's Guide", *Natick, Mass.:Mathwork*, 1993.

[8] S. Chen, and O.P. Malik, "H_∞ Optimization Based Power System Stabilizer Design", *IEE Proceedings. Part C*, vol. 142, no. 2, March 1995, pp. 179-184.

[9] S. Chen, and O.P. Malik, "Power System Stabilizer Design Using H_∞ Synthesis", *IEEE Trans. on Energy Conversion*, vol. 10, no. 1, March 1995, pp. 175-181.

[10] F. P. de Mello and C. Concordia, "Concepts of Synchronous Machine Stability as Affected by Excitation Control", *IEEE Trans. PAS-88*, pp.316-29, 1969.

[11] J.C.Doyle and A.Packard, " Uncertain Multivariable System from a State Space Perspective", *1987 ACC*, pp.2147-2152.

[12] J.C.Doyle and G.Stein, " Multivariable Feedback Design: Concepts for a Classical/Modern Synthesis", *IEEE Trans. Autom. Contr.*, vol.26.1, pp.1-16.1981.

[13] J.C.Doyle, " Analysis of FeedBack Systems with Structured Uncertainty", *IEE Proc., Part D*, vol.129, Nov.1982, pp.242-250.

[14] J.C. Doyle, "Structured uncertainty in control system design," in *Proceedings of the 24th Conference on Decision and Control*, 1985, pp. 260-265.

[15] A. El-Sakkary, "The gap metric: Robustness of stabilisation of feedback systems", *IEEE Trans. Automatic Control*,vol.30, pp 240-247.1985.

[16] IEEE Commitee Report, "Excitation System Models for Power System Stability Studies", *IEEE Trans. on Power Apparatus and Systems*, vol.PAS-100,pp.494-509, Feburary 1981.

[17] M. K.H. Fan, A.L.Tits, " Characterization and Efficient Computation of the Structured Singular Value", *IEEE Trans. Automat. Contr.*, vol.AC-31, pp.734-743, Aug.1986.

[18] M. K.H. Fan, A. L.Tits, and J. C.Doyle, " Robustness in the Presence of Mixed Parametric Uncertainty and Unmodeled Dynamics", *IEEE Trans. Automat. Contr.*, vol.36, pp.25-38, 1991.

[19] K.A.Folly, N.Yorino and H. Sasaki, "Robust Stabilization of Power System Using an Improved H_∞-PSS", *Proc. Int. Conf. on Electrical Engineering*, Beijing, August 1996, pp.188-192.

[20] Tryphon T. Geogiou, and Malcolm C. Smith, " Optimal Robustness in the Gap Metric", *IEEE Trans. Automat. Contr.*, vol.35, pp.673-686, 1990.

[21] Tryphon T. Geogiou, " On the computation of the Gap Metric", *System and Control Letters*, vol.11,pp253-257,1988.

[22] Graham Rogers, "Power System Oscillations", *Kluwer Academic Publishers*, 2000.

[23] M.H. Khammash, V. Vittal, and C.D. Pawloski, "Analysis of control performance for stability robustness of power systems", *IEEE Trans. on Power Systems*, vol. 9, no. 4, November 1994, pp. 1861-1867.

[24] E. Khutoryansky, and M.A. Pai, "Parametric Robust Stability of Power Systems Using Generalized Kharitonov's Theorem", *Proceedings of the 36th IEEE Conference on Decision and Control*, San Diego, California, 1997, pp. 3097-3099.

[25] M. Klien, L.X. Le, G. J. Rogers, and S. Farrokhpay, "H_∞ Damping Controller Design in Large Power Systems", *IEEE Trans. on Power Systems*, vol. 10, no. 1, Feburary 1995, pp158-166.

[26] P.Kundur, G.J.Rogers, and D.Y.Wong, " Extended Transient Midterm Stability Program Package: Version 2.0, user's manuals", *ERPI EL-6648*, December 1989.

[27] P. Kundur, M. Klein, G. J. Rogers, and M. Zwyno, "Applications of power system stabilizers for enhancement of overall system stability", *IEEE Trans. on Power Systems*, vol. 4, No. 2, May 1989, pp. 614-622.

[28] M. Klein, G. J. Rogers, and P. Kundur, "A Fundamental Study of Inter-area Oscillations in power systems", *IEEE Trans. on Power Systems*, vol. 6, 1991, pp. 914-921.

[29] P. Kundur, "Power System Stability and Control", *New York: McGrawHill Inc.*, 1993.

[30] E.V.Larsen and D.A.Swann, "Applying Power System Stabilizers, PartI-III", *IEEE Trans. on Power Apparatus and Systems*, vol.PAS-100, 1981, pp. 3017-3046.

[31] O.P.Malik, G.S.Hope,Y.M.Gorski, V.A.Ushakov, A.L.Rackevich, "Experimental Studies on Adaptive Micorprocessor Stabilizers for Synchronous Generators", *IFAC Power System and Power Plant Control*,Beijing, pp.125-130,1986.

[32] Miodrag Djukanovic, Mustafa Khammash, Vijay Vittal, " Application of the Structured Singular Value Theory for Robust Stability and Control Analysis in Multimachine Power Systems, Part-I: Framework Development and Part II: Numerical Simulation and Results", *IEEE Transaction on Power systems*, vol. 13, pp.1311-1316, Nov.1998

[33] Miodrag Djukanovic, Mustafa Khammash, Vijay Vittal, "Structured Singular Value Theory Based Stability Robustness of Power Systems, Part-I: Robust Analysis and Part II: Controller Synthesis", *Proceeding of the 36th IEEE Conference on Control and Decision*, vol. 3, 1997, pp. 2702-2707.

[34] Miodrag Djukanovic, Mustafa Khammash, Vijay Vittal, "Sequential Synthesis of Structured Singular Value Based Decentralized Controllers in Power Systems", *IEEE Transaction on Power systems*, vol. 14, no.2, May 1999, pp.635-641.

[35] Duncan McFarlane, and Keith Glover, " A Loop Shaping Design Procedure Using H_∞ Synthesis", *IEEE Transaction on Automatic Control*, vol.37, No.6, pp. 759-769, June 1992.

[36] G.L.Nemhauser, A.H.G.Rinnooy Kan and M.J.Todd, editors " *Optimization*, Vol 1, North-Holland, Amsterdam, 1989.

[37] Newlin, M.P. and Young, P.M., " Mixed μ Problems and Branch and Bound Techniques ", *Proceedings of the 31th Conference on Decision and Control*, pp.3175-3180, 1992.

[38] H.Othman, J.J.Sanchez-Gasca, "On the Design of Robust Power System Stablizers", *Proceedings of the 28th Conference on Decision and Control*, Tampa,Florida, pp. 1853-1857,December,1989.

[39] A.Packard, M.Fan, and J.Doyle, " A Power Method for the Structured Singular Value", *Proc. 28th IEEE CDC*, pp.2132-2137, 1988.

[40] R.F.Pannett, P.K.Chawdhry and C.R.Burrows, "Alternative robust control strategies for disturbance rejection in fluid power systems", *Proc. of the ACC* , San Diego, CA, June 1999.

[41] K.Qiu and E.J.Davison, "Pointwise Gap Metrics and Transfer Metrics", *IEEE Trans. Automatic Control*, vol.37,no.6, pp 770-780, 1992.

[42] S. Skogestad, and I. Postlethwaite, *Multivariable Feedback Control Analysis and Design*, Chichester:John Wiley & Sons, 1998.

[43] A.Sideris.. " Elimination of Frequency Search from Robustness Tests", *IEEE Trans. on AC*, vol.37, n.10, pp. 1635-1640, 1992.

[44] C.W.Taylor, " Improving Grid Behavior", *IEEE Spectrum*, vol.36, n.6, pp. 40-45, 1999.

[45] S. Venkataraman, M.H. Khammash, and V. Vittal, "Analysis and Synthesis of HVDC Controls for Stability of Power Systems", *IEEE Trans. on Power Systems*, vol. 10, no. 4, November 1995, pp. 1933-1939.

[46] M. Vidyasagar, "Control System Synthesis: A Factorization Approach", *MIT Press, Cambridge*, MA, 1985

[47] M. Vidyasagar, "The graph metric for unstable plants and robustness estimates for feedback stability", *IEEE Trans. Automatic Control*, vol.29, no.5,pp 403-417,1984.

[48] G.Vinnicombe, "Frequency Domain Uncertainty and the Graph Topology", *IEEE Trans. Automatic Control*, vol.38,no.9,pp 1371-1383,1993..

[49] G.Vinnicombe, "Measuring the Robustness of Feedback Systems", *Ph.D. Dissertation, Cambridge Univ.*, 1993..

[50] V. Vittal, "Transient Stability Test Systems for Direct Stability Methods", *IEEE Trans. on PAS*, vol. 7, No. 1, Feb. 1992, pp. 37-42.

[51] V.Vittal, M.Khammash, and M.Djukanovic, " Robust Analysis and Design of Control in Power Systems", *ERPI TR-111922*, Dec. 1998.

[52] Yu, Xuechun, " Robustness Analysis and Controller Design for Static Var Compensators in Power Systems", *Ph.D.dissertation, Iowa State University*, 2000.

[53] Young, P.M., " Robustness with Parameter and Dynamic Uncertainty", *Ph.D.dissertation, Cal.Ins.of Tech.*, 1993.

[54] Young, P.M., Doyle, J.C, " A Lower Bound for the Mixed μ Problem", *Automatic Control, IEEE Transactions on*, vol.42 1 , pp.123, Jan. 1997 , -128 .

[55] G.Zames, and A.K.El-Sakkary, "Unstable Systems and Feedback: The Gap Metric", *Proc. Allerton Conf.* pp 380-385.

[56] Q.Zhao and J.Jiang, "Robust Control Design for Generator Excitaion System", *IEEE Trans. on Energy Conv.*, vol.10, No.2, 1995, pp.201-209.

[57] K. Zhou, and J.C. Doyle, "Essentials of Robust Control", *New Jersey:Prentice-Hall*, 1998.

[58] K. Zhou, J.C. Doyle, and Keith Glover, "Robust and Optimal Control", *Upper Saddle River, N.J. : Prentice Hall*, c1996.